

# Accepted Manuscript

Synthesis, biological evaluation and molecular docking study of *N*-(2-methoxyphenyl)-6-((4-nitrophenyl)sulfonyl)benzamide derivatives as potent HIV-1 Vif antagonists

Meng Zhou, Rong-Hua Luo, Xue-Yan Hou, Rui-Rui Wang, Guo-Yi Yan, Huan Chen, Rong-Hong Zhang, Jian-You Shi, Yong-Tang Zheng, Rui Li, Yu-Quan Wei

PII: S0223-5234(17)30018-1

DOI: [10.1016/j.ejmech.2017.01.010](https://doi.org/10.1016/j.ejmech.2017.01.010)

Reference: EJMECH 9161

To appear in: *European Journal of Medicinal Chemistry*

Received Date: 6 December 2016

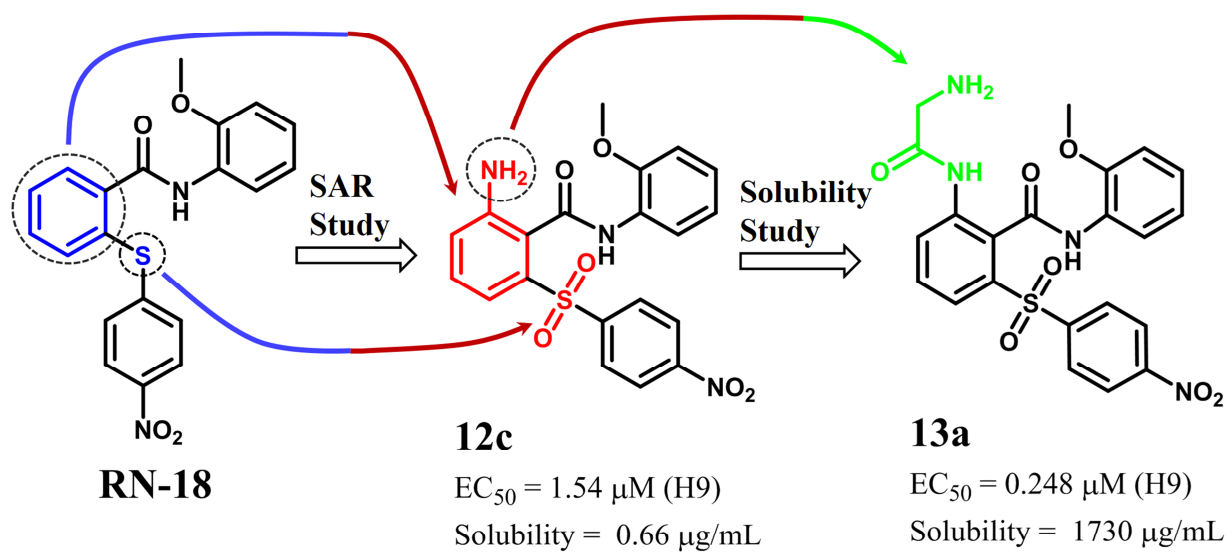
Revised Date: 6 January 2017

Accepted Date: 8 January 2017

Please cite this article as: M. Zhou, R.-H. Luo, X.-Y. Hou, R.-R. Wang, G.-Y. Yan, H. Chen, R.-H. Zhang, J.-Y. Shi, Y.-T. Zheng, R. Li, Y.-Q. Wei, Synthesis, biological evaluation and molecular docking study of *N*-(2-methoxyphenyl)-6-((4-nitrophenyl)sulfonyl)benzamide derivatives as potent HIV-1 Vif antagonists, *European Journal of Medicinal Chemistry* (2017), doi: 10.1016/j.ejmech.2017.01.010.

This is a PDF file of an unedited manuscript that has been accepted for publication. As a service to our customers we are providing this early version of the manuscript. The manuscript will undergo copyediting, typesetting, and review of the resulting proof before it is published in its final form. Please note that during the production process errors may be discovered which could affect the content, and all legal disclaimers that apply to the journal pertain.





# Synthesis, biological evaluation and molecular docking study of *N*-(2-methoxyphenyl)-6-((4-nitrophenyl)sulfonyl)benzamide derivatives as potent HIV-1 Vif antagonists

Meng Zhou<sup>a,c,d,1</sup>, Rong-Hua Luo<sup>b,1</sup>, Xue-Yan Hou<sup>a,1</sup>, Rui-Rui Wang<sup>b</sup>, Guo-Yi Yan<sup>a</sup>, Huan Chen<sup>b</sup>, Rong-Hong Zhang<sup>c</sup>, Jian-You Shi<sup>a</sup>, Yong-Tang Zheng<sup>b,\*</sup>, Rui Li<sup>a,\*</sup>, Yu-Quan Wei<sup>a</sup>

<sup>a</sup>State Key Laboratory of Biotherapy/Collaborative Innovation Center for Biotherapy, West China Hospital, Sichuan University, Chengdu, Sichuan 610041, P. R. China.

<sup>b</sup>Key Laboratory of Animal Models and Human Disease Mechanisms of Chinese Academy of Sciences & Yunnan Province, Kunming Institute of Zoology, Chinese Academy of Sciences, Kunming, Yunnan 650223, P. R. China.

<sup>c</sup>Engineering Research Center for the Development and Application of Ethnic Medicine and TCM, Ministry of Education, Guizhou Medical University, Guiyang 550004, Guizhou, China.

<sup>d</sup>National Engineering Research Center of Miao's Medicines, Guizhou Medical University, Guiyang 550004, Guizhou, China.

<sup>e</sup>Tissue Engineering and Stem Cell Research Center, Guizhou Medical University, Guiyang 550004, Guizhou, P. R. China.

<sup>1</sup>These authors contributed equally to this work.

\*Corresponding authors. E-mail addresses: lirui@scu.edu.cn (L. Rui), zhengyt@mail.kiz.ac.cn (Y-T, Zheng).

**Abstract.** Viral infectivity factor (Vif) is protective against APOBEC3G (A3G)-mediated viral cDNA hypermutations, and development of molecules that inhibit Vif mediated A3G degradation is a novel strategy for blocking HIV-1 replication. Through optimizations of the central ring of *N*-(2-methoxyphenyl)-2-((4-nitrophenyl)thio)benzamide (**RN-18**), we found a potent compound **12c** with EC<sub>50</sub> value of 1.54 μM, enhancing the antiviral activity more than 150-fold compared with **RN-18** in nonpermissive H9 cells. **12c** protected A3G from degradation by inhibiting Vif function. Besides, **12c** suppressed different HIV-1 clinical strains (HIV-1<sub>KM018</sub>, HIV-1<sub>TC-1</sub> and HIV-1<sub>WAN</sub>) and drug-resistant strains (NRTI, NNRTI, PI, and FI) with relatively high activities. Amidation of **12c** with glycine gave a prodrug **13a**, improving the water solubility about 2,600-fold compared with **12c**. Moreover, **13a** inhibited the virus replication efficiently with an EC<sub>50</sub> value of 0.228 μM. These results suggested that the prodrug **13a** is a promising candidate agent for the treatment of AIDS.

**Keywords.** Vif antagonists, Vif mediated A3G degradation, nonpermissive, antiviral activity.

## 1. Introduction

A major cellular host defense factor, APOBEC3G (A3G), which is an APOBEC3 family member, is reported to protect host cells from retroviral damage and severely weaken infectivity of human immunodeficiency virus type I (HIV-1) in nonpermissive cells (e.g., H9, CEM) [1, 2]. Antiviral effects of A3G include deaminase-dependent and -independent mechanisms. In the absence of viral infectivity factor (Vif), approximately seven copies of A3G are incorporated into budding virions by binding to the viral genomic (+) RNA or Gag [3, 4]. To initiate reverse transcription, A3G is released from RNA-induced multimer by RNase H and induces deamination of C-to-U on the first minus-strand viral cDNA [5, 6], which subsequently

inactivates viral proteins and produces noninfectious virions [7-10]. Also, A3G can inhibit numerous HIV-1 replication steps *via* a deaminase-independent mechanism. A3G inhibits tRNA<sup>Lys</sup><sub>3</sub> primer annealing, strand transfer, and nascent HIV-1 cDNA elongation [11, 12]. However, Vif recruits an E3 ubiquitin ligase complex composed of elongin B (ELOB) and C (ELOC), cullin 5 (CUL5), Rbx2 and CBF- $\beta$  and mediates A3G degradation [13-19]. Thus, inhibition of Vif may be an effective approach for preventing A3G from degradation and implementing antiviral activity [20].

**RN-18** (*N*-(2-methoxyphenyl)-6-((4-nitrophenyl)sulfonyl)benzamide, **1**, Fig. 1), a novel Vif antagonists discovered by Rana's group [21], offered an innovative approach to treating HIV. The derivatives of **1** reduce viral infectivity by enhancing A3G-dependent Vif degradation, increasing A3G incorporation into virions, and enhancing cytidine deamination of the viral genome [21-23]. Recent researches showed that replacement of amide functionality of **1** with a 1,2,3-triazole improved the potency [24], indicating the potential of **1** optimizations. Although structure-activity relationship of **1** on two branched chains (ring A and C, Fig. 1) has been well studied [23], the role of the central ring is remain unclear. Therefore, this study describes the design, synthesis and biological evaluation of a range of novel derivatives on this moiety of **1**.

## 2. Results and discussion

### 2.1. Chemistry

#### 2.1.1. Optimizing strategies on the central ring of **1** (Strategy I, II, and III)

The central ring B of **1** was optimized with two strategies: replacement of the benzene ring with a heteroaromatic ring (Strategy I, Fig. 1) and introduction of substituents to ring B (Strategy II, Fig. 1). Firstly, replacement of ring B with a heterocyclic thiophene (**2** and **3**) decreased EC<sub>50</sub>

5-fold compared to the reported Vif inhibitor (**1**) in nonpermissive H9 cells (reduced HIV-1 p24 antigen production by 50%, Table 1). It should be noted that the different  $EC_{50}$  values of **1** reported by Rana<sup>1, 21</sup> and this study might derive from the different testing systems. When replaced with a pyridine (**4**) [23],  $EC_{50}$  value decreased to 147  $\mu$ M. Then, addition of halogens or electron withdrawing groups to C5, such as a chlorine atom (**5**), fluorine (**6**), or a trifluoromethyl (**7**), nitro group (**8**), were investigated. Antiviral activities of **6**, **7**, and **8** were similar to **1**, but the activity of **5** was improved to 18.3  $\mu$ M. Interestingly, introduction of a chlorine atom to C5 of the pyrimidine ring of **4** got a similar result, and the activity of **9** was 3-fold greater than **4**, indicating the existence of a potential halogen bond (X-bond) [25]. The heteroatom serving as the X-bond acceptor was speculated to be a carbonyl oxygen of the peptide backbone, the most common X-bond acceptors in protein-inhibitor complexes [26]. The decreased activity of **8** confirmed that a hydrogen bond (H-bond) acceptor such as carbonyl should be used instead of an H-bond donor (hydroxyl, amide or thiol group); otherwise, the nitro group of **8** would form an H-bond with the target, conferring a greater activity. The activity of thiophene (**2** and **3**) was 3-fold greater than that of pyridine (**4**), which could be explained by an intermolecular C-S  $\sigma^*$  interaction with the carbonyl oxygen atom [27].

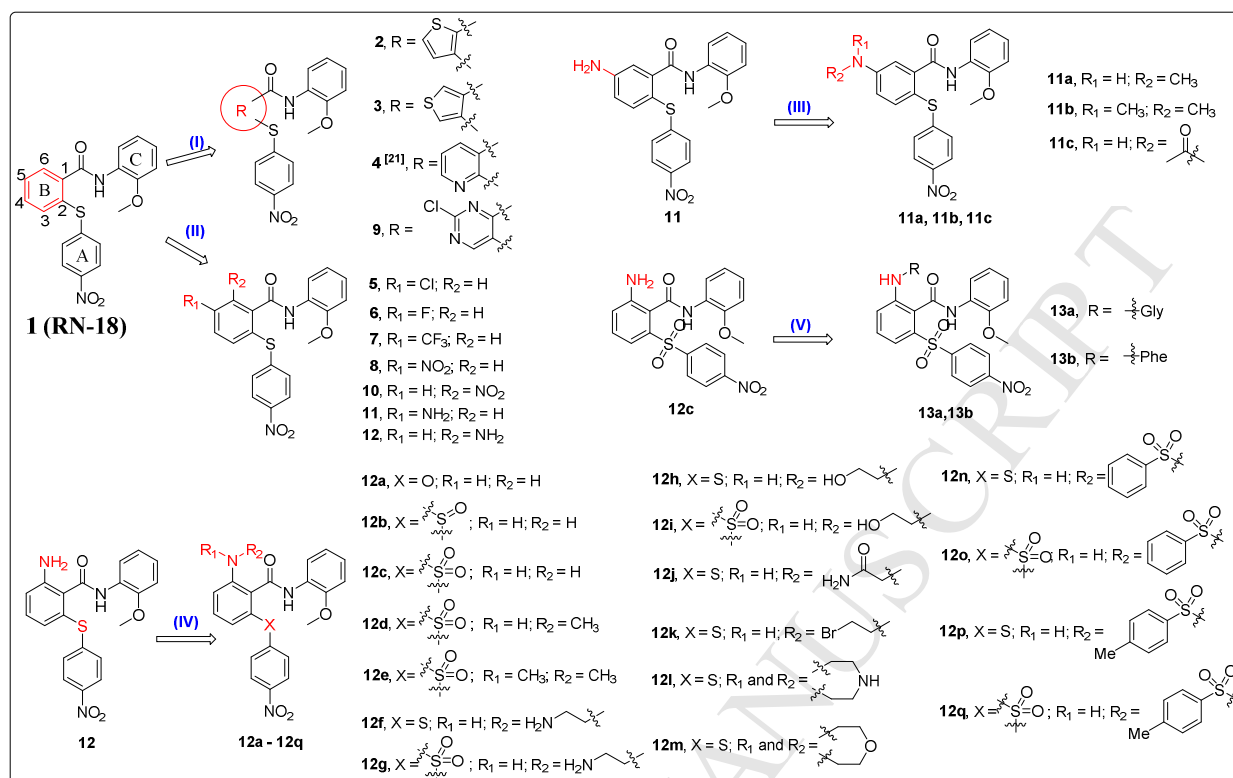


**Fig. 1.** Optimization strategies of **1** (I and II), **11** (III), **12** (IV), and **12c** (V).

**Table 1.** Antiviral activities of compound **1** derivatives in H9 cells.

Compound	CC <sub>50</sub>	EC <sub>50</sub>	TI <sup>a</sup>
<b>1</b>	N.A. <sup>b</sup>	263	N.A.
<b>2</b>	472	62.2	7.59
<b>3</b>	518	51.2	10.1
<b>4</b>	525	147	3.57
<b>5</b>	483	18.3	26.4
<b>6</b>	502	249	2.02
<b>7</b>	N.A.	223	N.A.
<b>8</b>	N.A.	235	N.A.
<b>9</b>	480	54.7	8.78
<b>10</b>	N.A.	235	N.A.
<b>11</b>	506	6.63	76.3
<b>11a</b>	302	240	1.26
<b>11b</b>	182	233	0.781
<b>11c</b>	171	457	0.374
<b>12</b>	387	1.87	207
<b>12a</b>	202	94.6	2.14
<b>12b</b>	335	10.5	31.9
<b>12c</b>	462	1.54	300
<b>12d</b>	200	278	0.719
<b>12e</b>	439	226	1.94

<b>12f</b>	38.2	45.4	0.841
<b>12g</b>	211	214	0.986
<b>12h</b>	265	43.6	6.08
<b>12i</b>	154	216	0.713
<b>12j</b>	35.5	41.8	0.849
<b>12k</b>	N.A.	221	N.A.
<b>12l</b>	30.6	8.24	3.71
<b>12m</b>	N.A.	242	N.A.
<b>12n</b>	N.A.	187	N.A.
<b>12o</b>	N.A.	176	N.A.
<b>12p</b>	364	30.6	11.9
<b>12q</b>	N.A.	172	N.A.
<b>13a</b>	196	0.248	790
<b>13b</b>	216	1.46	148

<sup>a</sup>TI: therapeutic index,  $TI = CC_{50}/EC_{50}$ . <sup>b</sup>NA: a  $CC_{50}$  values could not be obtained at the tested concentration range.

To verify our hypothesis, an amino group with two H-bond donors, was introduced to C5 (**11**) of the central ring, and we noted an increased activity ( $EC_{50}$  6.63  $\mu$ M), which might be ascribed to the H-bond interaction between the amino group and the nearby carbonyl group of the target. To understand the role of the amino group with respect to antiviral activity, the amino group of **11** was mono (**11a**)/dimethylated (**11b**), acetylated (**11c**) or translocated to the C6 position, respectively (Strategy III, Fig. 1). **11a**, **11b** and **11c** showed reduced activities, perhaps due to partial or total loss of the H-bond and increased steric hindrance (Table 1). However, when the amino group was transferred from C5 to C6 (**12**), activity obviously increased to 1.87  $\mu$ M. Subsequently, the sulfide bridge of **12** was replaced by an oxygen (**12a**), a sulfoxide (**12b**) or a sulphone (**12c**) (Strategy IV, Fig. 1). Results revealed that atom types and the sulfur oxidation states could influence the activity. When sulfur (**12**) was replaced by oxygen (**12a**), activity decreased ~50-fold; when sulfur was oxidized to sulfoxide (**12b**), activity decreased to 10.5  $\mu$ M; while activity increased to 1.54  $\mu$ M when sulfoxide was oxidized to sulphone (**12c**).

#### 2.1.2. Lowest conformation analysis of **12**, **12a**, **12b** and **12c**

To analyse the structure-activity relationship (SAR) of **12** and its analogues (**12a**, **12b**, and **12c**), the conformation of each compound was then studied. It was widely accepted that drugs bound to an enzyme in a particular conformation which was probably the lowest energy conformation or one close in energy to it [28-30]. Thus, the lowest energy conformation was usually used in quantitative structure activity relationship (QSAR) and docking researches [31-33]. The global minimum conformations of structure **12**, **12a**, **12b**, and **12c** were studied through a conformational search method by using Discovery Studio software (3.1) [34] with a systematic search method, which were then fully optimized using DFT at the B3LYP/6-31G(d) level, as implemented in the Gaussian 03 program package [35]. All of them displayed no imaginary frequencies. Results showed that the lowest conformation of four compounds (**12**, **12a**, **12b** and **12c**) all tended to form two intramolecular H-bonds: the amino group with the amide carbonyl group and the heteroatom of A-B ring bridge with the hydrogen of amide bond, conferring them structural rigidity (Fig. 2). Through superposition of their common aniline group, the lowest conformation of **12a** was unique (Supplementary Fig. S1), which was interpreted from the smaller radius of oxygen compared to sulfur. Regarding the torsion of ring B to C, with the torsion angle of the four compounds decreasing, the activities declined (Table 1 and 2), indicating that the direction in which ring B extended contributed to the activity. Compounds with better activities (**12** and **12c**) had similar angles between ring B and A, and hence the angle of **12c** might be ideal in the active conformation (104.97 degrees). Deviation of **12a** to the ideal angle was larger than that of **12b** by 10.40 degrees, which explained the obviously improved antiviral effect of **12b**. Thus, for **12** and **12c**, the active conformations might be related to their lowest conformations.

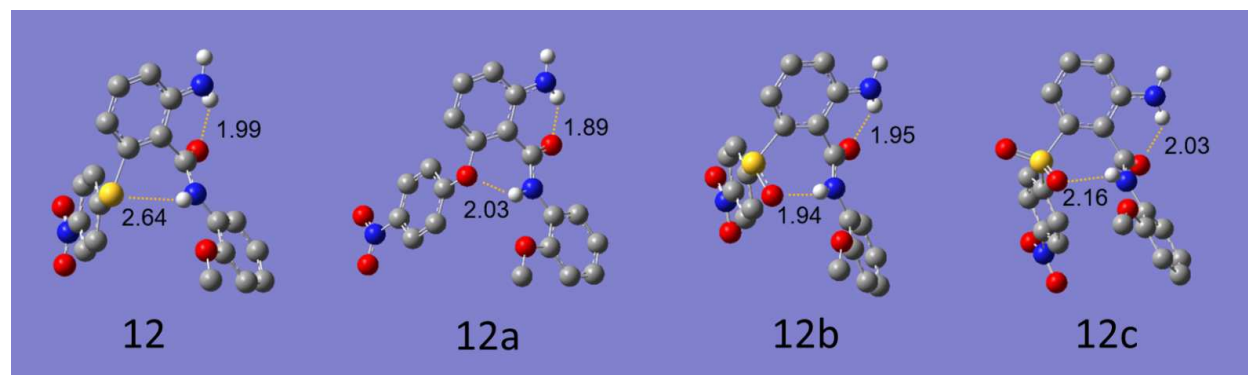


**Fig. 2.** The lowest conformations and intramolecular H-bonds of **12**, **12a**, **12b** and **12c**, respectively.

**Table 2.** The lowest conformational parameters of **12**, **12a**, **12b**, and **12c**, respectively.

Compound	B-C torsion	Deviation <sup>a</sup>	A-B angle	Deviation <sup>b</sup>
<b>12c</b>	53.82	0	104.97	0
<b>12</b>	46.23	7.59	104.67	0.30
<b>12b</b>	44.48	9.34	100.37	4.60
<b>12a</b>	27.85	25.97	119.97	15.00

<sup>a</sup>Deviation means the difference torsion between **12c** and **12**, **12b**, **12a**, respectively;

<sup>b</sup>Deviation means the difference angle between **12c** and **12**, **12b**, **12a**, respectively.

### 2.1.3. Optimizing strategies of **12** (Strategy IV, V, and VI)

Next, the amino group of **12c** was monomethylated (**12d**), and dimethylated (**12e**), and the activity declined for each (Strategy IV, Fig. 1), indicating that the two hydrogens of the amino group were important to antiviral activity as in the case of derivatives **11a**, **b**. One hydrogen was used to confer rigidity *via* an intramolecular H-bond with the carbonyl oxygen, and the other might interact with Vif. Thus, to study additional interaction sites in the vicinity, one hydrogen atom of the amino group was substituted. First, aminoethyl (**12f**, **12g**), xethyl (**12h**, **12i**) or acetamide (**12j**) groups were used to explore the possible neighboring H-bond. Whereas the antiviral activity of each modified compound was reduced (Table 1). Next, bromoethyl (**12k**),

piperazine (**12l**), morpholine (**12m**), benzenesulfonamide (**12n**, **12o**) and *p*-methylbenzenesulfonamide (**12p**, **12q**) were used to explore a possible X-bond and hydrophobic interaction, and again activity decreased for all compounds, indicating a narrow cavity in which the amino group was located. Interestingly, when the two hydrogens of the amino group were replaced by piperazine, **12l** retained activity (8.24  $\mu$ M), perhaps due to rigidity of the piperazine group that translocated the structure outward to ensure H-bond interaction between polar hydrogen on the piperazine group with the carbonyl oxygen. In contrast, with an amino group replaced by morpholine **12m** exhibited a reduced potency, confirming the presence of a carbonyl group in the amino group interaction region.

#### 2.1.4. Binding mode analysis

Since the complicated activity of Vif, the crystal structure of Vif complex was not resolved until recently [36], and the binding site of **1** was still unclear. Thus, to better understand the SARs, a binding mode of the most potent inhibitor **12c** with Vif (PDB ID 4N9F) was studied by using Autodock (4.2) [37]. We noted five major binding pockets on the surface of Vif (Supplementary Fig. S2, Table S1), and pocket 1 was the largest one but with no biological role. Pocket 2 was smaller than the former and it had a definite physiological function, interacting with ELOC and CUL5 [36, 38, 39]. Although pockets 3, 4 and 5 also bound A3G and CBF- $\beta$  [17, 36, 40, 41], they were too small to accommodate **12c**. Therefore, we focused on pocket 2 and after 100 repeated dockings on pocket 2 with **12c**, three major binding modes were found (Supplementary Fig. S3 and S4). Basing on the SAR of **12** derivatives, we speculated that mode 1, with the lowest binding energy ( $-7.31$  Kcal/mol), the highest occurrence rate (44%) and the most (five) intermolecular H-bonds, was the possible binding mode of **12c** (Table S2). Moreover,

its active conformation adopted the lowest conformation, bearing two intramolecular H-bonds (Fig. 3a). The ring C was buried in the hydrophobic cavity formed by Phe115, Tyr148, Ile155, and Pro157 and the oxygen of the *o*-methoxyl group formed an H-bond with Cys133. The amino group of central ring B formed H-bonds with Tyr148 and Gln136, and Tyr148 formed another H-bond with the carbonyl group of **12c**. With the intramolecular H-bond between the amino and the amide carbonyl group, a pseudo-four-membered ring structure formed, reinforcing the ligand interaction. Another carbonyl group was noted on His139 near the C-5 position of ring B (3.43 Å), which was not observed in the other two binding modes, indicating an origin of the X-bond with Cl and the C–S  $\sigma^*$  interaction with thiophene. The nitro group of ring A was near the main chain polar hydrogen of Ala153 and tended to form an H-bond. Although the sulphone linker was a little far from Lys156 (distance between sulphone and amino group on Lys156 = 3.91 Å), due to the flexibility of the side chain of Lys, the H-bond could be easily formed *via* an induced-fit process.

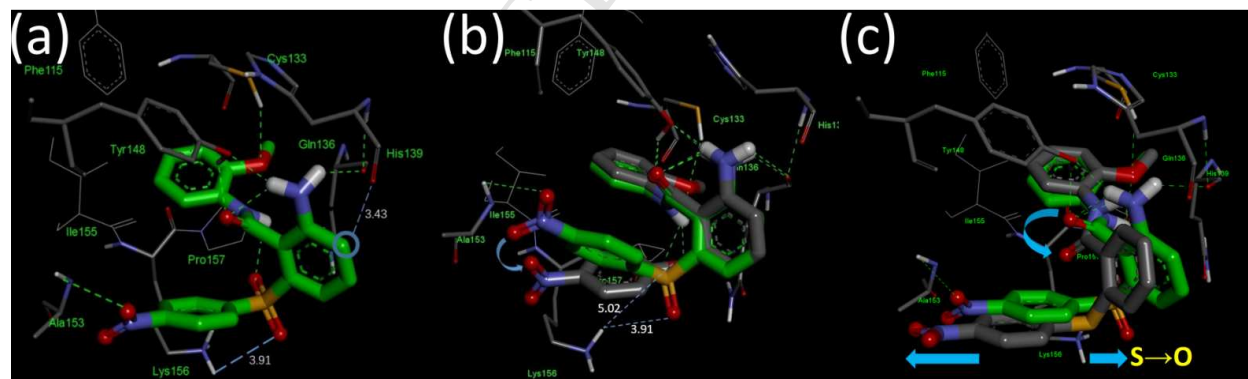


**Fig. 3.** Binding pose analysis of **1**, **12a** and **12c**. (a) The possible binding pose of **12c** with Vif. (b) Binding mode difference of **12a** (gray carbon) and **12c** (green carbon) with Vif. (c) The binding mode comparison of **1** (gray carbon) and **12c** (green carbon).

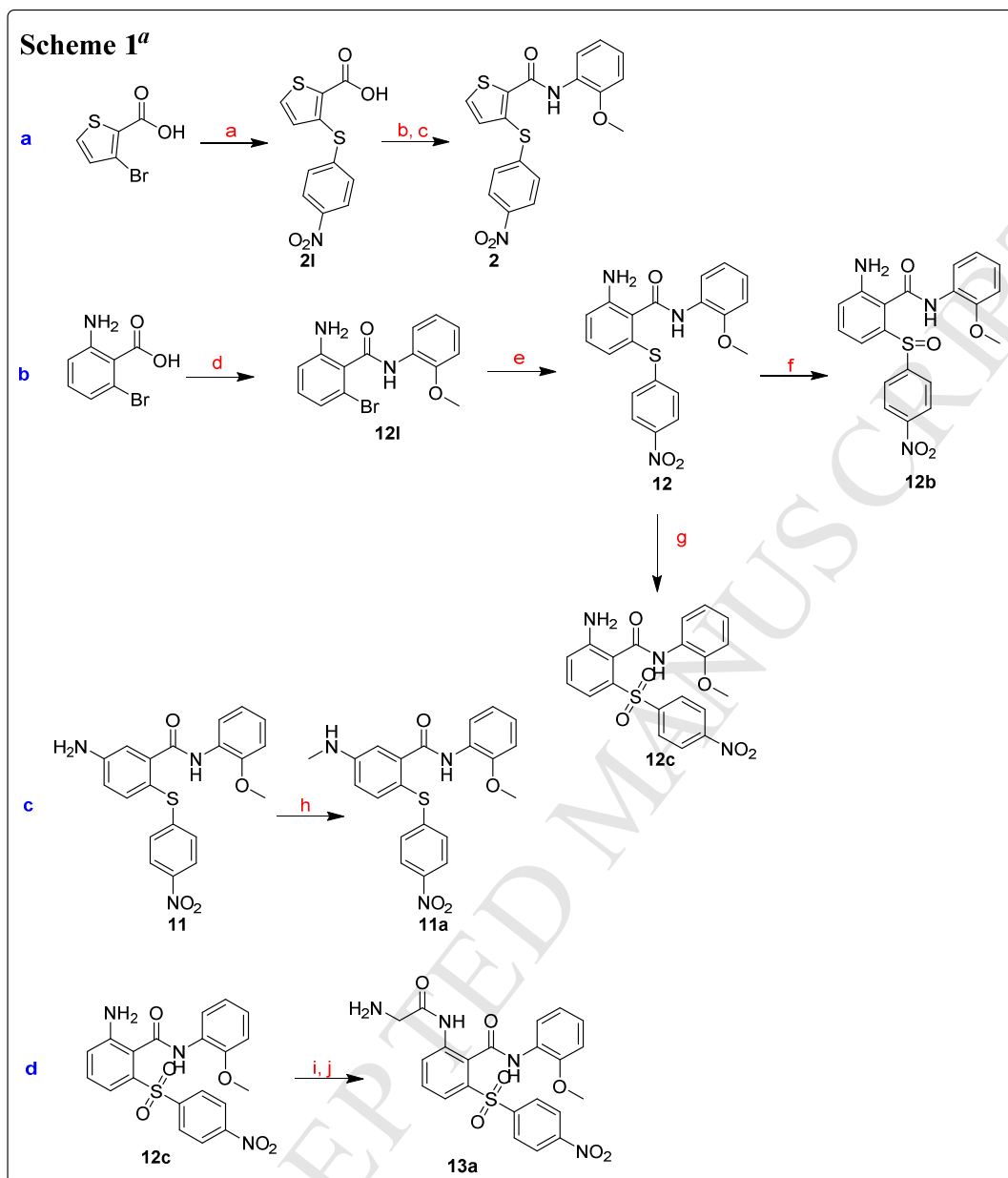
Through docking of **12a** to pocket 2, a similar active conformation with **12c** was observed, with B and C rings well superimposed (Fig. 3b). Due to the larger angle between ring A and B of **12a**, the whole ring A of **12a** moved downward, rendering the nitro group totally lose the H-bond interaction with Ala153. Besides, shorter C-O bond and smaller radius of oxygen increased the distance of ether oxygen to Lys156 (distance between ether oxygen and amino group on Lys156 = 5.02 Å), thus decreasing the possibility of H-bond formation.

As for **1**, this molecule adopted a similar active conformation with **12c**, with ring C buried into the hydrophobic cavity mentioned above and an H-bond was formed between the oxygen of *o*-methoxyl group and Cys133 (Fig. 3c). Differently, without the amino group, the H-bond between **1** and Tyr148 or Gln136 was not observed. Besides, without the restriction of amino intramolecular H-bond, torsion occurred on the amide bond, making carbonyl oxygen atom far away from Tyr148 and thereby losing another H-bond with Tyr148. Apart from that, A and B rings moved outward, and the distance between the nitro and Ala153 increased, which impaired the H-bond. When the sulfide bridge was replaced by ether oxygen, due to the smaller radius of oxygen and shorter C-O bond, the whole ring A moved inward and the distance of the nitro and Ala153 was decreased, which might partially restore the H-bond interaction. That is in agreement with the slightly improved activity of oxygen ether analogue of **1** in the reported researches (Supplementary Fig. S5) [22, 23].

#### 2.1.5. Synthetic routes of representative compounds

Processes for the preparation of compounds in this study were similar, and six typical compounds (**2**, **11a**, **12**, **12b**, **12c**, and **13a**) were described in Scheme 1. Synthetic procedure of other analogues was described in Experimental section. Intermediate **2I** was obtained through thiolation between 3-bromothiophene-2-carboxylic acid and 4-nitrobenzenethiol using base and

copper nanopowder, which was then converted to the corresponding acyl chloride and was further reacted with 2-methoxyaniline to afford **2** (Scheme 1a). For molecule **12**, in the presence of condensing agents, the intermediate **12I** was obtained by the amidation reaction between 2-amino-6-bromobenzoic acid and *o*-anisidine. Subsequently, **12I** was mixed with 4-nitrothiophenol in the presence of copper nanopowder and base to generate **12**. Afterwards, **12** was oxidized by hydrogen peroxide dissolving in methanol or acetic acid to give sulfoxide **12b** or sulfone **12c**, respectively (Scheme 1b). As for optimizations of the amino group of ring B, substituents were introduced under base condition. For example, **11a** was obtained in the presence of potassium carbonate and iodomethane (Scheme 1c). While for the synthesis of glycine prodrug **13a**, **12c** was reacted with boc-glycine under the condition of condensation agents to afford the intermediate, which was then generated **13a** through deprotection (Scheme 1d).



**Scheme 1.** Synthetic of representative compounds. <sup>a</sup>Reagents and conditions: (a) 4-Nitrothiophenol, copper nanopowder,  $K_2CO_3$ , DMF, 55 °C, 8 h. (b)  $SOCl_2$ , cat. DMF, 80 °C, 2 h. (c) 2-Methoxyaniline,  $Et_3N$ , benzene, 80 °C, 2 h. (d) 2-Methoxyaniline, EDCI, THF, RT, 2 h. (e) 4-Nitrothiophenol,  $K_2CO_3$ , copper nanopowder, DMF, 65 °C, 8 h. (f) 35%  $H_2O_2$ ,  $CH_3OH$ , 66 °C, 40min. (g) 35%  $H_2O_2$ , acetic acid (HAc), 55 °C, 3 h. (h) Iodomethane,  $K_2CO_3$ , DMF, 50 °C, 10 h. (i) Gly-Boc, DCC, HOBt, DCM, RT. (j) TFA/DCM (1:3), RT, 2 h.

## 2.2. Biological activity

### 2.2.1. **12c** protects APOBEC3G from Vif-mediated degradation.

Since Vif was reported to mediate the degradation of A3G [42], a fluorescent primary screening assay was used to measure **12c** effects on Vif-mediated A3G degradation. Results showed that the EYFP fluorescence of **12c**-treated cells were greater than those in DMSO-treated cells (Fig. 4a). Also, compared with **1**, **12c** protected A3G better at the same concentration, and **12c** protection of A3G against Vif-mediated degradation was dose-dependent (Fig. 4a and 4b). To verify that **12c** inhibited Vif-A3G interaction, TREX-hvif-15 cells were transfected with pcDNA3.1-APOBEC3G-HA and total cellular proteins were extracted 48 hours post-transfection for Vif and HA tag analysis. Results showed that A3G decreased in the presence of Vif and this was reversed with the addition of **12c**, and A3G increased with increasing concentrations of **12c** (Fig. 4c). In nonpermissive PBMCs infected with clinical strain HIV-1<sub>TC-1</sub>, Vif-mediated degradation of A3G was inhibited by **12c** and Vif expression was decreased with increasing concentration of **12c**, also, p24 expression was blocked (Fig. 4d). All these results proved that **12c** had the ability of inhibiting Vif-mediated A3G degradation.

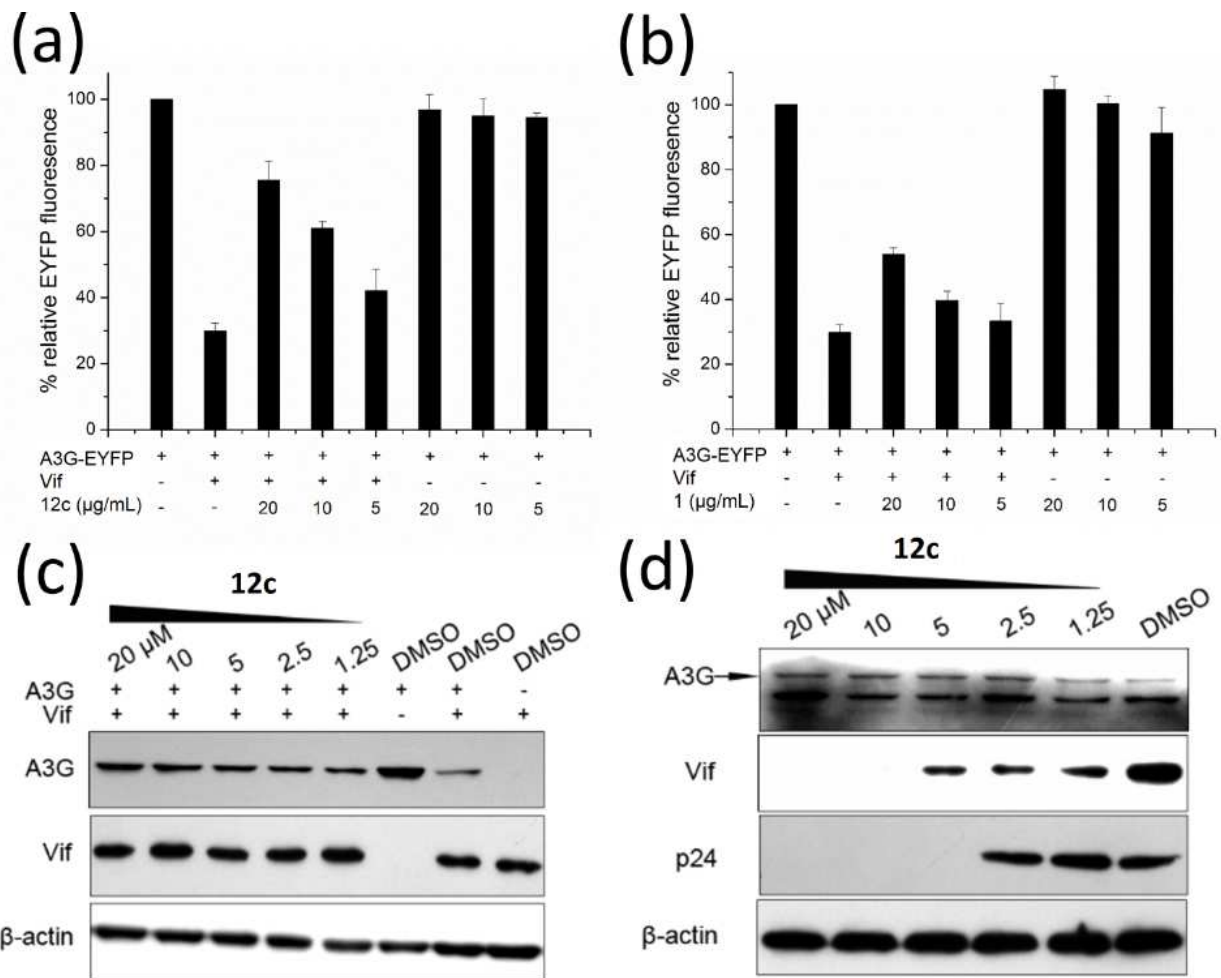


**Fig. 4.** Effects of **12c** on the expression of A3G, Vif, and p24. TREX-hvif-15 cells were transfected with EYFP-N1-hA3G, and Vif was induced by 1 μg/mL Dox. The cells were treated with or without **12c** (a) or **1** (b), respectively. The EYFP fluorescence was determined by flow cytometry and no Vif expression was set to 100%. (c) pcDNA3.1-APOBEC3G-HA was transfected into TREX-hvif-15 and Vif expression was induced by 0.1 μg/mL Dox. (d) PBMCs were infected with HIV-1<sub>TC-1</sub> in the presence or absence of **12c**. The total cellular protein was extracted, and the expression of A3G, Vif, HA tag, p24 and β-actin (internal control) were determined by western blot.

### 2.2.2. **12c** inhibits HIV-1 replication in different cell lines with relatively low cytotoxicity

The antiviral activity of **12c** was measured in H9 cells and PHA-stimulated PBMCs. H9 cells were infected with NL4-3 and PBMCs were infected with clinical strains HIV-1<sub>KM018</sub>, HIV-1<sub>TC-1</sub>, HIV-1<sub>WAN</sub>, and HIV-1<sub>SF162</sub>, the former three of which are prevalent in China [43, 44]. Result showed that **12c** effectively inhibited replication of different wild-type HIV-1 strains in different cell lines (Table 3). EC<sub>50</sub> values of **12c** against lab-adaptive strains ranged from 0.522-17.8  $\mu$ M. Moreover, **12c** had low cytotoxicity against H9 cells and PBMCs, with CC<sub>50</sub> values higher than 462  $\mu$ M.

**Table 3. Anti-HIV-1 activities of 12c in cell cultures<sup>a</sup>**

Cells	Virus	Subtype	CC <sub>50</sub> ( $\mu$ M) <sup>b</sup>	EC <sub>50</sub> ( $\mu$ M) <sup>c</sup>
H9	NL4-3	B	> 462	1.40 $\pm$ 0.13
PBMC	HIV-1 <sub>KM018</sub>	B/C <sup>d</sup>	> 468	17.8 $\pm$ 6.30
	HIV-1 <sub>SF162</sub>	B		17.8 $\pm$ 4.20
	HIV-1 <sub>TC-1</sub>	CRF01-AE		0.522 $\pm$ 0.11
	HIV-1 <sub>WAN</sub>	CRF01-AE		2.95 $\pm$ 1.14

<sup>a</sup>All data represent means  $\pm$  standard deviation for three separate experiments. <sup>b</sup>CC<sub>50</sub>, 50% cytotoxic concentration. <sup>c</sup>EC<sub>50</sub>, 50% effective concentration. <sup>d</sup>B/C, B/C recombinant.

### 2.3 Solubility optimizations of **12c**

The aqueous and organic solvent solubilities, partition coefficient (log p), and plasma protein binding of **12c** were measured. Data showed that aqueous solubility of **12c** was poor but organic solubility was high (Supplementary Table S3, S4, and S5). **12c** was readily bound to plasma protein (Fig. 5a), which might lead to potentially low activity after absorbed *in vivo*. In order to improve the aqueous solubility of **12c**, water-soluble glycine and phenylalanine prodrugs of **12c** were then synthesised (**13a** and **13b**, respectively, Strategy VII, Fig. 1) [45-50]. The water solubility was increased significantly, and the solubility of **13a** and **13b** were improved to 1730

and 120  $\mu\text{g/mL}$ , respectively (Supplementary Table S3). Moreover, **13a** and **13b** showed obviously enhanced activity in H9 cells (0.248 and 1.46  $\mu\text{M}$ , respectively, Table 1), probably because of the increased aqueous solubility. Protein analyses showed that **13a** reduced Vif level and improved A3G expression in a dose-dependent manner like **12c** (Fig. 5b). Considering potent antiviral activity, low-cost and synthetic efficiency, the glycine prodrug **13a** was chosen as a candidate prodrug of **12c**.

The forced degradation studies of **13a** were then studied using different pH buffer solutions and human liver microsomes (HLM). **13a** was stable at pH 4 and 7 (Fig. 5c), and about 50% of **13a** remained 180 h after exposure to pH 4 buffer. However, degradation of **13a** accelerated with increasing pH, and > 90% of **13a** was hydrolyzed at pH 9 in 15 h. Then, HLM metabolism studies were used to examine **13a** enzymatic degradation. Data showed that **13a** was degraded within 15 min (10 min, 76.3%; 15 min, 99.9%) to the parent **12c** (Fig. 5d, Supplementary Fig. S6 and S7). After 20 min, the prodrug was undetectable.

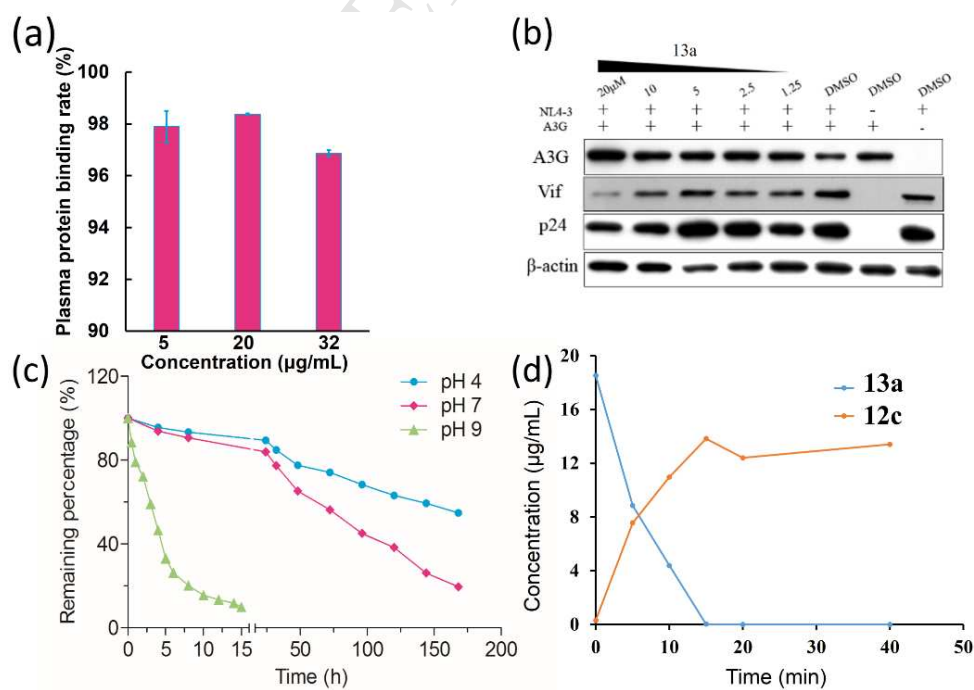


**Fig. 5.** Degradation researches and effects on the expression of A3G, Vif, and p24 of **13a**. (a) Plasma protein binding rate of **12c** at different concentrations (5, 20 and 32  $\mu\text{g/mL}$ ). (b) 293T cells were co-transfected with pcDNA3.1-APOBEC3G-HA and pNL4-3 in the presence or absence of **13a**. The total cellular protein was extracted, and the expression of A3G, Vif, HA tag, p24 and  $\beta$ -actin (internal control) were determined by western blot. (c) Degradation research of **13a** at pH 4, pH 7, and pH 9. (d) Degradation research of **13a** in human liver microsome (HLM) in 0.1 M phosphate buffer (pH 7.4) containing 36  $\mu\text{L}$  NADPH generating system at 37  $^{\circ}\text{C}$  for 0, 5, 10, 15, 20, 40 min, respectively.

### 3. Conclusions

In summary, through the optimizations on the central B ring of **1**, a new HIV-1 Vif antagonist **12c** was found. The SAR of **12c** derivatives revealed that two hydrogens of the amino group were crucial to improve the antiviral activity, with one hydrogen forming an H-bond with Vif, and the other hydrogen conferring rigidity *via* an intramolecular H-bond with the carbonyl oxygen. In nonpermissive H9 cells, **12c** showed improved activity about 150-fold compared with **1**. **12c** protected the expression of A3G more effectively than **1** at the same concentration. Meanwhile, **12c** significantly inhibited Vif-mediated degradation of A3G, and Vif expression was decreased with the concentration increasing, as well as p24 expression. Further biological activity assays showed a promising inhibitory effect of **12c** against various wild-type strains with low cytotoxicities. To improve the water solubility, amino acids (glycine and phenylalanine) was conjugated with **12c** and the glycine prodrug **13a** enhanced the aqueous solubility more than 2,600 times. In addition, the antiviral activity of **13a** was increased obviously compared with **12c** (0.228  $\mu\text{M}$ ). The efficient antiviral effect and good solubility make **13a** a potential drug for treating AIDS.

## 4. Experimental

### 4.1. General information

Proton magnetic resonance ( $^1\text{H}$  NMR) spectra was recorded on a Bruker (Avance III 400 MHz) spectrometer. Chemical shifts were reported in parts per million (ppm,  $\delta$  scale) relative to tetramethylsilane ( $\delta$  0.00). Data are represented as follows: chemical shift, multiplicity (s = singlet, d = doublet, t = triplet, q = quartet, m = multiple resonances, br = broad, app = apparent), integration, and coupling constant ( $J$ ) in Hertz. Splitting patterns that could not be easily interpreted are designated as multiplet (m) or broad (br). Carbon nuclear magnetic resonance ( $^{13}\text{C}$  NMR) spectra was recorded on a Bruker (Avance III 400 MHz) (100 MHz) spectrometer. High resolution Mass Spectroscopy (HRMS) was performed on an ESI-QTOF mass spectrometer (Micromass, UK) equipped with an interchangeable ESI Z-spray source. All final compounds were purified to > 95% purity as determined by HPLC (Dionex Ultimate 3000, USA) analysis using the following methods. Purity analysis of final compounds was performed through a  $\text{C}_{18}$  Acclaim 120 (particle size = 5  $\mu\text{m}$ , pore size = 12 nm, dimensions = 250  $\times$  4.6 mm) column. The injection volume was 10  $\mu\text{L}$  and the flow rate was 1.0 mL/min. Each analysis lasted for 20 minutes. The percentage of each solvent and retention times ( $R_{\text{T,HPLC}}$ ) and purity data (%) are displayed in the analytical data of the respective compounds in Experimental Section.

### 4.2. General procedure for the synthesis of **2-13**.

#### 4.2.1. 3-((4-nitrophenyl)thio)thiophene-2-carboxylic acid (**2I**)

3-bromothiophene-2-carboxylic acid (2070 mg, 10 mmol), 4-nitrobenzenethiol (1860 mg, 12 mmol), copper nanopowder (320 mg, 5 mmol) and anhydrous potassium carbonate (2760 mg, 20

mmol) was dissolved in DMF (50 mL), and the mixture was stirred at 55 °C for 8 hours the reaction was monitored using TLC. The reaction mixture was cooled to room temperature, filtered and washed with DMF (2 × 5 mL). The filtrate was acidified using 5N HCl leading to the precipitation of crude product. The crude residue was diluted with ethyl acetate (150 mL) and washed with water (2 × 50 mL). The organic layer was dried over anhydrous Na<sub>2</sub>SO<sub>4</sub>, filtered, and concentrated. The oily residue was applied to silica gel column chromatography (1:4 v/v ethyl acetate/petroleum ether) to afford a yellow solid (2166 mg, 77%). <sup>1</sup>H NMR (400 MHz, DMSO-*d*<sub>6</sub>) δ = 6.79 (d, *J* = 7.2Hz, 1H), 7.65 (d, *J* = 10Hz, 2H), 7.90 (d, *J* = 7.2Hz, 1H), 8.24 (d, *J* = 8.8Hz, 2H), 13.42 (s, 1H).

#### 4.2.2. *N*-(2-methoxyphenyl)-3-((4-nitrophenyl)thio)thiophene-2-carboxamide (2)

A solution of 3-((4-nitrophenyl)thio)thiophene-2-carbonyl chloride (prepared by stirring of **2I** (281 mg, 1 mmol) in SOCl<sub>2</sub> (15 mL) at 78 °C for 2 h followed by concentration of the mixture under reduced pressure) in anhydrous THF (25 mL) was added slowly to a stirred mixture of 2-methoxyaniline (98.4 mg, 0.8 mmol) and Et<sub>3</sub>N (0.416 mL, 3 mmol) dissolved in 10 mL THF at 0 °C. The reaction mixture was stirred for 2 hours at room temperature and concentrated under reduced pressure. The oily residue was diluted with ethyl acetate (50 mL) and washed with water (2 × 20 mL), dried over anhydrous Na<sub>2</sub>SO<sub>4</sub>, filtered, and concentrated under reduced pressure. The residue was applied to silica gel column chromatography (1:6 v/v ethyl acetate/petroleum ether) to afford a white solid (300.6 mg, 77.8%). m. p. 138.4–138.9 °C; <sup>1</sup>H NMR (400 MHz, CDCl<sub>3</sub>) δ = 3.75 (s, 3H), 6.86 (d, *J* = 8.0Hz, 1H), 6.98 (t, *J* = 8.0Hz, 1H), 7.07 (m, 1H), 7.16 (d, *J* = 5.2Hz, 1H), 7.26 (d, *J* = 8.8Hz, 2H), 7.67 (d, *J* = 4.8Hz, 1H), 8.14 (d, *J* = 8.4Hz, 2H), 8.45 (dd, *J* = 8.0,1.6Hz, 1H), 10.11 (s, 1H); HRMS (ESI) calcd for C<sub>18</sub>H<sub>15</sub>N<sub>2</sub>O<sub>4</sub>S<sub>2</sub> [M+H]<sup>+</sup>: 387.0473,

found: 387.0476;  $R_{T,HPLC}$  = 11.077 min, Purity > 99%, MeOH:H<sub>2</sub>O = 75:25, 30 °C. The same procedure was also followed for the syntheses of **3**, **4**, **5**, **6**, **7**, **8**, **9** and **10**.

#### 4.2.3. *N*-(2-methoxyphenyl)-4-((4-nitrophenyl)thio)thiophene-3-carboxamide (**3**)

Yellow solid; 63.7% yield; m. p. 137.0–137.9 °C; <sup>1</sup>H NMR (400 MHz, CDCl<sub>3</sub>)  $\delta$  = 3.80 (s, 3H), 6.85 (d,  $J$  = 8.0Hz, 1H), 6.95 (t,  $J$  = 8.0Hz, 1H), 7.05 (m, 1H), 7.18 (d,  $J$  = 6.8Hz, 2H), 7.75 (d,  $J$  = 3.6Hz, 1H), 8.08 (d,  $J$  = 6.8Hz, 2H), 8.41 (dd,  $J$  = 8.0,1.2Hz, 1H), 8.44 (d,  $J$  = 3.6Hz, 1H), 9.68 (s, 1H); HRMS (ESI) calcd for C<sub>18</sub>H<sub>15</sub>N<sub>2</sub>O<sub>4</sub>S<sub>2</sub> [M+H]<sup>+</sup>: 387.0473, found: 387.0479;  $R_{T,HPLC}$  = 15.677 min, Purity > 99%, MeOH:H<sub>2</sub>O = 75:25, 30 °C.

#### 4.2.4. *N*-(2-methoxyphenyl)-2-((4-nitrophenyl)thio)nicotinamide (**4**)

White solid; 67% yield; m. p. 132.9–133.2 °C; <sup>1</sup>H NMR (400 MHz, CDCl<sub>3</sub>)  $\delta$  = 3.91 (s, 3H), 6.94 (d,  $J$  = 8.0Hz, 1H), 7.04 (t,  $J$  = 7.6Hz, 1H), 7.14 (m, 1H), 7.27 (d,  $J$  = 12.0Hz, 2H), 7.66 (d,  $J$  = 8.4Hz, 1H), 7.98 (d,  $J$  = 7.6Hz, 1H), 8.20 (d,  $J$  = 8.8Hz, 2H), 8.49 (brs, 3H); HRMS (ESI) calcd for C<sub>19</sub>H<sub>16</sub>N<sub>3</sub>O<sub>4</sub>S [M+H]<sup>+</sup>: 382.0862, found: 382.0864;  $R_{T,HPLC}$  = 6.587 min, Purity > 99%, MeOH:H<sub>2</sub>O = 75:25, 30 °C.

#### 4.2.5. 5-chloro-*N*-(2-methoxyphenyl)-2-((4-nitrophenyl)thio)benzamide (**5**)

Yellow solid; 72% yield; m. p. 117.4–118.4 °C; <sup>1</sup>H NMR (400 MHz, CDCl<sub>3</sub>)  $\delta$  = 3.80 (s, 3H), 6.87 (d,  $J$  = 8.0Hz, 1H), 6.67 (t,  $J$  = 8.0Hz, 1H), 7.08 (m, 1H), 7.29 (d,  $J$  = 8.4Hz, 2H), 7.49 (m, 2H), 7.77 (s, 1H), 8.07 (d,  $J$  = 8.8Hz, 2H), 8.36 (s, 1H), 8.38 (s, 1H); HRMS (ESI) calcd for C<sub>20</sub>H<sub>16</sub>ClN<sub>2</sub>O<sub>4</sub>S<sub>2</sub> [M+H]<sup>+</sup>: 415.0519, found: 415.0520;  $R_{T,HPLC}$  = 14.180 min, Purity > 99%, MeOH:H<sub>2</sub>O = 75:25, 30 °C.

#### 4.2.6. 5-fluoro-*N*-(2-methoxyphenyl)-2-((4-nitrophenyl)thio)benzamide (**6**)

Yellow solid; 69.3% yield; m. p. 110.0–111.2 °C; <sup>1</sup>H NMR (400 MHz, CDCl<sub>3</sub>) δ = 3.77 (s, 3H), 6.86 (d, *J* = 8.0Hz, 1H), 6.97 (t, *J* = 7.6Hz, 1H), 7.08 (m, 1H), 7.25 (m, 3H), 7.55 (dd, *J* = 8.8, 2.8Hz, 1H), 7.62 (m, 1H), 8.06 (d, *J* = 8.8Hz, 2H), 8.37 (d, *J* = 7.2Hz, 1H), 8.45 (s, 1H); HRMS (ESI) calcd for C<sub>20</sub>H<sub>16</sub>FN<sub>2</sub>O<sub>4</sub>S [M+H]<sup>+</sup>: 399.0815, found: 399.0818; R<sub>T,HPLC</sub> = 10.170 min, Purity > 99%, MeOH:H<sub>2</sub>O = 75:25, 30 °C.

#### 4.2.7. *N*-(2-methoxyphenyl)-2-((4-nitrophenyl)thio)-5-(trifluoromethyl)benzamide (**7**)

Yellow solid; 77.9% yield; m. p. 99.9–101.7 °C; <sup>1</sup>H NMR (400 MHz, CDCl<sub>3</sub>) δ = 3.85 (s, 3H), 6.90 (d, *J* = 8.1Hz, 1H), 6.99 (t, *J* = 7.6Hz, 1H), 7.11 (td, *J* = 8.0, 1.5, 1H), 7.44 (d, *J* = 8.8, 2H), 7.52 (d, *J* = 8.3Hz, 1H), 7.67 (dd, *J* = 8.3, 1.5, 1H), 7.97 (s, 1H), 8.14 (t, *J* = 5.7, 2H), 8.39 (d, *J* = 6.2, 2H); HRMS (ESI) calcd for C<sub>21</sub>H<sub>16</sub>F<sub>3</sub>N<sub>2</sub>O<sub>4</sub>S [M+H]<sup>+</sup>: 449.0783, found: 449.0782; R<sub>T,HPLC</sub> = 14.587 min, Purity > 98%, MeOH:H<sub>2</sub>O = 75:25, 30 °C.

#### 4.2.8. *N*-(2-methoxyphenyl)-5-nitro-2-((4-nitrophenyl)thio)benzamide (**8**)

Yellow solid; 52% yield; <sup>1</sup>H NMR (400 MHz, DMSO-*d*<sub>6</sub>): δ = 3.938 (s, 3H), 6.76 (d, *J*=8.4 Hz, 1H), 7.06 (t, *J*=8 Hz, 1H), 7.18 (t, *J*=7.6 Hz, 1H), 7.70 (m, 2H), 8.15 (d, *J*=8.8 Hz, 2H), 8.23 (m, 3H), 8.39 (m, 2H); HRMS (ESI) calcd for C<sub>20</sub>H<sub>15</sub>N<sub>3</sub>NaO<sub>6</sub>S [M+Na]<sup>+</sup>: 448.0579, found: 448.0584; R<sub>T,HPLC</sub> = 12.427 min, Purity > 99%, MeOH:H<sub>2</sub>O = 75:25, 30 °C.

#### 4.2.9. *N*-(2-chloro-5-((4-nitrophenyl)thio)pyrimidin-4-yl)-2-methoxybenzamide (**9**)

White solid; 59.2% yield; m. p. 84.9–87.2 °C; <sup>1</sup>H NMR (400 MHz, CDCl<sub>3</sub>) δ = 4.00 (s, 3H), 7.05 (m, 3H), 7.56 (t, *J* = 7.6Hz, 1H), 7.71 (t, *J* = 7.6Hz, 2H), 7.86 (d, *J* = 8.8Hz, 1H), 8.28 (d, *J*

=8.24, 2H); HRMS (ESI) calcd for  $C_{18}H_{14}ClN_4O_4S$   $[M+H]^+$ : 417.0424, found: 417.0426;  $R_{T,HPLC}$  = 12.073 min, Purity > 98%, MeOH:H<sub>2</sub>O = 75:25, 30 °C.

#### 4.2.10. *N*-(2-aminophenyl)-2-nitro-6-((4-nitrophenyl)thio)benzamide (**10**)

White solid; 68.5% yield; m. p. 200.7–201.6 °C; <sup>1</sup>H NMR (400 MHz, CDCl<sub>3</sub>)  $\delta$  = 3.57 (brs, 2H), 6.83 (d,  $J$  = 8.0Hz, 2H), 7.14 (t,  $J$  = 7.2Hz, 1H), 7.22 (d,  $J$  = 8.0Hz, 2H), 7.40 (d,  $J$  = 8.0Hz, 2H), 7.68 (t,  $J$  = 7.6Hz, 1H), 7.85 (d,  $J$  = 8.0Hz, 1H), 7.09 (d,  $J$  = 8.0Hz, 2H), 8.31 (d,  $J$  = 8.0Hz, 1H); HRMS (ESI) calcd for  $C_{19}H_{15}N_4O_5S$   $[M+H]^+$ : 411.0763, found: 411.0761;  $R_{T,HPLC}$  = 4.287 min, Purity > 99%, MeOH:H<sub>2</sub>O = 75:25, 30 °C.

#### 4.2.11. 5-amino-*N*-(2-methoxyphenyl)-2-((4-nitrophenyl)thio)benzamide (**11**)

Yellow solid; 84% yield; m. p. 141.0–142.3 °C; <sup>1</sup>H NMR (400 MHz, CDCl<sub>3</sub>)  $\delta$  = 3.71 (s, 3H), 4.20 (brs, 2H), 6.82 (m, 2H), 6.95 (t,  $J$  = 7.6Hz, 1H), 7.04 (t,  $J$  = 8.0Hz, 1H), 7.14 (m, 3H), 7.42 (d,  $J$  = 8.0Hz, 1H), 8.03 (d,  $J$  = 9.2Hz, 2H), 8.40 (d,  $J$  = 8.0Hz, 1H), 8.45 (brs, 1H); HRMS (ESI) calcd for  $C_{20}H_{18}N_3O_4S$   $[M+H]^+$ : 396.1018, found: 396.1021;  $R_{T,HPLC}$  = 7.207 min, Purity > 99%, MeOH:H<sub>2</sub>O = 75:25, 30 °C.

#### 4.2.12. *N*-(2-methoxyphenyl)-5-(methylamino)-2-((4-nitrophenyl)thio)benzamide (**11a**)

**11** (395 mg, 1 mmol) was dissolved in DMF (40 mL) and treated with anhydrous potassium carbonate (276 mg, 2 mmol) at room temperature. To this mixture was added iodomethane (56  $\mu$ L, 0.9 mmol) *via* a micro syringe. After being stirred for 10 hours at 50 °C, the reaction mixture was poured into ice-cold water (200 mL) to get crude product. The crude solid was filtered and washed several times with water and purified by silica gel column chromatography (1:6 v/v ethyl acetate/petroleum ether) to provide a yellow solid (176.3 mg, 43% yield). m. p. 150.4–151.6 °C;

$^1\text{H}$  NMR (400 MHz,  $\text{CDCl}_3$ )  $\delta$  = 2.93 (s, 3H), 3.69 (s, 3H), 4.24 (brs, 1H), 7.72 (d,  $J$  = 8.4Hz, 1H), 6.82 (d,  $J$  = 8.0Hz, 1H), 6.94 (t,  $J$  = 6.4Hz, 1H), 7.03 (m, 2H), 7.13 (d,  $J$  = 8.8Hz, 2H), 7.43 (d,  $J$  = 8.4Hz, 1H), 8.02 (d,  $J$  = 8.8Hz, 2H), 8.41 (d,  $J$  = 8.0Hz, 1H), 8.45 (brs, 1H); HRMS (ESI) calcd for  $\text{C}_{21}\text{H}_{20}\text{N}_3\text{O}_4\text{S}$   $[\text{M}+\text{H}]^+$ : 410.1175, found: 410.1179;  $R_{\text{T,HPLC}}$  = 11.117 min, Purity > 99%, MeOH:H<sub>2</sub>O = 75:25, 30 °C. The same procedure was also followed for the syntheses of **12d**, **12f**, **12h**, **12j** and **12k**.

#### 4.2.13. 5-(dimethylamino)-*N*-(2-methoxyphenyl)-2-((4-nitrophenyl)thio)benzamide (**11b**)

**11** (395 mg, 1 mmol) was dissolved in DMF (40 mL) and treated with anhydrous potassium carbonate (552 mg, 4 mmol) at room temperature. To this mixture was added iodomethane (156  $\mu\text{L}$ , 2.5 mmol) *via* a micro syringe. After being stirred for 10 hours at 60 °C, the reaction mixture was poured into ice-cold water (200 mL) to get crude product. The crude solid was filtered and washed several times with water and purified by silica gel column chromatography (1:8 v/v ethyl acetate/petroleum ether) to provide a yellow solid (330.8 mg, 78.1% yield).  $^1\text{H}$  NMR (400 MHz,  $\text{CDCl}_3$ )  $\delta$  = 3.09 (s, 6H), 3.69 (s, 3H), 6.83 (m, 2H), 6.95 (t,  $J$  = 6.8Hz, 1H), 7.04 (t,  $J$  = 7.6Hz, 1H), 7.13 (m, 3H), 7.47 (d,  $J$  = 8.4Hz, 1H), 8.03 (d,  $J$  = 9.2Hz, 2H), 8.43 (dd,  $J$  = 8.0, 1.2Hz, 1H), 8.48 (brs, 1H); HRMS (ESI) calcd for  $\text{C}_{22}\text{H}_{22}\text{N}_3\text{O}_4\text{S}$   $[\text{M}+\text{H}]^+$ : 424.1331, found: 424.1336;  $R_{\text{T,HPLC}}$  = 6.953 min, Purity > 98%, MeOH:H<sub>2</sub>O = 75:25, 30 °C. The same procedure was also followed for the syntheses of **12e**.

#### 4.2.14. 5-acetamido-*N*-(2-methoxyphenyl)-2-((4-nitrophenyl)thio)benzamide (**11c**)

**11** (395 mg, 1 mmol) was dissolved in DCM (30 mL) at room temperature. To this mixture was added acetic anhydride (122 mg, 1.2 mmol), followed by the addition of DMAP (61 mg, 0.5 mmol). After being stirred for 5 hours at room temperature, the reaction mixture was

concentrated under reduced pressure. The crude residue was diluted ethyl acetate (60 mL), washed with water ( $2 \times 15$  mL), dried over anhydrous  $\text{Na}_2\text{SO}_4$ , filtered, and concentrated under reduced pressure. The residue was purified by silica gel column chromatography (1:6 v/v ethyl acetate/petroleum ether) to provide a yellow solid (420 mg, 96% yield). m. p. 191.4–193.2 °C;  $^1\text{H}$  NMR (400 MHz,  $\text{CDCl}_3$ )  $\delta$  = 2.18 (s, 3H), 3.73 (s, 3H), 6.85 (d,  $J$  = 8.4Hz, 1H), 6.95 (t,  $J$  = 7.6Hz, 1H), 7.07 (t,  $J$  = 8.0Hz, 1H), 7.19 (d,  $J$  = 8.8Hz, 2H), 7.56 (d,  $J$  = 8.8Hz, 1H), 7.83 (d,  $J$  = 1.6Hz, 1H), 7.94 (d,  $J$  = 8.0Hz, 1H), 7.98 (brs, 1H), 8.04 (d,  $J$  = 9.2Hz, 2H), 8.35 (d,  $J$  = 7.6Hz, 1H), 8.51 (brs, 1H); HRMS (ESI) calcd for  $\text{C}_{22}\text{H}_{20}\text{N}_3\text{O}_5\text{S}$   $[\text{M}+\text{H}]^+$ : 438.1124, found: 438.1127;  $R_{\text{T,HPLC}}$  = 7.240 min, Purity > 99%, MeOH:H<sub>2</sub>O = 75:25, 30 °C.

#### 4.2.15. Synthesis of 2-amino-6-bromo-*N*-(2-methoxyphenyl)benzamide (**12I**)

2-methoxyaniline (369 mg, 3 mmol) and EDCI (230 mg, 1.2 mmol) were mixed in tetrahydrofuran (30 mL) with a magnetic stirrer for 5 min at room temperature (RT), and to this mixture was slowly added a solution of 2-amino-6-bromobenzoic acid (215 mg, 1 mmol) in tetrahydrofuran (20 mL). After stirred for 2 hours at RT, the reaction mixture was concentrated under reduced pressure and then was diluted with water (30 mL). The aqueous layer was extracted with ethyl acetate ( $3 \times 15$  mL) and the combined organic layers were dried over anhydrous sodium sulfate, filtered, and concentrated. The oily residue was applied to silica gel column chromatography (1:5 v/v ethyl acetate/petroleum ether) to afford **12I** as a white amorphous solid (243 mg, 76% yield). m. p. 124.1–125.3 °C;  $^1\text{H}$  NMR (400 MHz,  $\text{DMSO}-d_6$ )  $\delta$  = 3.80 (s, 3H), 5.33 (s, 2H), 6.72 (d,  $J$  = 8Hz, 1H), 6.78 (d,  $J$  = 8Hz, 1H), 6.99 (m, 2H), 7.07 (d,  $J$  = 8.4Hz, 1H), 7.18 (t,  $J$  = 7.6Hz, 1H), 7.85 (t,  $J$  = 7.2Hz, 1H), 9.43 (s, 1H);  $^{13}\text{C}$  NMR (100 MHz,  $\text{DMSO}-d_6$ )  $\delta$  = 55.8, 111.5, 114.3, 119.2, 119.6, 120.3, 123.5, 123.9, 125.8, 126.6, 130.7, 147.2,

151.2, 165.1; HRMS (ESI) calcd for  $C_{14}H_{14}BrN_2O_2$   $[M+H]^+$ : 321.0239, found: 321.0240;  $R_{T,HPLC}$  = 6.187 min, Purity > 98%. MeOH:H<sub>2</sub>O = 70:30, 30 °C.

#### 4.2.16. Synthesis of 2-amino-*N*-(2-methoxyphenyl)-6-((4-nitrophenyl)thio)benzamide (**12**)

**12I** (320 mg, 1 mmol), 4-nitrothiophenol (310 mg, 2 mmol), copper nanopowder (32 mg, 0.5 mmol) and anhydrous potassium carbonate (414 mg, 3 mmol) were mixed in DMF (40 mL) at RT. Then the reaction flask was heated in an oil bath at 65 °C. After 8 hours, the heating bath was removed and the reaction flask was allowed to cool to RT. The reaction mixture was filtered and the liquid layer was diluted with water (40 mL), extracted with ethyl acetate (3 × 20 mL), washed with water (6 × 15 mL), dried over anhydrous Na<sub>2</sub>SO<sub>4</sub>, filtered, and concentrated under reduced pressure. The residue was purified by silica gel column chromatography (1:3 v/v ethyl acetate/petroleum ether) to provide the product **12** as a yellow amorphous solid (296.3 mg, 75% yield); m. p. 135.0–136.0 °C; <sup>1</sup>H NMR (400 MHz, CDCl<sub>3</sub>)  $\delta$  = 3.69 (s, 3H), 4.54 (br, 2H), 6.84 (d,  $J$  = 8Hz, 2H), 6.95 (m, 2H), 7.06 (t,  $J$  = 8Hz, 1H), 7.22 (m, 3H), 8.03 (d,  $J$  = 7.6Hz, 2H), 8.23 (s, 1H), 8.32 (d,  $J$  = 7.6Hz, 1H); <sup>13</sup>C NMR (100 MHz, DMSO-*d*<sub>6</sub>)  $\delta$  = 55.6, 111.3, 117.0, 120.2, 122.9, 123.3, 123.9, 125.4, 126.6, 126.9, 130.7, 144.7, 146.9, 148.5, 150.7, 165.1; HRMS (ESI) calcd for  $C_{20}H_{18}N_3O_4S$   $[M+H]^+$ : 396.1018, found: 396.1020;  $R_{T,HPLC}$  = 12.583 min, Purity > 99%, MeOH:H<sub>2</sub>O = 60:40, 30 °C. The same procedure was also followed for the syntheses of **11** and **12a**.

#### 4.2.17. 2-amino-*N*-(2-methoxyphenyl)-6-(4-nitrophenoxy)benzamide (**12a**)

Yellow solid; 38% yield; m. p. 136.3–137.9 °C; <sup>1</sup>H NMR (400 MHz, CDCl<sub>3</sub>)  $\delta$  = 3.77 (s, 3H), 5.88 (brs, 2H), 6.28 (d,  $J$  = 8Hz, 1H), 6.60 (d,  $J$  = 8Hz, 1H), 6.90 (m, 2H), 7.67 (t,  $J$  = 8Hz, 1H), 7.00 (d,  $J$  = 8Hz, 2H), 7.18 (t,  $J$  = 8Hz, 1H), 8.21 (d,  $J$  = 8.8Hz, 2H), 8.42 (d,  $J$  = 8Hz, 1H), 9.49

(s, 1H); HRMS (ESI) calcd for  $C_{20}H_{17}N_3NaO_5$   $[M+Na]^+$ : 402.1066, found: 402.1052;  $R_{T,HPLC}$  = 9.533 min, Purity > 98%, MeOH:H<sub>2</sub>O = 75:25, 30 °C.

#### 4.2.18. 2-amino-*N*-(2-methoxyphenyl)-6-((4-nitrophenyl)sulfinyl)benzamide (**12b**)

**12** (395 mg, 1 mmol) was dissolved in CH<sub>3</sub>OH (30 mL) with a magnetic stirrer at RT, and 35% H<sub>2</sub>O<sub>2</sub> (0.258 mL, 3 mmol) was added slowly to this solution. This reaction mixture was heated in an oil bath at 66 °C and monitored using TLC. The reaction was quenched with MnO<sub>2</sub> at RT. The mixture was filtered and the residue was washed with ethyl acetate (3 × 5 mL). The liquid layer was concentrated under reduced pressure and the oily residue was purified by silica gel column chromatography (1:4 v/v ethyl acetate/petroleum ether) to provide a yellow solid; 44.3% yield; m. p. 192.7–194.2 °C; <sup>1</sup>H NMR (400 MHz, CDCl<sub>3</sub>)  $\delta$  = 3.90 (s, 3H), 4.46 (brs, 2H), 6.88 (d,  $J$  = 8.0Hz, 1H), 6.96 (d,  $J$  = 8.0Hz, 1H), 7.04 (t,  $J$  = 7.6Hz, 1H), 7.17 (t,  $J$  = 8.0Hz, 1H), 7.41 (t,  $J$  = 8.0Hz, 1H), 7.47 (d,  $J$  = 7.2Hz, 1H), 7.91 (d,  $J$  = 8.8Hz, 2H), 8.21 (d,  $J$  = 8.8Hz, 2H), 8.28 (d,  $J$  = 7.2Hz, 1H), 8.75 (brs, 1H); HRMS (ESI) calcd for  $C_{20}H_{17}N_3NaO_5S$   $[M+Na]^+$ : 434.0787, found: 434.0784;  $R_{T,HPLC}$  = 4.913 min, Purity > 96%, MeOH:H<sub>2</sub>O = 75:25, 30 °C.

#### 4.2.19. 2-amino-*N*-(2-methoxyphenyl)-6-((4-nitrophenyl)sulfonyl)benzamide (**12c**)

**12** (395 mg, 1 mmol) was dissolved in acetic acid (30 mL) with a magnetic stirrer at RT, and H<sub>2</sub>O<sub>2</sub> (0.233 mL, 3 mmol) was added to this solution. This reaction mixture was heated in an oil bath at 55 °C and the reaction was monitored using TLC. The reaction was quenched with MnO<sub>2</sub> (305 mg, 3.5 mmol) at RT. The mixture was filtered and the residue was washed with ethyl acetate (3 × 10 mL). The liquid layer was concentrated under reduced pressure and the oily residue was purified by silica gel column chromatography (1:2 v/v ethyl acetate/petroleum ether) to provide the product **12c** as a yellow amorphous solid (162.4 mg, 38% yield). m. p. 217.0–

218.8 °C;  $^1\text{H}$  NMR (400 MHz, DMSO- $d_6$ )  $\delta$  = 3.79 (s, 3H), 5.57 (s, 2H), 7.01 (t,  $J$  = 7.6Hz, 1H), 7.08 (m, 2H), 7.22 (t,  $J$  = 7.6Hz, 1H), 7.29 (d,  $J$  = 7.6Hz, 1H), 7.36 (t,  $J$  = 7.6Hz, 1H), 7.76 (d,  $J$  = 7.6Hz, 1H), 8.16 (d,  $J$  = 8.8Hz, 2H), 8.36 (d,  $J$  = 8.8Hz, 2H), 9.71 (s, 1H);  $^{13}\text{C}$  NMR (100 MHz, DMSO- $d_6$ )  $\delta$  = 55.7, 111.5, 116.8, 120.4, 121.0, 124.4, 124.9, 126.2, 126.5, 129.2, 130.0, 136.6, 146.7, 147.2, 149.9, 151.9, 164.2; HRMS (ESI) calcd for  $\text{C}_{20}\text{H}_{18}\text{N}_3\text{O}_6\text{S}$   $[\text{M}+\text{H}]^+$ : 428.0916, found: 428.0920;  $R_{\text{T,HPLC}}$  = 9.797 min, Purity > 97%, MeOH:H<sub>2</sub>O = 60:40, 30 °C. The same procedure was also followed for the syntheses of **12g**, **12i**, **12o**, and **12p**.

#### 4.2.20. *N*-(2-methoxyphenyl)-2-(methylamino)-6-((4-nitrophenyl)sulfonyl)benzamide (**12d**)

White solid; 85.2% yield; m. p. 262.9–265.7 °C;  $^1\text{H}$  NMR (400 MHz, CDCl<sub>3</sub>)  $\delta$  = 3.29 (s, 3H), 4.03 (s, 3H), 4.73 (brs, 1H), 6.66 (dd,  $J$  = 8.0,0.8Hz, 1H), 7.04 (td,  $J$  = 8.0,1.2Hz, 1H), 7.15 (dd,  $J$  = 8.0,1.2Hz, 1H), 7.24 (m, 3H), 7.41 (m, 2H), 7.57 (m, 2H), 7.95 (d,  $J$  = 12.0Hz, 2H); HRMS (ESI) calcd for  $\text{C}_{21}\text{H}_{19}\text{N}_3\text{NaO}_6\text{S}$   $[\text{M}+\text{Na}]^+$ : 464.0892, found: 464.0894;  $R_{\text{T,HPLC}}$  = 3.910 min, Purity > 98%, MeOH:H<sub>2</sub>O = 80:20, 30 °C.

#### 4.2.21. 2-(dimethylamino)-*N*-(2-methoxyphenyl)-6-((4-nitrophenyl)sulfonyl)benzamide (**12e**)

Yellow solid; 77.2% yield; m. p. 118.5–119.2 °C;  $^1\text{H}$  NMR (400MHz, CDCl<sub>3</sub>)  $\delta$  = 2.76 (d,  $J$  = 4.8Hz, 3H), 3.28 (s, 3H), 4.08 (s, 3H), 6.61 (d,  $J$  = 8.0Hz, 1H), 7.09 (t,  $J$  = 7.6Hz, 1H), 7.13 (d,  $J$  = 8.0Hz, 1H), 7.21 (d,  $J$  = 7.6Hz, 2H), 7.36 (m, 2H), 7.43 (t,  $J$  = 6.4Hz, 1H), 7.60 (d,  $J$  = 9.2Hz, 2H), 7.91 (d,  $J$  = 8.0Hz, 2H); HRMS (ESI) calcd for  $\text{C}_{22}\text{H}_{21}\text{N}_3\text{NaO}_6\text{S}$   $[\text{M}+\text{Na}]^+$ : 478.1049, found: 478.1047;  $R_{\text{T,HPLC}}$  = 4.487 min, Purity > 98%, MeOH:H<sub>2</sub>O = 80:20, 30 °C.

#### 4.2.22. 2-((2-aminoethyl)amino)-*N*-(2-methoxyphenyl)-6-((4-nitrophenyl)thio)benzamide (**12f**)

Yellow solid; 51% yield;  $^1\text{H NMR}$  (400 MHz,  $\text{DMSO-}d_6$ )  $\delta$  = 2.73 (t,  $J$  = 6.8Hz, 1H), 3.01 (t,  $J$  = 6.4Hz, 1H), 3.19 (t,  $J$  = 6.8Hz, 1H), 3.32 (brs, 2H), 3.42 (t,  $J$  = 6.8Hz, 1H), 3.63 (s, 3H), 6.91 (m, 3H), 6.98 (d,  $J$  = 8.0Hz, 1H), 7.08 (t,  $J$  = 7.6Hz, 1H), 7.22 (d,  $J$  = 7.6Hz, 1H), 67.43 (m, 2H), 7.93 (m, 1H), 8.02 (d,  $J$  = 9.2Hz, 2H), 8.75 (br, 1H), 9.40 (br, 1H); HRMS (ESI) calcd for  $\text{C}_{22}\text{H}_{23}\text{N}_4\text{O}_4\text{S}$   $[\text{M}+\text{H}]^+$ : 439.1440, found: 439.1443;  $R_{\text{T,HPLC}}$  = 6.953 min, Purity > 98%, MeOH:H<sub>2</sub>O = 75:25, 30 °C.

4.2.23. *2-((2-aminoethyl)amino)-N-(2-methoxyphenyl)-6-((4-nitrophenyl)sulfonyl)benzamide (12g)*

Yellow solid; 49% yield; m. p. 119.3–121.0 °C;  $^1\text{H NMR}$  (400 MHz,  $\text{DMSO-}d_6$ )  $\delta$  = 3.16 (t,  $J$  = 6Hz, 2H), 3.51 (t,  $J$  = 6.4Hz, 2H), 3.73 (s, 3H), 6.89 (d,  $J$  = 8.0Hz, 1H), 7.00 (m, 3H), 7.14 (t,  $J$  = 8Hz, 1H), 7.62 (t,  $J$  = 8.0Hz, 1H), 7.77 (d,  $J$  = 8.0Hz, 1H), 7.83 (d,  $J$  = 8.0Hz, 1H), 8.15 (d,  $J$  = 9.2Hz, 2H), 8.25 (d,  $J$  = 7.2Hz, 1H), 8.45 (s, 1H); HRMS (ESI) calcd for  $\text{C}_{22}\text{H}_{23}\text{N}_4\text{O}_6\text{S}$   $[\text{M}+\text{H}]^+$ : 471.1338, found: 471.1338;  $R_{\text{T,HPLC}}$  = 5.070 min, Purity > 96%, MeOH:H<sub>2</sub>O = 75:25, 30 °C.

4.2.24. *2-((2-hydroxyethyl)amino)-N-(2-methoxyphenyl)-6-((4-nitrophenyl)thio)benzamide (12h)*

Yellow solid; 66% yield; m. p. 82.2–83.6 °C;  $^1\text{H NMR}$  (400 MHz,  $\text{CDCl}_3$ )  $\delta$  = 3.66 (m, 4H), 3.90 (s, 3H), 6.44 (d,  $J$  = 8.0Hz, 1H), 6.77 (d,  $J$  = 6.7Hz, 1H), 7.02 (m, 3H), 7.37 (m, 4H), 7.57 (m, 1H), 7.97 (d,  $J$  = 6.8Hz, 2H), 8.19 (s, 1H); HRMS (ESI) calcd for  $\text{C}_{22}\text{H}_{21}\text{N}_3\text{NaO}_5\text{S}$   $[\text{M}+\text{Na}]^+$ : 462.1100, found: 462.1100;  $R_{\text{T,HPLC}}$  = 4.677 min, Purity > 98%, MeOH:H<sub>2</sub>O = 70:30, 30 °C.

4.2.25. *2-((2-hydroxyethyl)amino)-N-(2-methoxyphenyl)-6-((4-nitrophenyl)sulfonyl)benzamide (12i)*

Yellow solid; 43% yield;  $^1\text{H NMR}$  (400 MHz,  $\text{CDCl}_3$ )  $\delta$  = 3.67 (m, 2H), 3.96 (t,  $J$  = 8.4Hz, 2H), 4.02 (s, 3H), 4.75 (br, 1H), 6.69 (d,  $J$  = 8.0Hz, 1H), 7.07 (t,  $J$  = 8.0Hz, 1H), 7.14 (d,  $J$  = 8.0Hz, 1H), 7.24 (m, 3H), 7.43 (m, 2H), 7.57 (d,  $J$  = 8.0Hz, 3H), 7.99 (d,  $J$  = 7.6Hz, 2H); HRMS (ESI) calcd for  $\text{C}_{22}\text{H}_{21}\text{N}_3\text{NaO}_7\text{S}$   $[\text{M}+\text{Na}]^+$ : 494.0998, found: 494.0999;  $R_{\text{T,HPLC}}$  = 4.017 min, Purity > 96%, MeOH:H<sub>2</sub>O = 75:25, 30 °C.

4.2.26. 2-((2-amino-2-oxoethyl)amino)-*N*-(2-methoxyphenyl)-6-(4-nitrophenylthio)benzamide (**12j**)

White solid; m. p. 204.4–205.4 °C; 86.1% yield;  $^1\text{H NMR}$  (400 MHz,  $\text{DMSO}-d_6$ )  $\delta$  = 3.78 (s, 3H), 5.34 (brs, 2H), 5.85 (s, 2H), 6.46 (m, 2H), 6.67 (t,  $J$  = 7.2Hz, 2H), 6.76 (t,  $J$  = 7.2Hz, 2H), 6.99 (d,  $J$  = 8.0Hz, 2H), 7.16 (m, 3H), 7.43 (d,  $J$  = 7.2Hz, 1H), 7.55 (s, 1H); HRMS (ESI) calcd for  $\text{C}_{22}\text{H}_{21}\text{N}_4\text{O}_5\text{S}$   $[\text{M}+\text{H}]^+$ : 453.1233, found: 453.1234;  $R_{\text{T,HPLC}}$  = 3.697 min, Purity > 97%, MeOH:H<sub>2</sub>O = 75:25, 30 °C.

4.2.27. 2-((2-bromoethyl)amino)-*N*-(2-methoxyphenyl)-6-(4-nitrophenylthio)benzamide (**12k**)

Yellow solid; 59.5% yield; m. p. 111.3–113.0 °C;  $^1\text{H NMR}$  (400 MHz,  $\text{CDCl}_3$ )  $\delta$  = 3.3 (m, 2H), 3.57 (t,  $J$  = 6Hz, 2H), 3.81 (s, 3H), 4.14 (brs, 1H), 6.47 (d,  $J$  = 8Hz, 1H), 6.58 (d,  $J$  = 6.4Hz, 1H), 7.00 (m, 3H), 7.22 (m, 1H), 7.37 (m, 3H), 7.56 (m, 1H), 8.03 (m, 1H), 8.23 (s, 1H); HRMS (ESI) calcd for  $\text{C}_{22}\text{H}_{21}\text{BrN}_3\text{O}_4\text{S}$   $[\text{M}+\text{H}]^+$ : 502.0436, found: 502.0438;  $R_{\text{T,HPLC}}$  = 5.560 min, Purity > 97%, MeOH:H<sub>2</sub>O = 80:20, 30 °C.

4.2.28. *N*-(2-methoxyphenyl)-2-((4-nitrophenylthio)-6-(piperazin-1-yl)benzamide (**12l**)

**12** (395 mg, 1 mmol) was dissolved in DMF (40 mL) at room temperature. To this mixture was added bis(2-bromoethyl)amine (231 mg, 1 mmol), followed by the addition of NaOH (0.08

g, 2 mmol). After being stirred for 2 hours at room temperature, the reaction mixture was poured into ice-cold water (200 mL) to get crude product. The crude solid was filtered and washed several times with water and purified by silica gel column chromatography (1:3 v/v ethyl acetate/petroleum ether) to provide a yellow solid (380.9 mg, 82% yield). m. p. 297.3–299.6 °C; <sup>1</sup>H NMR (400 MHz, DMSO-*d*<sub>6</sub>) δ = 3.36 (m, 5H), 3.56 (m, 3H), 3.82 (s, 3H), 6.46 (d, *J* = 8.0Hz, 1H), 6.58 (m, 1H), 6.99 (m, 2H), 7.22 (m, 1H), 7.37 (m, 3H), 7.57 (m, 1H), 8.04 (m, 2H), 8.25 (s, 1H); HRMS (ESI) calcd for C<sub>24</sub>H<sub>25</sub>N<sub>4</sub>O<sub>4</sub>S [M+H]<sup>+</sup>: 465.1597, found: 465.1590; R<sub>T,HPLC</sub> = 5.553 min, Purity > 97%, MeOH:H<sub>2</sub>O = 80:20, 30 °C. The same procedure was also followed for the syntheses of **12m**.

#### 4.2.29. Synthesis of *N*-(2-methoxyphenyl)-2-morpholino-6-((4-nitrophenyl)thio)benzamide (**12m**)

Yellow solid; 67% yield; m. p. 292.0–292.9 °C; <sup>1</sup>H NMR (400 MHz, CDCl<sub>3</sub>) δ = 2.95 (m, 1H), 3.16 (m, 4H), 3.56 (t, *J* = 12.4Hz, 1H), 3.71 (m, 4H), 3.85 (m, 1H), 6.80 (s, 1H), 6.97 (d, *J* = 8.4Hz, 1H), 7.08 (d, *J* = 9.2Hz, 2H), 7.34(t, *J* = 6.8Hz, 1H), 7.43 (m, 3H), 7.55 (d, *J* = 6.4Hz, 1H), 8.18 (d, *J* = 8.8Hz, 2H); HRMS (ESI) calcd for C<sub>24</sub>H<sub>24</sub>N<sub>3</sub>O<sub>5</sub>S [M+H]<sup>+</sup>: 466.1437, found: 466.1440; R<sub>T,HPLC</sub> = 6.247 min, Purity > 99%, MeOH:H<sub>2</sub>O = 75:25, 30 °C.

#### 4.2.30. *N*-(2-methoxyphenyl)-2-((4-nitrophenyl)thio)-6-(phenylsulfonamido)benzamide (**12n**)

**12** (395 mg, 1 mmol) was dissolved in azabenzene (40 mL) at room temperature. To this mixture was added benzenesulfonyl chloride (0.211 g, 1.2 mmol). After being stirred for 10 hours at room temperature, the reaction mixture was concentrated under reduced pressure. The crude residue was diluted ethyl acetate (50 mL), washed with water (3 × 20 mL), dried over anhydrous Na<sub>2</sub>SO<sub>4</sub>, filtered, and concentrated under reduced pressure. The residue was purified by silica gel column chromatography (1:4 v/v ethyl acetate/petroleum ether) to provide a white

solid (358.9 mg, 67% yield). m. p. 153.1–155.7 °C;  $^1\text{H NMR}$  (400 MHz,  $\text{CDCl}_3$ )  $\delta$  = 3.65 (s, 3H), 6.74 (d,  $J$  = 8.0Hz, 1H), 6.85 (t,  $J$  = 7.6Hz, 1H), 6.91 (d,  $J$  = 8.0Hz, 1H), 7.02 (t,  $J$  = 7.6Hz, 1H), 7.28 (m, 1H), 7.37 (t,  $J$  = 8.0Hz, 1H), 7.47 (t,  $J$  = 7.6Hz, 3H), 7.64 (m, 3H), 8.01 (m, 5H), 8.93 (s, 1H); HRMS (ESI) calcd for  $\text{C}_{26}\text{H}_{21}\text{N}_3\text{NaO}_6\text{S}_2$   $[\text{M}+\text{Na}]^+$ : 558.0769, found: 558.0772;  $R_{\text{T,HPLC}}$  = 13.533 min, Purity > 97%, MeOH:H<sub>2</sub>O = 80:20, 30 °C. The same procedure was also followed for the syntheses of **12p**.

4.2.31. *N*-(2-methoxyphenyl)-2-((4-nitrophenyl)sulfonyl)-6-(phenylsulfonamido)benzamide (**12o**)

White solid; 62% yield; m. p. 179.6–181.5 °C;  $^1\text{H NMR}$  (400 MHz,  $\text{CDCl}_3$ )  $\delta$  = 3.69 (s, 3H), 6.77 (d,  $J$  = 7.2Hz, 1H), 6.95 (m, 2H), 7.09 (t,  $J$  = 8.0Hz, 1H), 7.44 (t,  $J$  = 8.0Hz, 2H), 7.49 (t,  $J$  = 7.2Hz, 1H), 7.61 (t,  $J$  = 7.2Hz, 2H), 7.95 (d,  $J$  = 7.2Hz, 3H), 8.10 (d,  $J$  = 9.2Hz, 1H), 8.27 (d,  $J$  = 7.2Hz, 2H), 8.32 (d,  $J$  = 7.2Hz, 2H), 9.18 (s, 1H); HRMS (ESI) calcd for  $\text{C}_{26}\text{H}_{21}\text{N}_3\text{NaO}_8\text{S}_2$   $[\text{M}+\text{Na}]^+$ : 590.0668, found: 590.0677;  $R_{\text{T,HPLC}}$  = 9.433 min, Purity > 99%, MeOH:H<sub>2</sub>O = 80:20, 30 °C.

4.2.32. *N*-(2-methoxyphenyl)-2-(4-methylphenylsulfonamido)-6-((4-nitrophenyl)thio)benzamide (**12p**)

White solid; m. p. 220.6–223.8 °C; 83.8% yield;  $^1\text{H NMR}$  (400 MHz,  $\text{CDCl}_3$ )  $\delta$  = 2.17 (s, 3H), 3.69 (s, 3H), 6.8 (d,  $J$  = 8Hz, 1H), 6.95 (d,  $J$  = 8.8Hz, 3H), 7.09 (m, 3H), 7.38 (d,  $J$  = 8.0Hz, 1H), 7.47 (t,  $J$  = 8.0Hz, 1H), 7.54 (d,  $J$  = 8.0Hz, 2H), 7.81 (d,  $J$  = 8.0Hz, 1H), 7.95 (s, 1H), 8.01 (d,  $J$  = 8.8Hz, 2H), 8.16 (d,  $J$  = 8.0Hz, 1H), 8.42 (s, 1H); HRMS (ESI) calcd for  $\text{C}_{27}\text{H}_{23}\text{N}_3\text{NaO}_6\text{S}_2$   $[\text{M}+\text{Na}]^+$ : 572.0926, found: 572.0921;  $R_{\text{T,HPLC}}$  = 7.887 min, Purity > 96%, MeOH:H<sub>2</sub>O = 80:20, 30 °C.

4.2.33. *N*-(2-methoxyphenyl)-2-(4-methylphenylsulfonamido)-6-((4-nitrophenyl)sulfonyl)benzamide (**12q**)

White solid; 55% yield;  $^1\text{H}$  NMR (400 MHz,  $\text{CDCl}_3$ )  $\delta$  = 2.05 (s, 3H), 3.64 (s, 3H), 6.77 (d,  $J$  = 8.0Hz, 1H), 6.95 (m, 2H), 7.09 (t,  $J$  = 7.2Hz, 1H), 7.19 (d,  $J$  = 8.0Hz, 1H), 7.42 (t,  $J$  = 7.2Hz, 2H), 7.61 (t,  $J$  = 7.2Hz, 1H), 7.81 (d,  $J$  = 7.6Hz, 1H), 7.95 (d,  $J$  = 7.6Hz, 2H), 8.10 (d,  $J$  = 8.0Hz, 1H), 8.26 (d,  $J$  = 8.4Hz, 2H), 8.33 (d,  $J$  = 8.4Hz, 2H), 9.18 (s, 1H); HRMS (ESI) calcd for  $\text{C}_{27}\text{H}_{23}\text{N}_3\text{NaO}_8\text{S}_2$   $[\text{M}+\text{Na}]^+$ : 604.0824, found: 604.0821;  $R_{\text{T,HPLC}}$  = 9.417 min, Purity > 99%, MeOH:H<sub>2</sub>O = 80:20, 30 °C.

4.3.51. 2-(2-aminoacetamido)-*N*-(2-methoxyphenyl)-6-((4-nitrophenyl)sulfonyl)benzamideHydrochloride (**13a**)

Boc-Gly (350 mg, 2 mmol), DCC (384 mg, 2 mmol) and HOBt (270 mg, 2 mmol) were mixed in dichloromethane (30 mL) with a magnetic stirrer for 5 min at RT, and to this mixture was slowly added a solution of **12c** (427 mg, 1 mmol) in dichloromethane (30 mL). After stirred for 12H at RT, the reaction mixture was filtered and the liquid layer was washed with water (3 × 15 mL), dried over anhydrous sodium sulfate, concentrated under reduced pressure. The oily residue was dissolved in DCM (20 mL) at RT, and into this mixture was added trifluoroacetic acid (7 mL) with a magnetic stirrer for 2H at RT. Then the mixture was filtered and the residue was washed sequentially with ethanol (2 × 10 mL) and dichloromethane (15 × 5 mL) to afford **13a** as a pale yellow amorphous solid (224 mg, 43% yield). m. p. 226.5–229.0 °C;  $^1\text{H}$  NMR (400 MHz,  $\text{DMSO}-d_6$ )  $\delta$  = 3.73 (s, 2H), 3.82 (s, 3H), 7.02 (t,  $J$  = 6.8Hz, 1H), 7.09 (d,  $J$  = 7.6Hz, 1H), 7.19 (t,  $J$  = 7.2Hz, 1H), 7.77 (t,  $J$  = 6.8Hz, 1H), 8.01 (t,  $J$  = 7.6Hz, 2H), 8.08 (d,  $J$  = 7.6Hz, 1H), 8.23 (d,  $J$  = 8.4Hz, 2H), 8.39 (m, 4H), 9.89 (s, 1H), 10.00 (br, 2H);  $^{13}\text{C}$  NMR (100 MHz,  $\text{DMSO}-d_6$ )  $\delta$  =

55.8, 111.5, 120.2, 123.5, 124.5, 125.5, 126.7, 127.2, 129.4, 130.1, 131.7, 131.8, 135.0, 137.0, 146.5, 150.2, 150.8, 162.3, 166.0; HRMS (ESI) calcd for  $C_{22}H_{21}N_4O_7S$   $[M+H]^+$ : 485.1131, found: 485.1132;  $R_{T,HPLC}$  = 10.700 min, Purity > 98%, MeOH:H<sub>2</sub>O = 60:40, 30 °C. The same procedure was also followed for the syntheses of **13b**.

#### 4.3.52. 2-(2-amino-3-phenylpropanamido)-N-(2-methoxyphenyl)-6-((4-nitrophenyl)sulfonyl)benzamide (**13b**)

Yellow solid; 43% yield; m. p. 286.2–288.5 °C; <sup>1</sup>H NMR (400 MHz, DMSO-*d*<sub>6</sub>)  $\delta$  = 2.88 (m, 1H), 3.14 (d, *J* = 16.0Hz, 1H), 3.44 (d, *J* = 8.0Hz, 1H), 3.69 (s, 3H), 4.34 (brs, 2H), 6.99 (m, 2H), 7.12 (t, *J* = 8.0Hz, 1H), 7.23 (d, *J* = 8.0Hz, 4H), 7.77 (t, *J* = 8.0Hz, 1H), 7.94 (d, *J* = 4.0Hz, 1H), 8.10 (d, *J* = 8.0Hz, 1H), 8.31 (m, 7H), 9.88 (s, 1H); HRMS (ESI) calcd for  $C_{29}H_{27}N_4O_7S$   $[M+H]^+$ : 575.1600, found: 575.1601;  $R_{T,HPLC}$  = 7.130 min, Purity > 96%, MeOH:H<sub>2</sub>O = 75:25, 30 °C.

### 4.3. Computational chemistry

#### 4.3.1 Lowest conformation searching

By using generate conformation protocol with systematic search method of Discovery Studio 3.1, conformations of **12**, **12a**, **12b**, and **12c** were obtained. Then, the lowest conformation was subjected to *ab initio* optimization at B3LYP/6-311G (d, p) level by Gaussian03.

#### 4.3.2. Molecular Docking

HIV-1 Vif was chosen as the target receptor, and the 3D structure of the receptor was gained from Protein Data Bank (PDB ID 4N9F). The ligand (**1**, **12a**, **12c**) prepared for docking was

described in our previous work [51]. Docking studies were performed with the AutoDock (4.2) suite of programs. Binding sites were defined from receptor cavities by using “define and edit binding site” method of Discovery Studio 3.1, and the binding site ( $X = 72.881$ ,  $Y = -69.580$ ,  $Z = -181.951$ ) was selected for docking studies. The 3D affinity map was a cube with  $60 \text{ \AA} \times 60 \text{ \AA} \times 60 \text{ \AA}$  grid points separated by  $0.375 \text{ \AA}$ . The docking parameters were identical to our previous work [51].

#### 4.4. Bioactivity evaluation methods

##### 4.4.1 Cells, virus and plasmids

T cell lines were maintained in RPMI medium 1640 (Gibco) containing 10% fetal bovine serum (FBS, Gibco), 100 units/mL penicillin and 100 units/mL streptomycin. 293T and TREX-hvif-15 cell lines were maintained with Dulbecco’s modified Eagle medium (DMEM, Gibco) containing 10% FBS. Peripheral Blood Mononuclear Cells (PBMCs) (Ethical Approval Number: SWYX-2012020) were isolated from healthy donors’ peripheral blood [52]. PBMCs were stimulated by  $5 \mu\text{g/mL}$  phytohemagglutinin (PHA, Sigma) for 72 h and cultured in RPMI-1640 containing 10% FBS and  $0.05 \text{ unit/mL}$  IL-2. HIV-1<sub>IIB</sub>, and pNL4-3<sub>gp41 (36G) V38A, N42T</sub> were propagated in H9 cells.  $\Delta\text{Vif}$  HIV-1 produced by transfecting plasmid pNL $\Delta\text{Vif}$  to 293T and NL4-3 produced by transfecting plasmid pNL4-3 was propagated in H9 cells, respectively. Clinical isolated strains, HIV-1<sub>KM018</sub>, HIV-1<sub>TC-1</sub>, and HIV-1<sub>WAN</sub> were isolated from local AIDS patients (Ethical Approval Number: SWYX-2006011) and propagated by co-culture with healthy PBMCs. All virus stocks were stored in small aliquots at  $-70 \text{ }^\circ\text{C}$ .

##### 4.4.2. Cytotoxicity assays

The cytotoxicity of the compounds on H9 and PBMCs were determined by MTT colorimetric assay described previously [53].  $4 \times 10^4$  cells/well H9 or  $5 \times 10^5$  cells/well PBMCs were co-incubated with serial diluted compounds in 96-well plate at 37 °C, 5% CO<sub>2</sub>. After incubating for three days (PBMCs and H9 for seven days), the cell viability was determined by using MTT, and the 50% cytotoxicity concentration (CC<sub>50</sub>) was calculated [54].

#### 4.4.3 Antiviral assays

The antiviral activities of the compounds were determined by the HIV-1 p24 assay. H9 cells were infected with NL4-3 at a multiplicity of infection (MOI) of 0.03 for 2 h, then washed three times to remove free virus and resuspended with RPMI-1640. Serial diluted compounds and  $4 \times 10^4$  cells/well infected cells were added into 96-well cell culture plates and incubated for 7 days. The p24 level of the culture supernatant was measured by in-house ELISA assay [55]. The antiviral activities in clinical isolated strains were determined in PBMCs. PHA-stimulated PBMCs were infected with HIV-1<sub>SF162</sub>, HIV-1<sub>KM018</sub>, HIV-1<sub>TC-1</sub> or HIV-1<sub>WAN</sub> for 2 h and then free viruses were washed away.  $5 \times 10^5$  cells/well infected PBMCs and serial diluted compounds were added into 96-well plate and incubated at 37 °C, 5% CO<sub>2</sub> for 7 days. The p24 level was determined by in-house ELISA assay [55]. The 50% effective concentrations (EC<sub>50</sub>) were calculated.

#### 4.4.4. Fluorescence-based primary screening assays

The expression of Vif in TREX-hvif-15 cell line was regulated by a Tet-On system.  $2 \times 10^5$  cells/well TREX-hvif-15 cells were plated in 24-well cell culture plate and incubated overnight. EYFP-N1-hA3G was transfected into TREX-hvif-15 when the cell confluence was about 80% by using Lipofectamine 2000. 6 hours later, the supernatant was removed and cells were washed

with DMEM. Compounds with different concentration were added into the wells and 0.1 µg/mL doxycycline (Dox, Clontech, USA) was added to induce Vif expression [56] and Vif inhibitor 1 was used as a control. Cells were harvested by trypsin treatment 48 h post-transfection. Enhanced yellow fluorescent protein (EYFP) positive cells were analysed with BD Influx flow cytometer.

#### 4.4.5. Western blot assays

Cells were collected, lysed with cell lysis buffer for western (Beyotime, China), and the total protein was collected. The information of the antibodies was as follow: anti-APOBEC3GP antibody (sc-130689, Santa Cruz Biotechnology, Inc, USA); anti-HIV-1 Vif antibody [319] (ab66643, Abcam, UK); anti-HA antibody [HA-7] (H3663, Sigma Aldrich, USA); anti-β-actin antibody (cw0096a, CWBIO, China); anti-p24 antibody was homemade [55]. The target proteins were separated by SDS polyacrylamide gel electrophoresis and transferred to polyvinylidene difluoride (PVDF) membranes. The PVDF membranes with proteins were incubated overnight with primary antibodies at 4 °C. Membranes were probed with horseradish peroxidase (HRP)-conjugated secondary antibodies at room temperature for 1-2 h. The membranes were washed thoroughly, stained with Chemiluminescent HRP Substrate (Millipore, USA), and exposed to X-ray film.

#### 4.4.6. The infection assay and transfection assay for protein analyse

Proteins in 293T cells, TREX-hvif-15 cells and PBMCs were analysed using western blot mentioned above.  $2 \times 10^5$  cells/well 293T were plated in 24-well cell culture plate and incubated overnight. The cells were co-transfected with pcDNA3.1-APOBEC3G-HA and pNL4-3 using Lipofectamine 2000 when the cell confluence was about 80%. The supernatant was removed,

and cells were washed with DMEM once 6 h post-transfection. Then the fresh DMEM (with 10% FBS) was added into the wells. Compounds with different concentrations were added into the wells and incubated for 48 h, and the HA tag, Vif, p24 and  $\beta$ -actin (internal control) was analysed.

In TREX-hvif-15 cells,  $2 \times 10^5$  cells/well were plated in 24-well cell culture plate and incubated overnight. The pcDNA3.1-APOBEC3G-HA was transfected using Lipofectamine 2000 when the cell confluence was about 80%. After 6 h post-transfection, the supernatant was removed and cells were washed once with DMEM. Then the fresh DMEM (with 10% FBS) was added to the wells. Compounds with different concentration were added into the wells and 0.1  $\mu\text{g}/\text{mL}$  doxycycline (Clontech, USA) was used to induce Vif expression. The HA tag, Vif and  $\beta$ -actin was measured.

In PBMCs,  $5 \times 10^6$  cells/well PHA-stimulated PBMC were infected with HIV-1<sub>TC-1</sub> or  $\Delta$ Vif NL4-3 (MOI = 0.5). 4 h post-infection, cells were washed twice with PBS, resuspended with fresh RPMI (with or without serial diluted compounds) and incubated. After 7 days incubating, cells were collected, lysed, and total cell protein was collected. The expression of A3G, Vif, p24, and  $\beta$ -actin in the cell was determined with western blot assay.

#### 4.5. Solubility studies

##### 4.5.1. Partition coefficient determination of **12c**

In order to achieve a saturation state, high purity analytical grade n-octanol 1 L was shaken with ultra-pure water 500 mL for 24 h on a mechanical shaker at 120 rpm and 37 °C, then separated to obtain aqueous phase (water pre-saturated with n-octanol) and octanol phase (n-

octanol pre-saturated with water). The partition coefficient (Log P of **12c** was determined by the shake flask method.

The shake flask method is considered a gold standard for Log P determination. An excess amount of **12c** was added to octanol phase followed by sonication to dissolve the drug. Solution was centrifuged for 3 min at 12,000 rpm and the supernatant was collected for further study. The effects of different shaking time were investigated, firstly. Experiment was carried out in triplicate through the volume ratio of 1:1 (octanol/aqueous phase, v/v) and three different shaking time of 2, 4 and 7 h, respectively. In order to obtain uniform dispersion of two phases, all samples were kept in 10 mL test tubes and shaken by a Water-bathing Constant Temperature Vibrator (SH2-A, Shanghai) at 120 rpm and 37 °C. Then, the test samples in each phase were separated for 5 min at 12,000 rpm and quantitated by HPLC.

The effects of different volume ratios of octanol/aqueous phase were also studied through ratio of 1:1, 1:4 and 1:9, respectively. The experiment was carried out according to the method above, and the partition coefficients were calculated by the following equation:

$$\text{Log P} = \text{Lg} (C_o/C_w)$$

where  $C_o$  is the concentration of drug in the octanol phase and  $C_w$  is the concentration of drug in the aqueous phase.

#### 4.5.2. Solubility determination of **12c**

The solubility of **12c** was measured by equilibrium method (shake-flask technique). In this experiment, an excess amount of **12c** was added to series of solvent, including water, methanol, ethanol, acetonitrile, ethyl acetate and acetone, respectively. The resulting suspensions were

shaken for 24-72 h at controlled temperature (25 °C), and undissolved material was separated by filtration with a 0.22 µm dialysis membrane. The compound dissolved in the supernatant was diluted accordingly and measured using HPLC (flow rate: 1 mL/min; mobile phase: methanol/water, 70/30, v/v; C<sub>18</sub> column: 250 × 4.6 mm, 5 µm; UV wavelength: 251 nm).

#### 4.5.3. Degradation studies of **13a**

The buffer solution at different pH were prepared according to manufacturer's protocols (i.e., the different pH powers were dissolved in 900 mL deionized water at room temperature, stirred and then added deionized water to make the total volume was 1 L). **13a** was added to different buffer solutions (pH 4, pH 7 and pH 9) to make the final concentration 100 µM. Samples were shaken by a Water-bathing Constant Temperature Vibrator (SH2-A, Shanghai) at 100 rpm and 37 °C. Samples were withdraw and analyzed by HPLC system (Dionex Ultimate 3000, USA; flow rate: 0.5 mL/min; mobile phase: acetonitrile/water with 0.1% triethylamine, 70/30, v/v; C<sub>18</sub> column: 4.6 × 250 mm, 5 µm; UV wavelength: 248 nm; sample injection volume: 10 µL, Acclaim 120, USA) at the appropriate time interval (pH 4 and pH 7: 0, 4, 8, 24, 32, 48, 72, 96, 120, 144 and 168 h; pH 9: 0, 0.5, 1, 2, 3, 4, 5, 6, 8, 10, 12, 14 and 15 h).

#### 4.5.4. Plasma protein binding of **12c**

Arterial blood samples were taken from Sprague-Dawley rats (male and female, respectively) and separate to obtain male and female plasma, respectively. Arterial blood was collected by heparin-treated syringes and centrifuged at 6000 rpm for 5 min at room temperature to separate plasma. Stock solution of **12c** (800 µg/mL) and appropriate PBS (pH 7.4) solutions were mixed and vortexed for several minutes. Then, the samples were centrifuged at 13000 rpm for 3 min and the supernatants were collected and diluted to different concentrations. The fresh rat plasma

(400  $\mu\text{L}$ ) was added to supernatants above (100  $\mu\text{L}$ ) and incubated at 37  $^{\circ}\text{C}$  for 2 h. The final concentrations of **12c** were 30, 20 and 5  $\mu\text{g}/\text{mL}$ , respectively. Furthermore, drug-plasma solutions were transferred to ultracentrifuge tubes (30 KD, Merck Millipore Corporation, Billerica, MA) and centrifuged with a refrigerated centrifuge apparatus (2000 g, 4  $^{\circ}\text{C}$ , 15 min). The filtrates were collected for HPLC analysis (flow rate: 1 mL/min; mobile phase: methanol/water, 70/30, v/v;  $\text{C}_{18}$  column: 4.6  $\times$ 250 mm column, Acclaim 120, USA; UV wavelength: 251 nm) and the plasma protein binding rate was calculated by the following equation:

$$r (\%) = (D_t - D_f) / D_t \times 100 \%$$

where  $r$  is the plasma protein binding rate,  $D_t$  is the total drug concentration in the plasma and  $D_f$  is defined as the free drug concentration of samples.

#### 4.5.5. HLM metabolism studies of **13a**

The prodrug **13a** (1.5 mg/mL) 1.5  $\mu\text{L}$  was incubated with human liver microsome (HLM, purchased from Wuhan PrimeTox Bio-medical Technology Co., LTD, China) in 0.1 M phosphate buffer (pH 7.4) containing 36  $\mu\text{L}$  NADPH generating system at 37  $^{\circ}\text{C}$  for 0, 5, 10, 15, 20, 40 min, respectively. The total incubation volume was 150  $\mu\text{L}$ . The incubation was terminated by the addition of 400  $\mu\text{L}$  methanol followed with vortex for 3 min. Samples were centrifuged for 10 min at 12000 rpm. Supernatants were collected, evaporated to dryness under nitrogen, and the residues were dissolved in the mobile phase prior to analysis using high-performance liquid chromatography (HPLC) and high-performance liquid chromatography-mass spectrometer (HPLC-MS). HPLC was performed as follows: flow rate, 1 mL/min; mobile phase, methanol/water = 60/40, v/v;  $\text{C}_{18}$  column, 4.6  $\times$ 250 mm column, Acclaim 120, USA; UV

wavelength, 251 nm. The LC-MS system consisted of a high performance liquid chromatography system (Dionex Ultimate 3000, USA) and an electrospray ionization mass spectrometer (Bruker amaZon SL, Germany). Samples were introduced via an autosampler and reversed-phase chromatography was carried out with a C<sub>18</sub> column (5 μm, 4.6 ×250 mm, Acclaim 120, Dionex). Mobile phase A: methanol, phase B: water. Chromatography was performed at 0.3 mL/min and starting at 60% A. The eluent from HPLC system was connected directly to the ESI interface of the ion trap mass spectrometer. The mass spectrometer was operated in positive mode for analysis and the mass range of 70-800 *m/z* was scanned. The desolvation gas was nitrogen and its temperature was kept at 250 °C. The data was processed by Compass Data Analysis 4.0 software.

Ethics statement: The methods were performed in accordance with all relevant guidelines and regulations. The study and all the animal experiments were approved by the Animal Care and Use Committee of Sichuan University (Chengdu, Sichuan, China). Informed consent was obtained from all subjects before participation in the study. All experimental procedures involving cells, virus and plasmids were approved by the internal review board of Kunming Institute of Zoology, Chinese Academy of Sciences (approval ID: SWYX-2012020).

### **Acknowledgments**

Vif stably expressed cell line TREX-hvif-15 and APOBEC3G expressed plasmid EYFP-N1-hA3G were kindly donated by Prof. Guangxia Gao (Institute of Biophysics, Chinese Academy of Sciences). Plasmid pNLΔVif was kindly provided by Prof. Yonghui Zheng (Michigan State University) and Tariq M Rana (Sanford-Burnham Medical Research Institute). We would like to

thank NIH AIDS Reagent Program for pcDNA3.1-APOBEC3G-HA, pNL4-3 and HIV-1 strains. We also thank Medical Research Council, AIDS Reagent Project for human T cell lines H9. This study was support by the National Key Program of China during the 12th Five-Year Plan Period (Grant 2012ZX09103101-022, 2012ZX10001-006), the National Natural Science Foundation of China (81102483, 81472780), and the Innovation Team of Natural Science Foundation of Department of Education of Guizhou Province (No. QJHRCTDZ [2015] 57). We thank LetPub ([www.letpub.com](http://www.letpub.com)) for its linguistic assistance during the preparation of this manuscript.

## REFERENCES

- [1] K.M. Rose, M. Marin, S.L. Kozak, D. Kabat, Regulated production and anti-HIV type 1 activities of cytidine deaminases APOBEC3B, 3F, and 3G, *AIDS Res Hum. Retroviruses* 21 (2005) 611-619.
- [2] A.M. Sheehy, N.C. Gaddis, J.D. Choi, M.H. Malim, Isolation of a human gene that inhibits HIV-1 infection and is suppressed by the viral Vif protein, *Nature* 418 (2002) 646-650.
- [3] K. Strelbel, M.A. Khan, APOBEC3G encapsidation into HIV-1 virions: which RNA is it?, *Retrovirology* 5 (2008) 55.
- [4] H. Xu, E. Chertova, J. Chen, D.E. Ott, J.D. Roser, W.S. Hu, V.K. Pathak, Stoichiometry of the antiviral protein APOBEC3G in HIV-1 virions, *Virology* 360 (2007) 247-256.
- [5] A. Burnett, P. Spearman, APOBEC3G multimers are recruited to the plasma membrane for packaging into human immunodeficiency virus type 1 virus-like particles in an RNA-dependent process requiring the NC basic linker, *J. Virol.* 81 (2007) 5000-5013.
- [6] V.B. Soros, W. Yonemoto, W.C. Greene, Newly synthesized APOBEC3G is incorporated into HIV virions, inhibited by HIV RNA, and subsequently activated by RNase H, *PLoS Pathog.* 3 (2007) e15.
- [7] K.N. Bishop, R.K. Holmes, A.M. Sheehy, N.O. Davidson, S.J. Cho, M.H. Malim, Cytidine deamination of retroviral DNA by diverse APOBEC proteins, *Curr. Biol.* 14 (2004) 1392-1396.
- [8] R.S. Harris, K.N. Bishop, A.M. Sheehy, H.M. Craig, S.K. Petersen-Mahrt, I.N. Watt, M.S. Neuberger, M.H. Malim, DNA deamination mediates innate immunity to retroviral infection, *Cell* 113 (2003) 803-809.
- [9] D. Lecossier, F. Bouchonnet, F. Clavel, A.J. Hance, Hypermutation of HIV-1 DNA in the absence of the Vif protein, *Science* 300 (2003) 1112.
- [10] B. Mangeat, P. Turelli, G. Caron, M. Friedli, L. Perrin, D. Trono, Broad antiretroviral defence by human APOBEC3G through lethal editing of nascent reverse transcripts, *Nature* 424 (2003) 99-103.
- [11] X.Y. Li, F. Guo, L. Zhang, L. Kleiman, S. Cen, APOBEC3G inhibits DNA strand transfer during HIV-1 reverse transcription, *J. Biol. Chem.* 282 (2007) 32065-32074.
- [12] K.N. Bishop, M. Verma, E.Y. Kim, S.M. Wolinsky, M.H. Malim, APOBEC3G inhibits elongation of HIV-1 reverse transcripts, *PLoS Pathog.* 4 (2008) e1000231.
- [13] K. Luo, Z. Xiao, E. Ehrlich, Y. Yu, B. Liu, S. Zheng, X.F. Yu, Primate lentiviral virion infectivity factors are substrate receptors that assemble with cullin 5-E3 ligase through a HCCH motif to suppress APOBEC3G, *Proc. Natl. Acad. Sci. U. S. A.* 102 (2005) 11444-11449.
- [14] A. Mehle, J. Goncalves, M. Santa-Marta, M. McPike, D. Gabuzda, Phosphorylation of a novel SOCS-box regulates assembly of the HIV-1 Vif-Cul5 complex that promotes APOBEC3G degradation, *Genes Dev.* 18 (2004) 2861-2866.
- [15] X. Yu, Y. Yu, B. Liu, K. Luo, W. Kong, P. Mao, X.F. Yu, Induction of APOBEC3G ubiquitination and degradation by an HIV-1 Vif-Cul5-SCF complex, *Science* 302 (2003) 1056-1060.
- [16] W. Zhang, J. Du, S.L. Evans, Y. Yu, X.F. Yu, T-cell differentiation factor CBF-beta regulates HIV-1 Vif-mediated evasion of host restriction, *Nature* 481 (2012) 376-379.
- [17] S. Jager, D.Y. Kim, J.F. Hultquist, K. Shindo, R.S. LaRue, E. Kwon, M. Li, B.D. Anderson, L. Yen, D. Stanley, C. Mahon, J. Kane, K. Franks-Skiba, P. Cimermancic, A. Burlingame,

- A. Sali, C.S. Craik, R.S. Harris, J.D. Gross, N.J. Krogan, Vif hijacks CBF-beta to degrade APOBEC3G and promote HIV-1 infection, *Nature* 481 (2012) 371-375.
- [18] J.F. Hultquist, M. Binka, R.S. LaRue, V. Simon, R.S. Harris, Vif proteins of human and simian immunodeficiency viruses require cellular CBFbeta to degrade APOBEC3 restriction factors, *J. Virol.* 86 (2012) 2874-2877.
- [19] J. Batisse, S. Guerrero, S. Bernacchi, D. Sleiman, C. Gabus, J.L. Darlix, R. Marquet, C. Tisne, J.C. Paillart, The role of Vif oligomerization and RNA chaperone activity in HIV-1 replication, *Virus Res.* 169 (2012) 361-376.
- [20] T. Pan, X. He, B. Chen, H. Chen, G. Geng, H. Luo, H. Zhang, C. Bai, Development of benzimidazole derivatives to inhibit HIV-1 replication through protecting APOBEC3G protein, *Eur. J. Med. Chem.* 95 (2015) 500-513.
- [21] R. Nathans, H. Cao, N. Sharova, A. Ali, M. Sharkey, R. Stranska, M. Stevenson, T.M. Rana, Small-molecule inhibition of HIV-1 Vif, *Nat. Biotechnol.* 26 (2008) 1187-1192.
- [22] A. Ali, J. Wang, R.S. Nathans, H. Cao, N. Sharova, M. Stevenson, T.M. Rana, Synthesis and structure-activity relationship studies of HIV-1 virion infectivity factor (Vif) inhibitors that block viral replication, *ChemMedChem* 7 (2012) 1217-1229.
- [23] I. Mohammed, M.K. Parai, X. Jiang, N. Sharova, G. Singh, M. Stevenson, T.M. Rana, SAR and Lead Optimization of an HIV-1 Vif-APOBEC3G Axis Inhibitor, *ACS Med. Chem. Lett.* 3 (2012) 465-469.
- [24] I. Mohammed, I.R. Kummetha, G. Singh, N. Sharova, G. Lichinchi, J. Dang, M. Stevenson, T.M. Rana, 1,2,3-Triazoles as Amide Bioisosteres: Discovery of a New Class of Potent HIV-1 Vif Antagonists, *J. Med. Chem.* 59 (2016) 7677-7682.
- [25] P. Metrangolo, F. Meyer, T. Pilati, G. Resnati, G. Terraneo, Halogen bonding in supramolecular chemistry, *Angew. Chem. Int. Ed. Engl.* 47 (2008) 6114-6127.
- [26] Y. Lu, Y. Wang, W. Zhu, Nonbonding interactions of organic halogens in biological systems: implications for drug discovery and biomolecular design, *Phys. Chem. Chem. Phys.* 12 (2010) 4543-4551.
- [27] B.R. Beno, K.S. Yeung, M.D. Barberger, L.D. Pennington, N.A. Meanwell, A Survey of the Role of Noncovalent Sulfur Interactions in Drug Design, *J. Med. Chem.* 58 (2015) 4383-4438.
- [28] M.D. Segall, M.C. Payne, R.N. Boyesy, An ab initio study of the conformational energy map of acetylcholine, *Mol. Phys.* 93 (1998) 365-370.
- [29] N. Kamiya, Y. Yonezawa, H. Nakamura, J. Higo, Protein-inhibitor flexible docking by a multicanonical sampling: native complex structure with the lowest free energy and a free-energy barrier distinguishing the native complex from the others, *Proteins* 70 (2008) 41-53.
- [30] D. Sanfelice, P.A. Temussi, The conformation of enkephalin bound to its receptor: an "elusive goal" becoming reality, *Front. Mol. Biosci.* 1 (2014) 14.
- [31] J.G. Briard, M. Fernandez, P. De Luna, T.K. Woo, R.N. Ben, QSAR Accelerated Discovery of Potent Ice Recrystallization Inhibitors, *Sci Rep.* 6 (2016) 26403.
- [32] O. Mekenyan, N. Nikolova, P. Schmieder, Dynamic 3D QSAR techniques: applications in toxicology, *Journal of Molecular Structure: THEOCHEM*, 622 (2003) 147-165.
- [33] M.G. Damale, S.N. Harke, F.A. Kalam Khan, D.B. Shinde, J.N. Sangshetti, Recent advances in multidimensional QSAR (4D-6D): a critical review, *Mini-Rev. Med. Chem.* 14 (2014) 35-55.
- [34] Discovery Studio, version 3.1; Accelrys Inc.: San Diego, CA, in, 2011.

- [35] Gaussian 03, Revision A.1, M. J. Frisch, G. W. Trucks, H. B. Schlegel, G. E. Scuseria, M. A. Robb, J. R. Cheeseman, J. A. Montgomery, Jr., T. Vreven, K. N. Kudin, J. C. Burant, J. M. Millam, S. S. Iyengar, J. Tomasi, V. Barone, B. Mennucci, M. Cossi, G. Scalmani, N. Rega, G. A. Petersson, H. Nakatsuji, M. Hada, M. Ehara, K. Toyota, R. Fukuda, J. Hasegawa, M. Ishida, T. Nakajima, Y. Honda, O. Kitao, H. Nakai, M. Klene, X. Li, J. E. Knox, H. P. Hratchian, J. B. Cross, C. Adamo, J. Jaramillo, R. Gomperts, R. E. Stratmann, O. Yazyev, A. J. Austin, R. Cammi, C. Pomelli, J. W. Ochterski, P. Y. Ayala, K. Morokuma, G. A. Voth, P. Salvador, J. J. Dannenberg, V. G. Zakrzewski, S. Dapprich, A. D. Daniels, M. C. Strain, O. Farkas, D. K. Malick, A. D. Rabuck, K. Raghavachari, J. B. Foresman, J. V. Ortiz, Q. Cui, A. G. Baboul, S. Clifford, J. Cioslowski, B. B. Stefanov, G. Liu, A. Liashenko, P. Piskorz, I. Komaromi, R. L. Martin, D. J. Fox, T. Keith, M. A. Al-Laham, C.Y. Peng, A. Nanayakkara, M. Challacombe, P. M. W. Gill, B. Johnson, W. Chen, M. W. Wong, C. Gonzalez, and J. A. Pople, Gaussian, Inc., Pittsburgh PA, 2003.
- [36] Y.Y. Guo, L.Y. Dong, X.L. Qiu, Y.S. Wang, B.L. Zhang, H.N. Liu, Y. Yu, Y. Zang, M.J. Yang, Z.W. Huang, Structural basis for hijacking CBF-beta and CUL5 E3 ligase complex by HIV-1 Vif, *Nature* 505 (2014) 229-233.
- [37] G.M. Morris, R. Huey, W. Lindstrom, M.F. Sanner, R.K. Belew, D.S. Goodsell, A.J. Olson, AutoDock4 and AutoDockTools4: Automated docking with selective receptor flexibility, *J. Comput. Chem.* 30 (2009) 2785-2791.
- [38] A. Mehle, E.R. Thomas, K.S. Rajendran, D. Gabuzda, A zinc-binding region in Vif binds Cul5 and determines cullin selection, *J. Biol. Chem.* 281 (2006) 17259-17265.
- [39] T. Kamura, K. Maenaka, S. Kotoshiba, M. Matsumoto, D. Kohda, R.C. Conaway, J.W. Conaway, K.I. Nakayama, VHL-box and SOCS-box domains determine binding specificity for Cul2-Rbx1 and Cul5-Rbx2 modules of ubiquitin ligases, *Genes Dev.* 18 (2004) 3055-3065.
- [40] E. Pery, K.S. Rajendran, A.J. Brazier, D. Gabuzda, Regulation of APOBEC3 proteins by a novel YXXL motif in human immunodeficiency virus type 1 Vif and simian immunodeficiency virus SIVagm Vif, *J. Virol.* 83 (2009) 2374-2381.
- [41] R.A. Russell, J. Smith, R. Barr, D. Bhattacharyya, V.K. Pathak, Distinct domains within APOBEC3G and APOBEC3F interact with separate regions of human immunodeficiency virus type 1 Vif, *J. Virol.* 83 (2009) 1992-2003.
- [42] S.G. Conticello, R.S. Harris, M.S. Neuberger, The Vif protein of HIV triggers degradation of the human antiretroviral DNA deaminase APOBEC3G, *Curr. Biol.* 13 (2003) 2009-2013.
- [43] X. He, H. Xing, Y. Ruan, K. Hong, C. Cheng, Y. Hu, R. Xin, J. Wei, Y. Feng, J.H. Hsi, Y. Takebe, Y. Shao, H.I.V.M.E.S. Group for, A comprehensive mapping of HIV-1 genotypes in various risk groups and regions across China based on a nationwide molecular epidemiologic survey, *PLoS One* 7 (2012) e47289.
- [44] R.R. Wang, Q.H. Yang, R.H. Luo, Y.M. Peng, S.X. Dai, X.J. Zhang, H. Chen, X.Q. Cui, Y.J. Liu, J.F. Huang, J.B. Chang, Y.T. Zheng, Azvudine, a novel nucleoside reverse transcriptase inhibitor showed good drug combination features and better inhibition on drug-resistant strains than lamivudine in vitro, *PLoS One* 9 (2014) e105617.
- [45] S. Trombino, T. Ferrarelli, R. Cassano, A new pro-prodrug aminoacid-based for trans-ferulic Acid and silybin intestinal release, *J. Funct. Biomater.* 5 (2014) 99-110.
- [46] A. Mishra, S. Agrawal, K. Pathak, Naproxen glycine conjugate-synthesis, pharmaceutical preformulation and pharmacodynamic evaluation, *Drug Deliv.* 19 (2012) 102-111.

- [47] T.D. Bradshaw, J.E. Wren, M. Bruce, D.A. Barrett, C.O. Leong, M. Gaskell, E.K. Wright, P.B. Farmer, C.J. Henderson, R. Wolf, M.F. Stevens, Preclinical toxicokinetic evaluation of phortress [2-(4-amino-3-methylphenyl)-5-fluorobenzothiazole lysylamide dihydrochloride] in two rodent species, *Pharmacology* 83 (2009) 99-109.
- [48] B.S. Vig, K.M. Huttunen, K. Laine, J. Rautio, Amino acids as promoieties in prodrug design and development, *Adv. Drug Deliv. Rev.* 65 (2013) 1370-1385.
- [49] M. Tsuda, T. Terada, M. Irie, T. Katsura, A. Niida, K. Tomita, N. Fujii, K. Inui, Transport characteristics of a novel peptide transporter 1 substrate, antihypertensive drug midodrine, and its amino acid derivatives, *J. Pharmacol. Exp. Ther.* 318 (2006) 455-460.
- [50] I. Hutchinson, S.A. Jennings, B.R. Vishnuvajjala, A.D. Westwell, M.F. Stevens, Antitumor benzothiazoles. 16. Synthesis and pharmaceutical properties of antitumor 2-(4-aminophenyl)benzothiazole amino acid prodrugs, *J. Med. Chem.* 45 (2002) 744-747.
- [51] M. Zhou, H. Luo, R. Li, Z.Y. Ding, Exploring the binding mode of HIV-1 Vif inhibitors by blind docking, molecular dynamics and MM/GBSA, *Rsc Adv.* 3 (2013) 22532-22543.
- [52] A.M. Vandamme, M. Witvrouw, C. Pannecouque, J. Balzarini, K. Van Laethem, J.C. Schmit, J. Desmyter, E. De Clercq, Evaluating Clinical Isolates for Their Phenotypic and Genotypic Resistance Against Anti-HIV Drugs, *Methods Mol. Med.* 24 (2000) 223-258.
- [53] R.R. Wang, L.M. Yang, Y.H. Wang, W. Pang, S.C. Tam, P. Tien, Y.T. Zheng, Sifuvirtide, a potent HIV fusion inhibitor peptide, *Biochem. Biophys. Res. Commun.* 382 (2009) 540-544.
- [54] X.J. Zhang, L.H. Lu, R.R. Wang, Y.P. Wang, R.H. Luo, C. Cong Lai, L.M. Yang, Y.P. He, Y.T. Zheng, DB-02, a C-6-cyclohexylmethyl substituted pyrimidinone HIV-1 reverse transcriptase inhibitor with nanomolar activity, displays an improved sensitivity against K103N or Y181C than S-DABOs, *PLoS One* 8 (2013) e81489.
- [55] G.J. Liu, J.P. Wang, J.C. Xiao, Z.W. Zhao, Y. Zheng, Preparation and characterization of three monoclonal antibodies against HIV-1 p24 capsid protein, *Cell. Mol. Immunol.* 4 (2007) 203-208.
- [56] B. Nowotny, T. Schneider, G. Pradel, T. Schirmeister, A. Rethwilm, M. Kirschner, Inducible APOBEC3G-Vif double stable cell line as a high-throughput screening platform to identify antiviral compounds, *Antimicrob. Agents Chemother.* 54 (2010) 78-87.

- A more potent Vif antagonist **12c** was obtained through the optimizations of **RN-18**.
- **12c** protected APOBEC3G from degradation by inhibiting Vif function.
- The glycine prodrug **13a** showed an obviously improved drug-like property than **12c**.

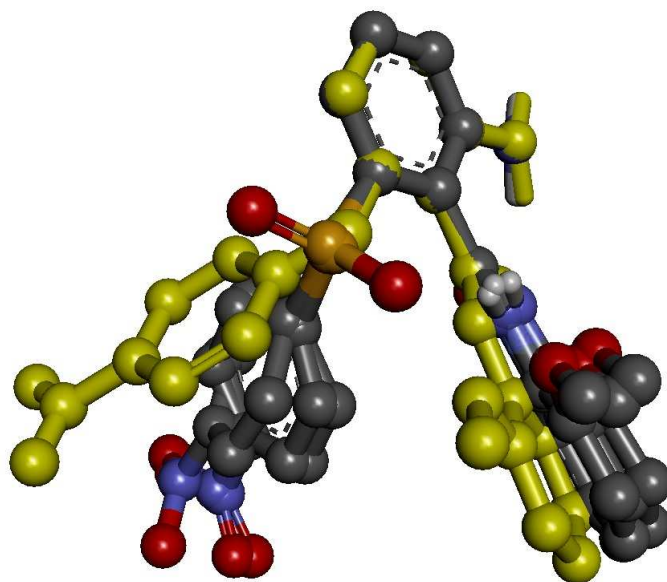
**Supporting Information****Synthesis, biological evaluation and molecular docking study of  
*N*-(2-methoxyphenyl)-6-((4-nitrophenyl)sulfonyl)benzamide  
derivatives as potent HIV-1 Vif antagonists**

Meng Zhou, Rong-Hua Luo, Xue-Yan Hou, Rui-Rui Wang, Guo-Yi Yan, Huan Chen,  
Rong-Hong Zhang, Jian-You Shi, Yong-Tang Zheng, Rui Li, and Yu-Quan Wei

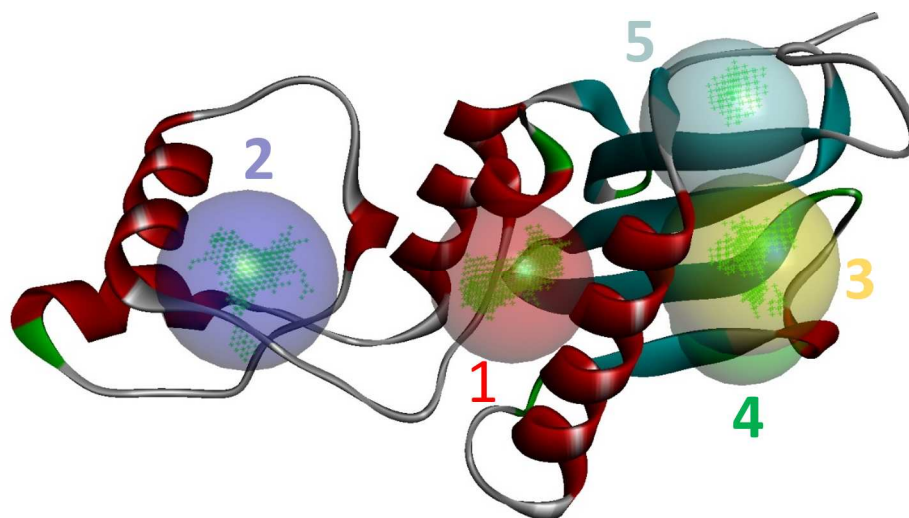
**Table of Content****1. Supporting Figures and Tables**

Figure S1.....	2
Figure S2.....	3
Figure S3.....	4
Figure S4.....	5
Figure S5.....	6
Figure S6.....	7
Figure S7.....	8
Table S1.....	9
Table S2.....	10
Table S3.....	11
Table S4.....	12
Table S5.....	13
<b>2. <sup>1</sup>H and <sup>13</sup>C NMR spectra of compounds.....</b>	<b>14</b>

## 1. Supporting Figures and Tables



**Figure S1.** Superposition of **12**, **12a** (yellow), **12b**, and **12c** by the common aniline group.



**Figure S2.** Binding site analysis on the surface of Vif.

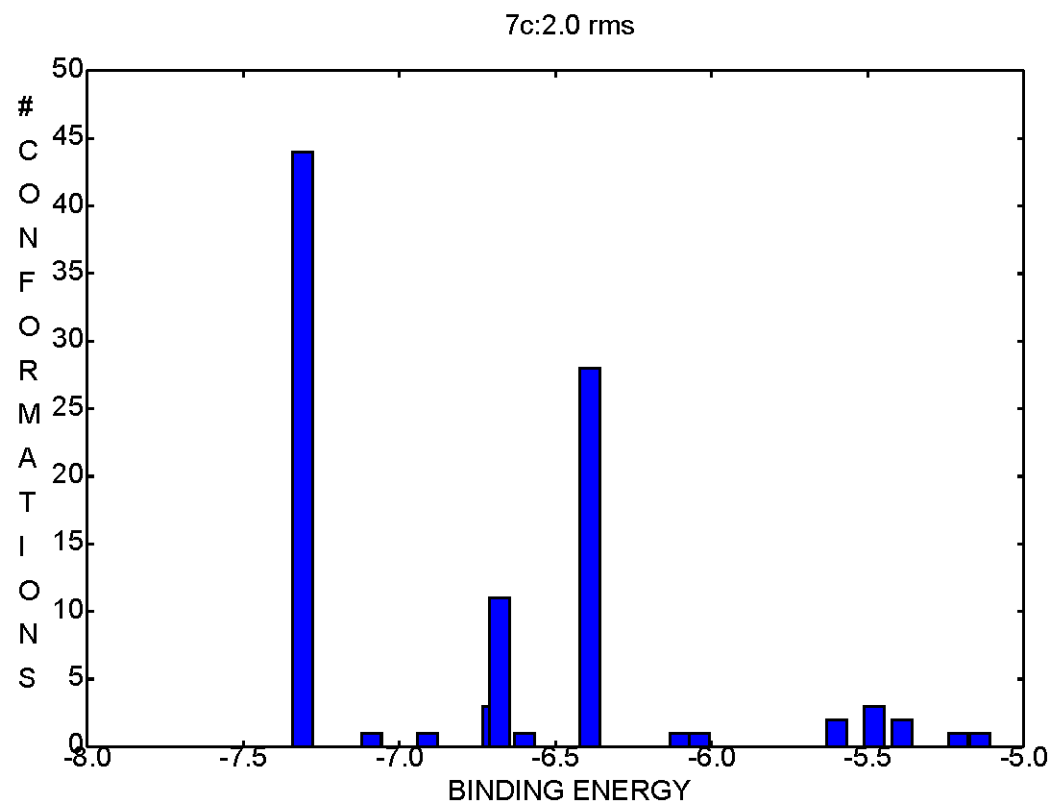
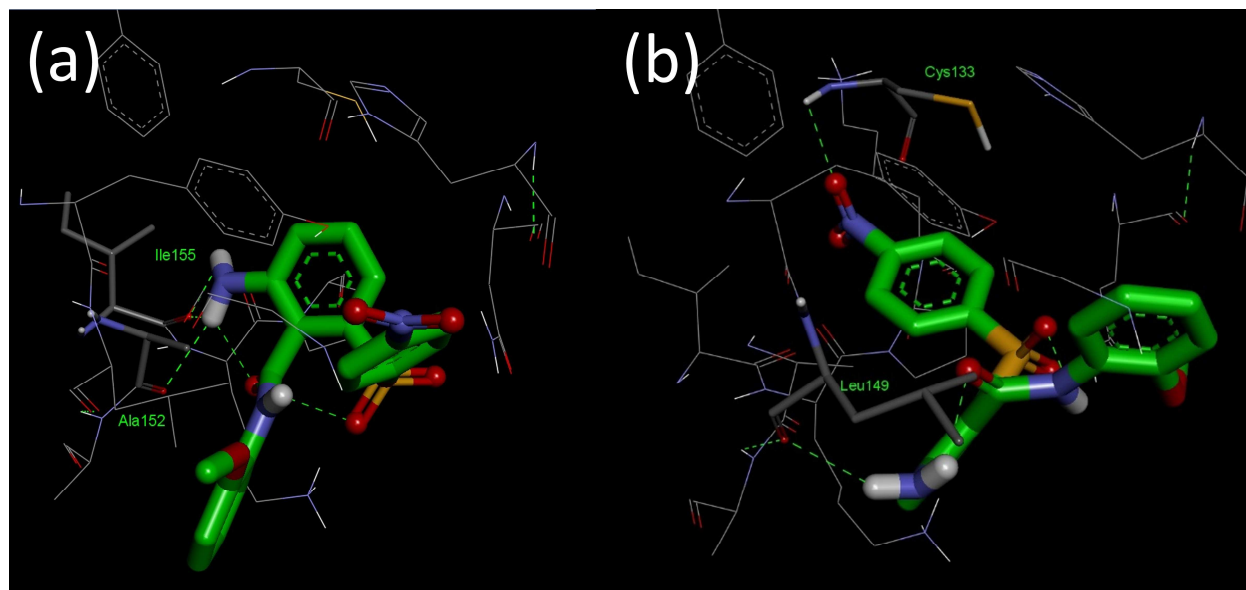
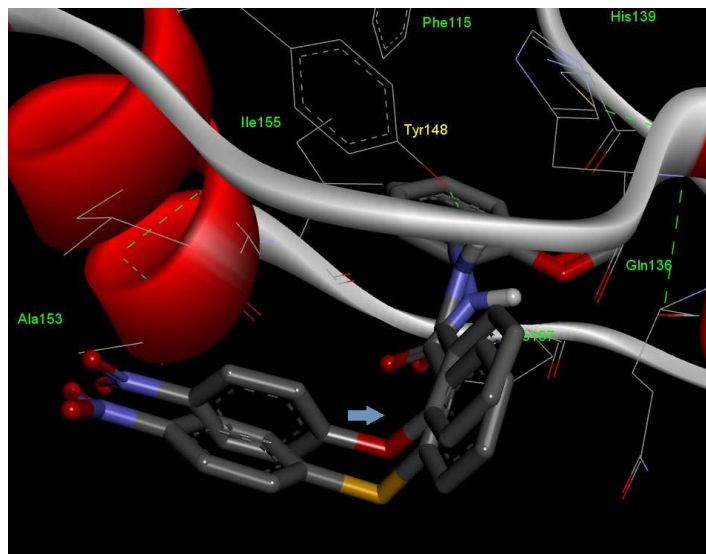


Figure S3. Docking result of **12c** with Vif.



**Figure S4.** Binding pose analysis of mode 2 (a) and mode 3 (b). (a) Ring B was buried into the hydrophobic cavity formed by Phe115, Try148, Ile155 and Pro157. The amino group formed two H-bonds with Ile155 and one H-bond with Ala152. (b) Ring A was buried into the hydrophobic cavity formed by Phe115, Try148, Ile155 and Pro157. It had two H-bonds with Vif, one was the nitro group with Cys133, the other was the amino group with Leu149.



**Figure S5.** Binding mode comparison of compound **1** and its oxygen ether analogue.

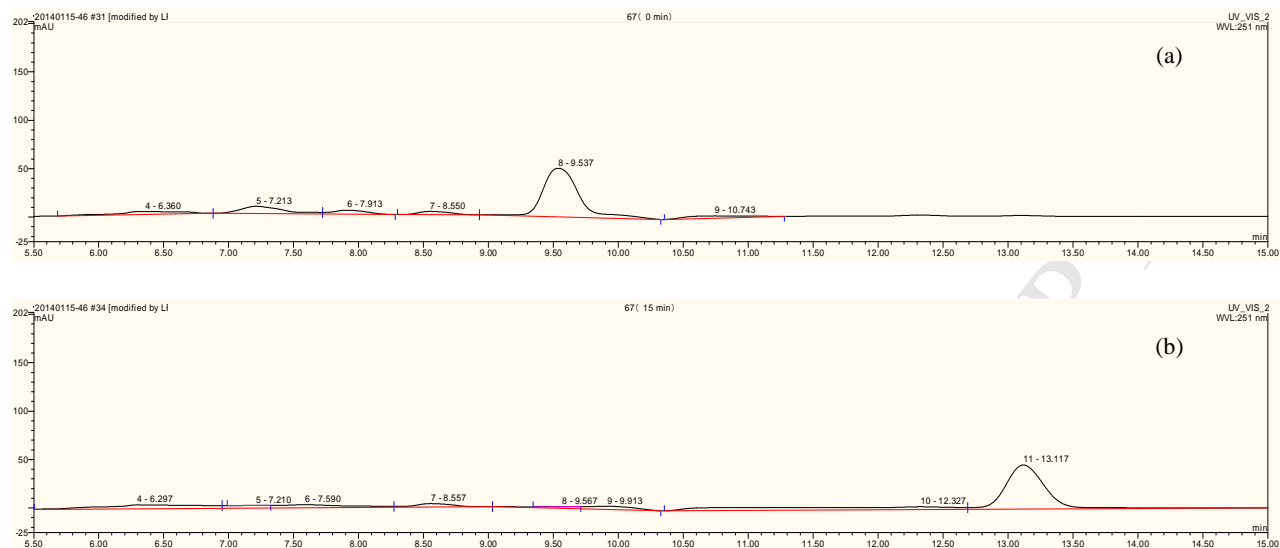


**Figure S6.** HPLC chromatograms of metabolite for 0 (a) and 15 min (b) of prodrug 13a.

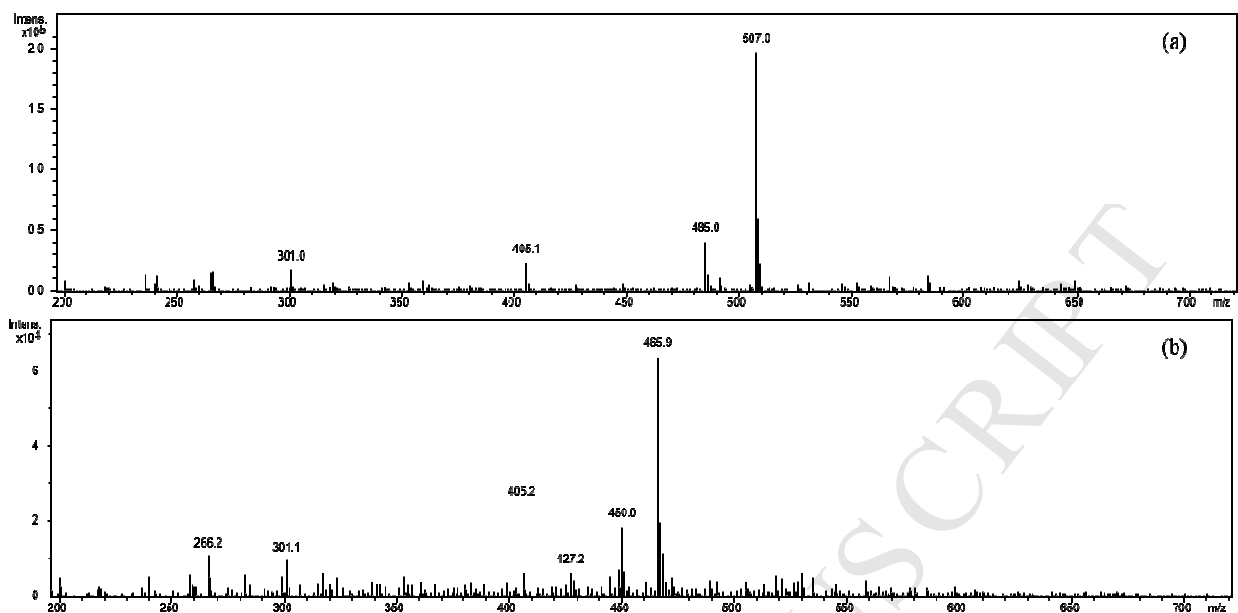


**Figure S7.** LC/ESI-MS spectra of metabolite for 0 (a, RT = 9.5 min, **13a**) and 15 min (b, RT = 13.1 min, **12c**) of prodrug **13a**.

**Table S1. Binding site analysis of Vif.**

<b>Binding Site</b>	<b>X</b>	<b>Y</b>	<b>Z</b>	<b>Volume</b>	<b>Color</b>	<b>Function</b>
1	70.99	-87.49	-180.10	57.50	Red	Unclear
2	72.88	-69.58	-181.95	43.25	Blue	Interacting with ELOC and CUL5
3	67.09	-100.83	-181.88	27.13	Yellow	Interacting with A3G
4	55.44	-97.50	-187.19	14.50	Green	Interacting with A3G
5	72.84	-100.88	-188.21	13.75	Cyan	Interacting with CBF- $\beta$

**Table S2. Docking result analysis of 12c with Vif.**

<b>Mode</b>	<b>Occurrence rate</b>	<b>Lowest energy</b>	<b>H-bond number</b>
<b>1</b>	<i>44</i>	<i>-7.31</i>	<i>5</i>
<b>2</b>	<i>11</i>	<i>-6.45</i>	<i>3</i>
<b>3</b>	<i>28</i>	<i>-5.17</i>	<i>2</i>

**Table S3. Aqueous and organic solvents solubility of 12c and its derivatives.**

Compound	Experimentally determined solubility ( $\mu\text{g/mL}$ ) <sup>a</sup>					
	Water	Methanol	Ethanol	Acetonitrile	Ethyl acetate	Acetone
<b>12c</b>	0.66 $\pm$ 0.12	814 $\pm$ 59	284 $\pm$ 15	9090 $\pm$ 77	4380 $\pm$ 40	22400 $\pm$ 49
<b>13a</b>	1730 $\pm$ 25	-	-	-	-	-
<b>13b</b>	120 $\pm$ 5	-	-	-	-	-

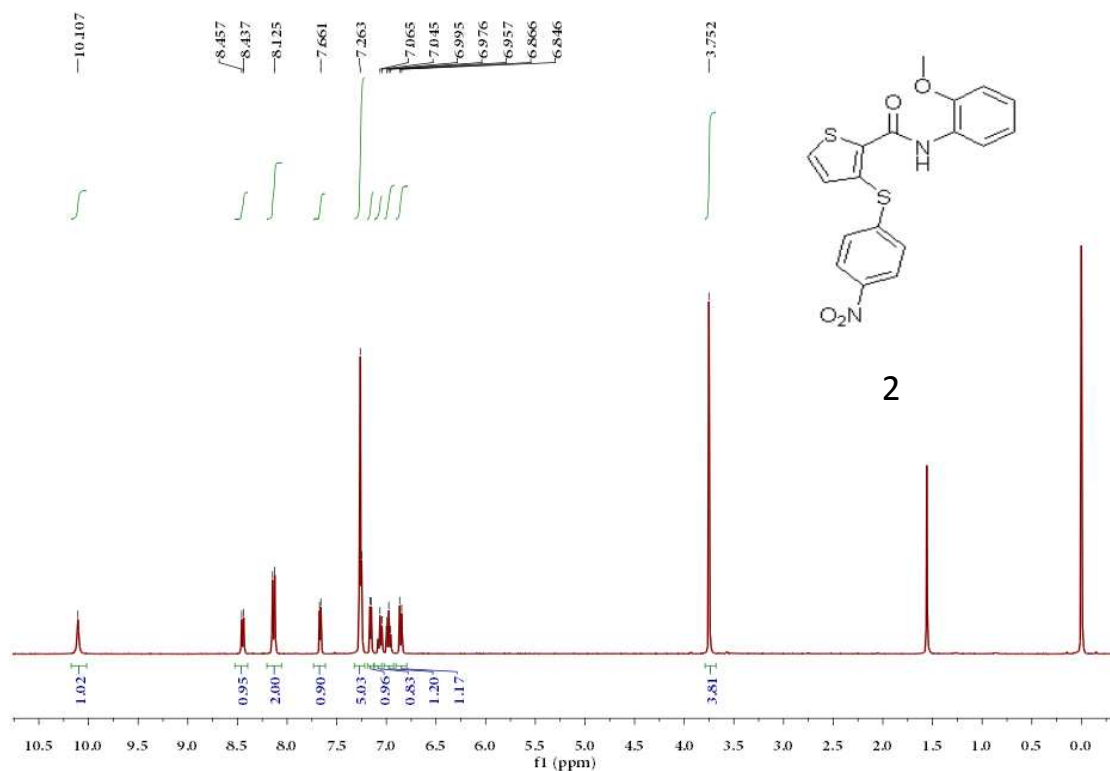
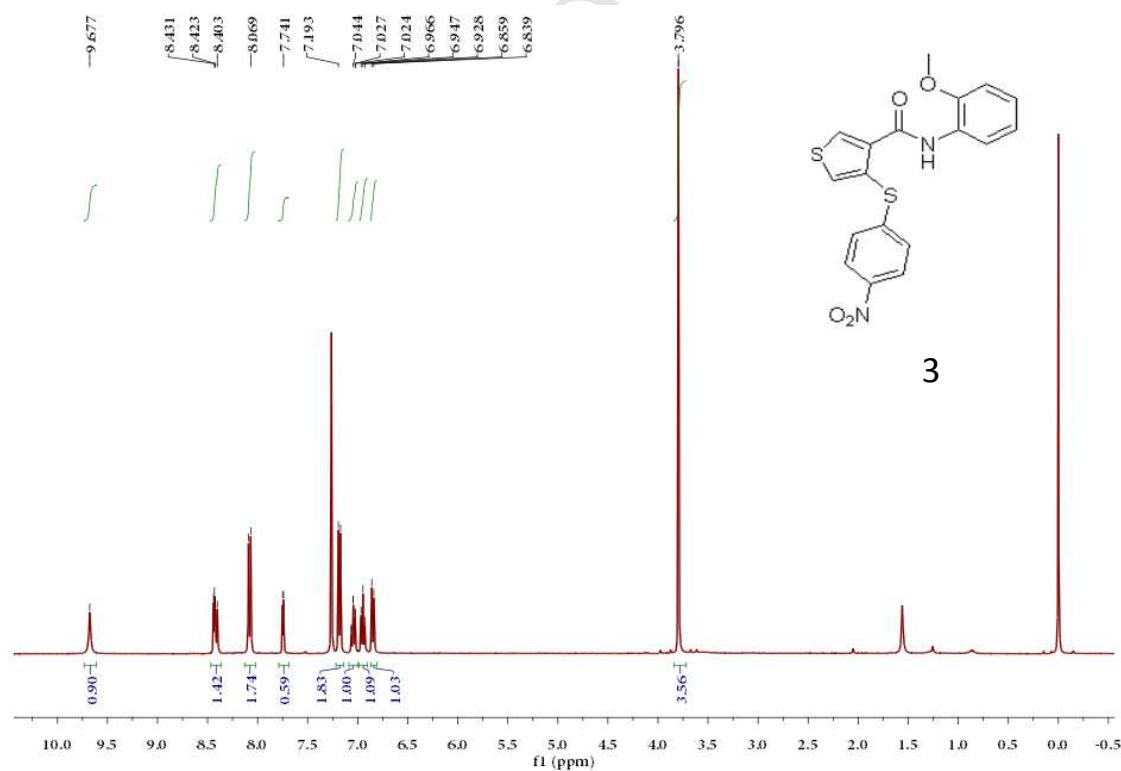
<sup>a</sup>n=3, values are described as mean + SD. <sup>b</sup>-, not test.

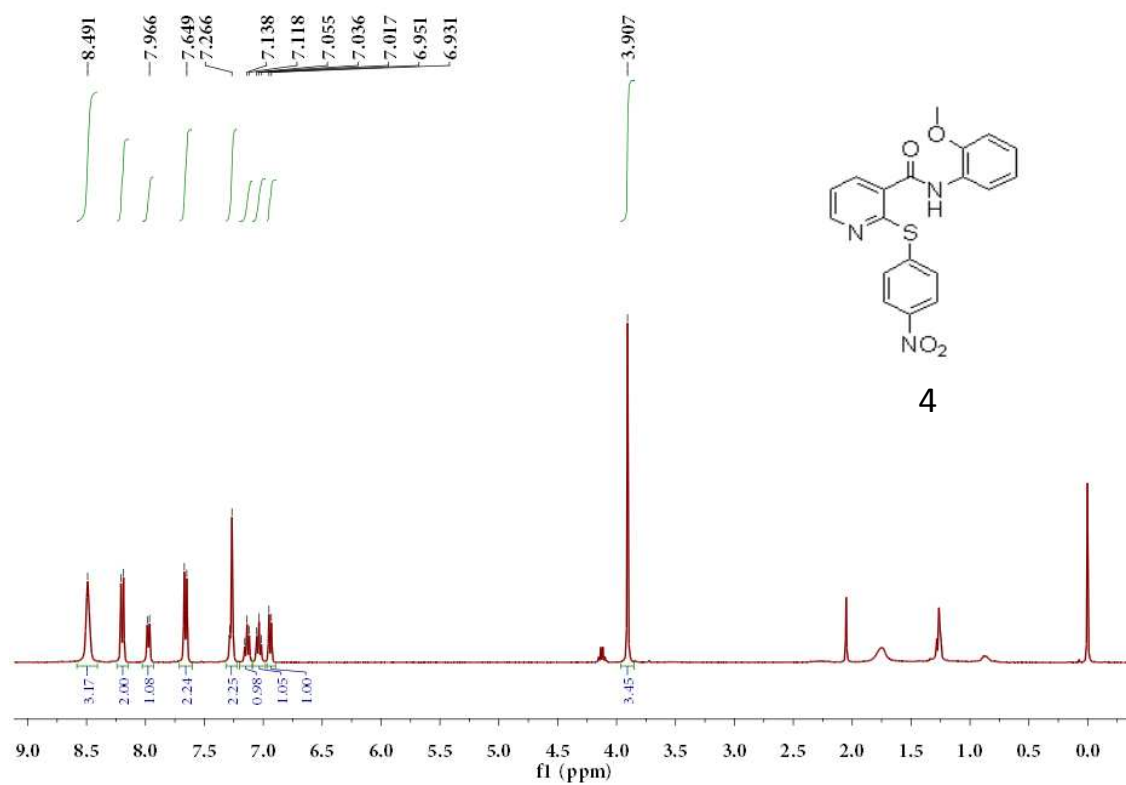
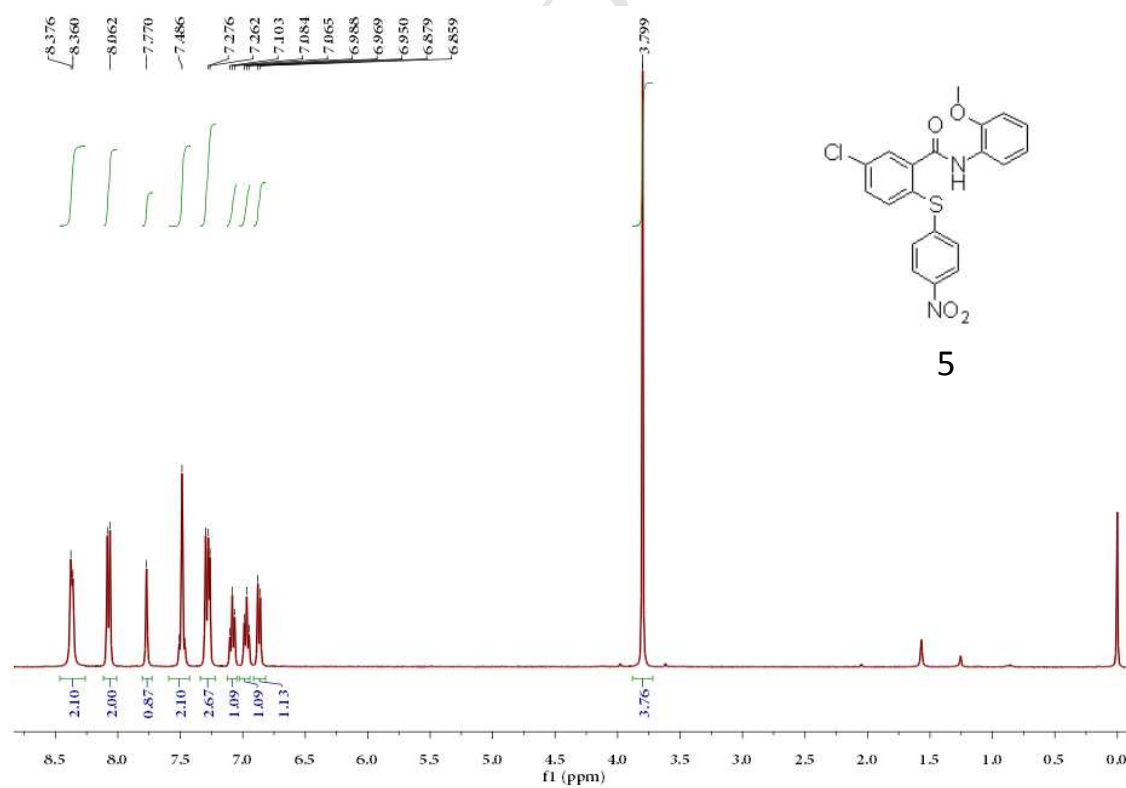
**Table S4. Experimental partition coefficient of 12c at different time.**

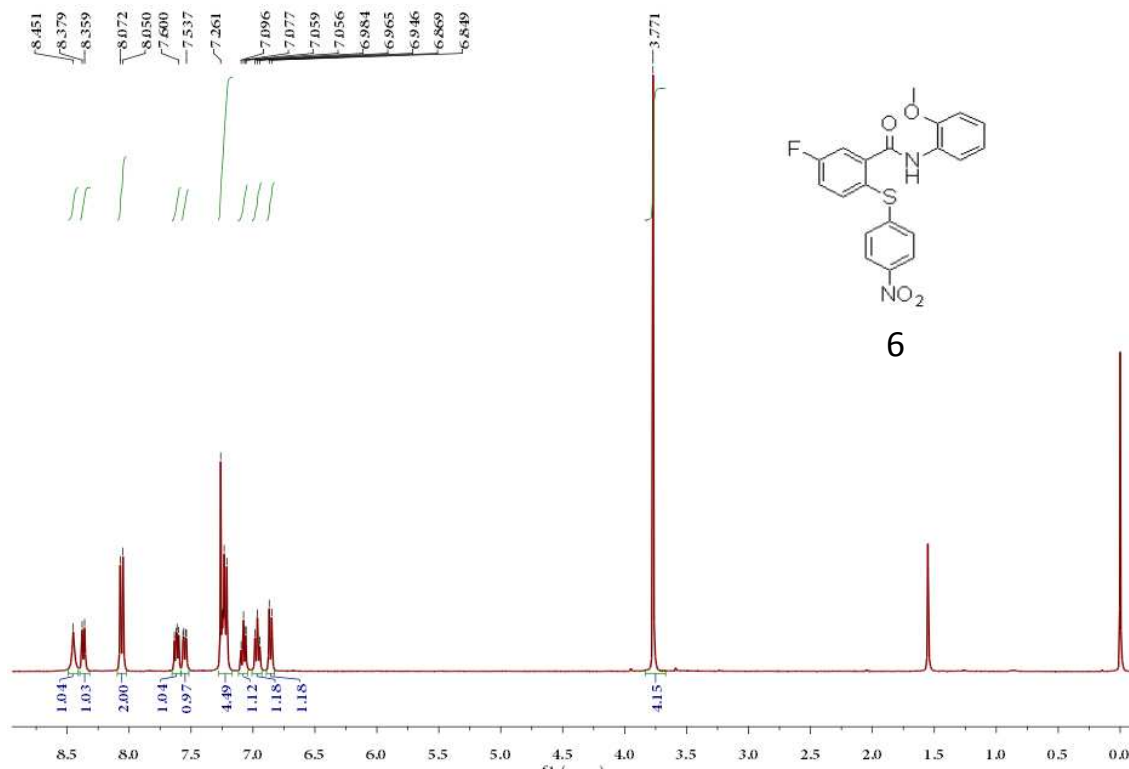
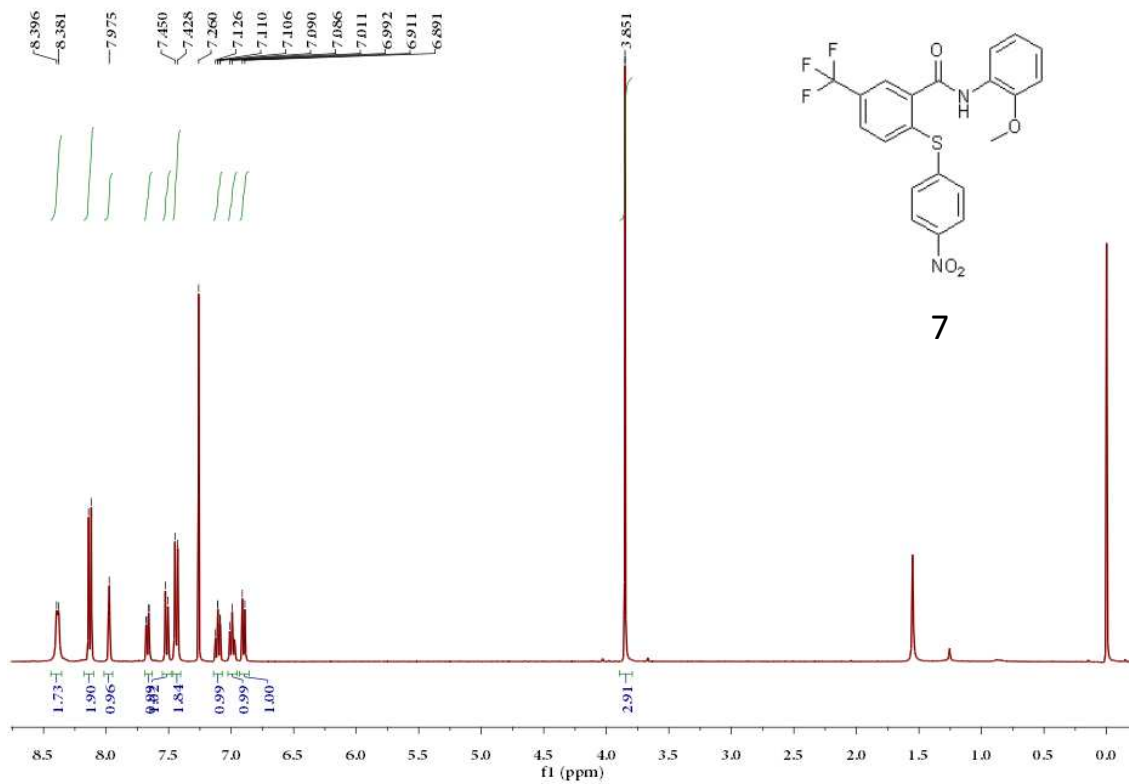
Shaking time	Partition coefficient (Log P)	Mean $\pm$ SD
2 h	2.45	2.41 $\pm$ 0.04
	2.38	
	2.39	
4 h	2.42	2.40 $\pm$ 0.01
	2.39	
	2.39	
	2.41	
7 h	2.40	2.40 $\pm$ 0.01
	2.40	
	2.39	

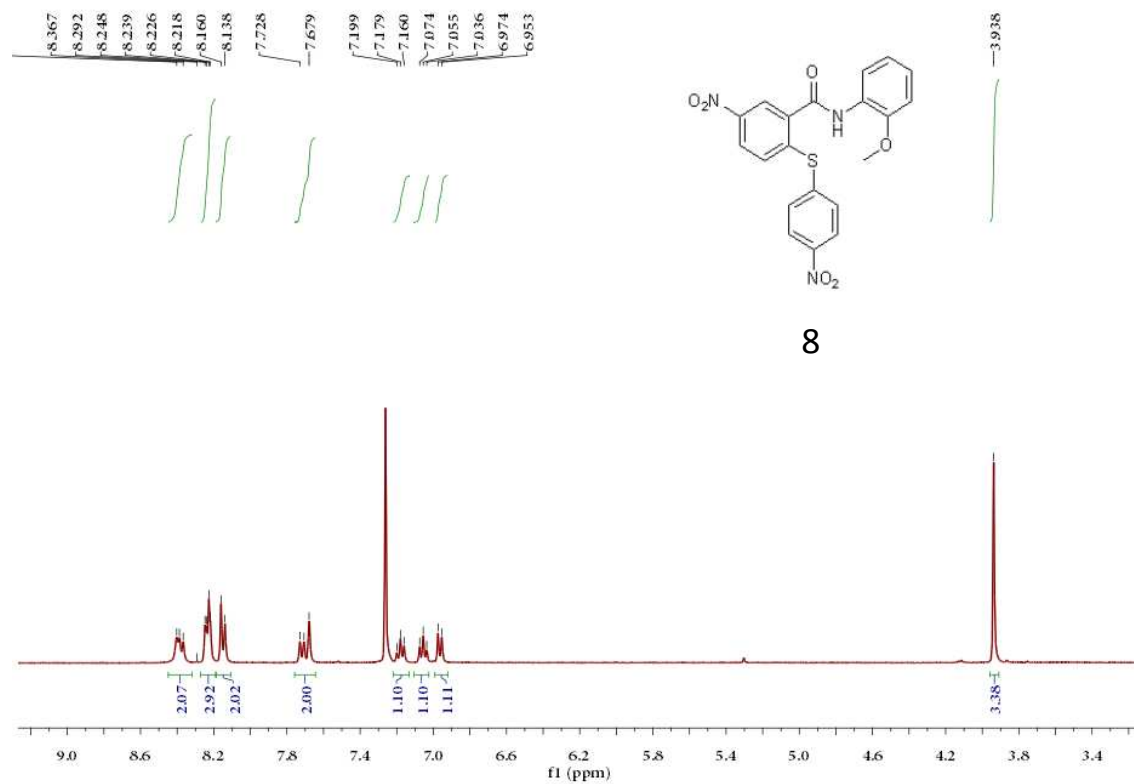
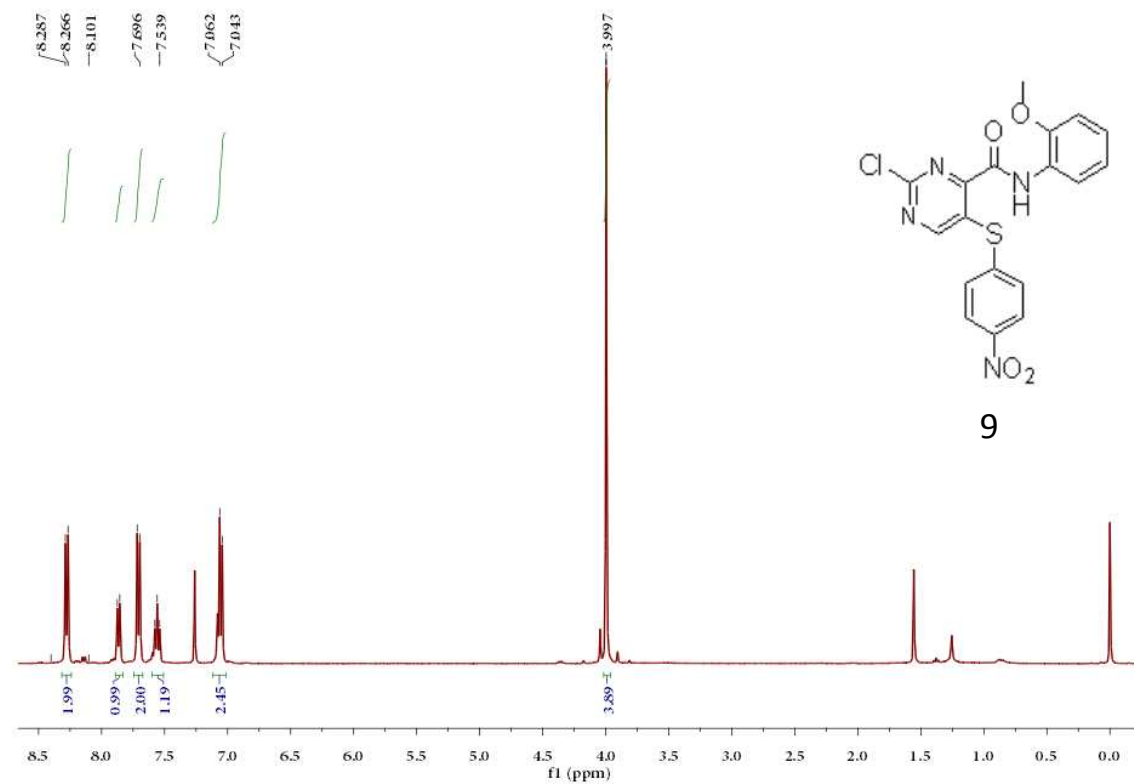
**Table S5. Experimental partition coefficient of 12c with different volume ratios of *n*-octanol to water.**

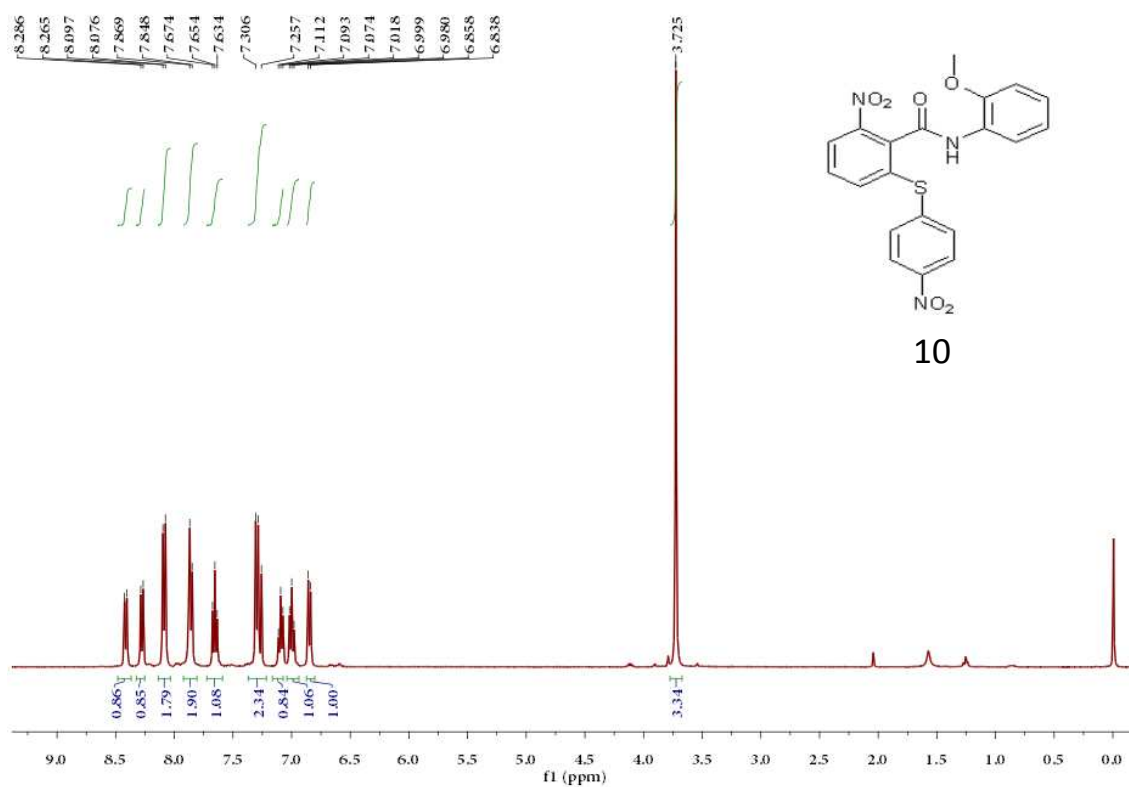
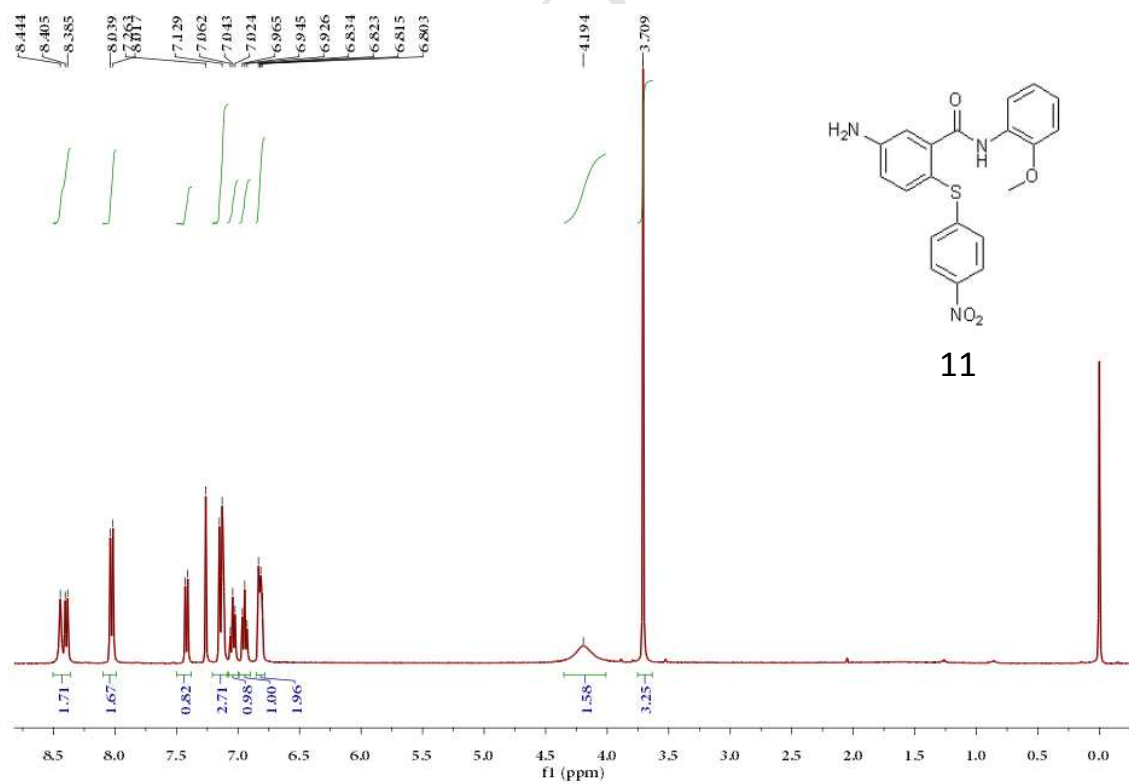
Phase ratio	Partition coefficient (Log P)	Mean $\pm$ SD
	2.40	
1:1	2.40	2.40 $\pm$ 0.01
	2.41	
	2.51	
1:4	2.55	2.53 $\pm$ 0.02
	2.53	
	2.52	
1:9	2.52	2.55 $\pm$ 0.05
	2.60	

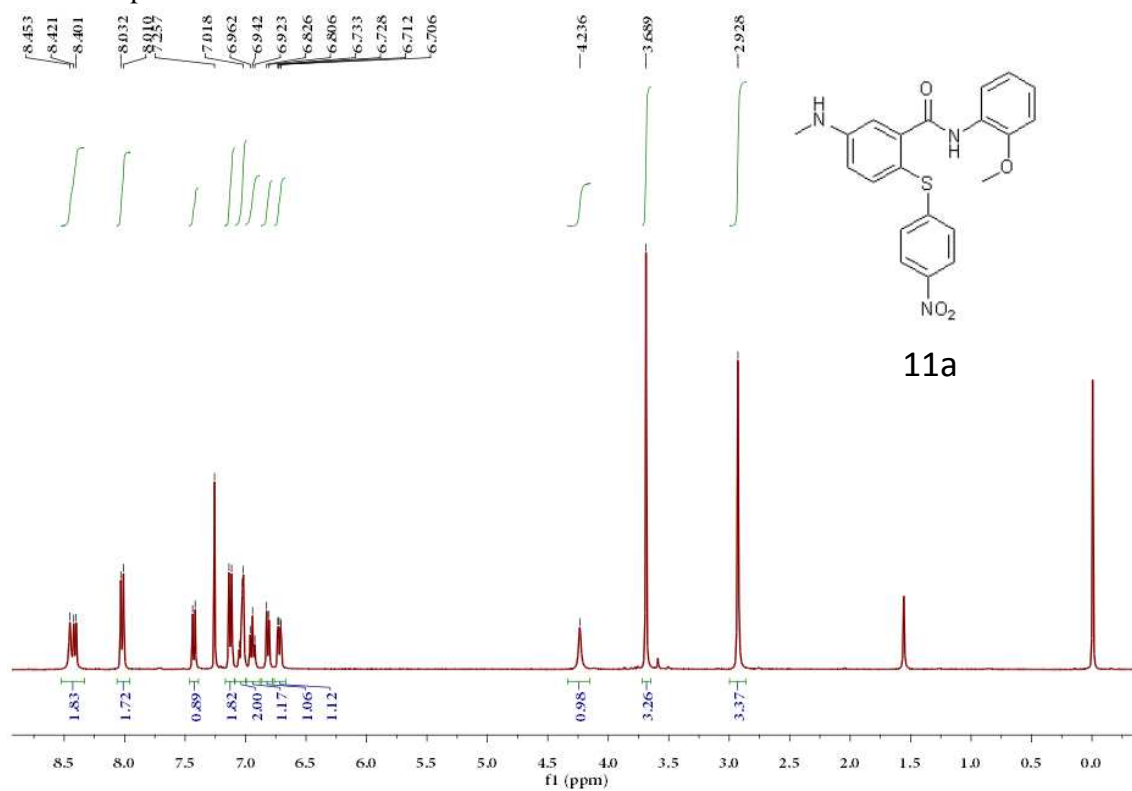
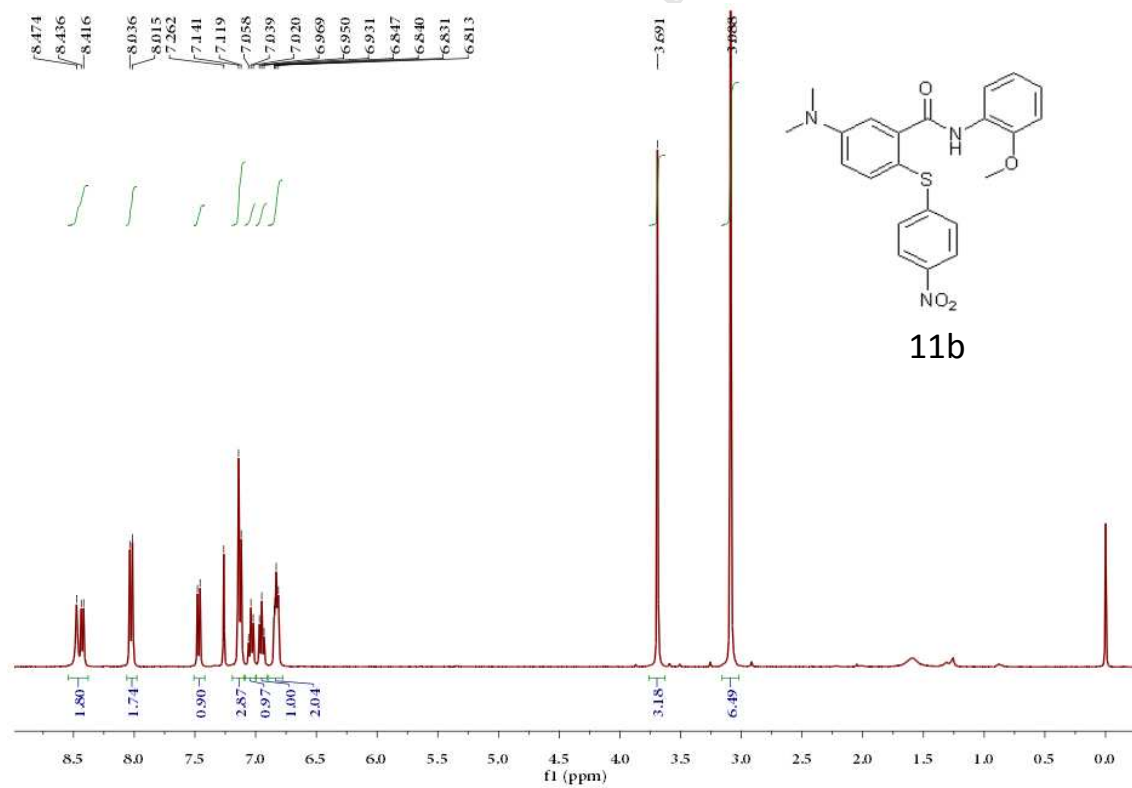
**2.  $^1\text{H}$  and  $^{13}\text{C}$  NMR spectra of compounds** **$^1\text{H}$  NMR spectra of 2** **$^1\text{H}$  NMR spectra of 3**

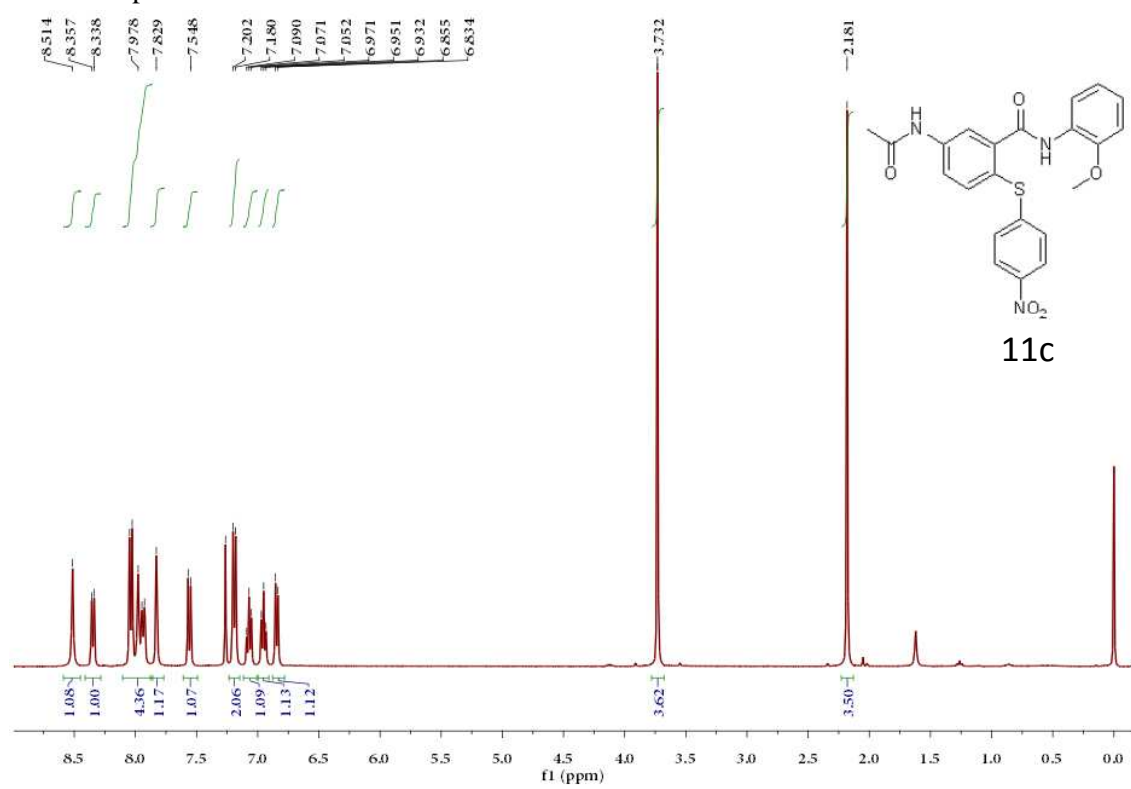
<sup>1</sup>H NMR spectra of **4**<sup>1</sup>H NMR spectra of **5**

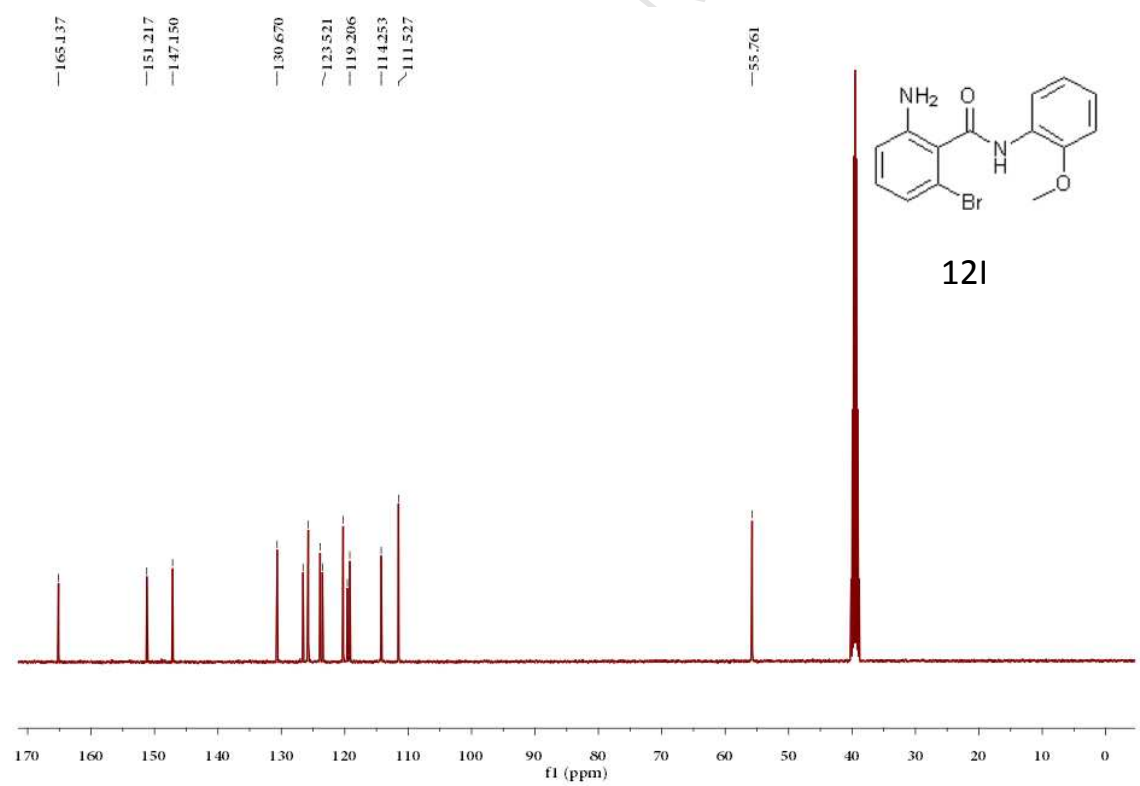
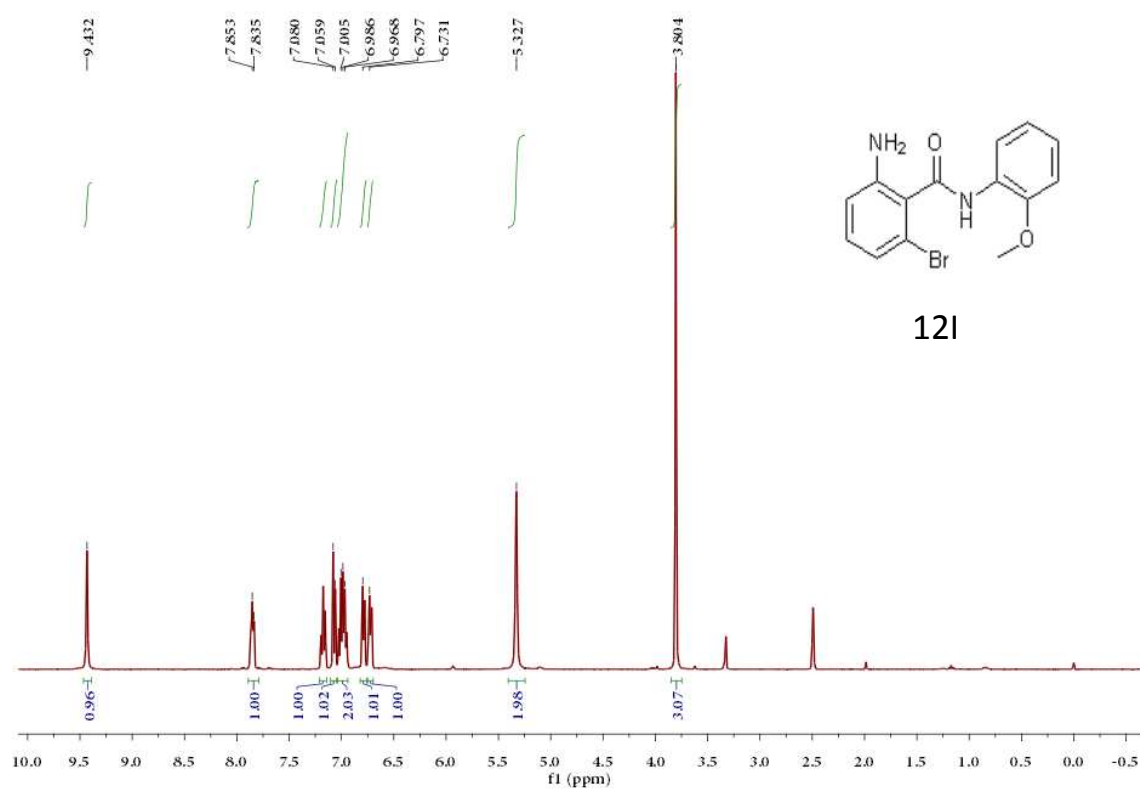
<sup>1</sup>H NMR spectra of **6**<sup>1</sup>H NMR spectra of **7**

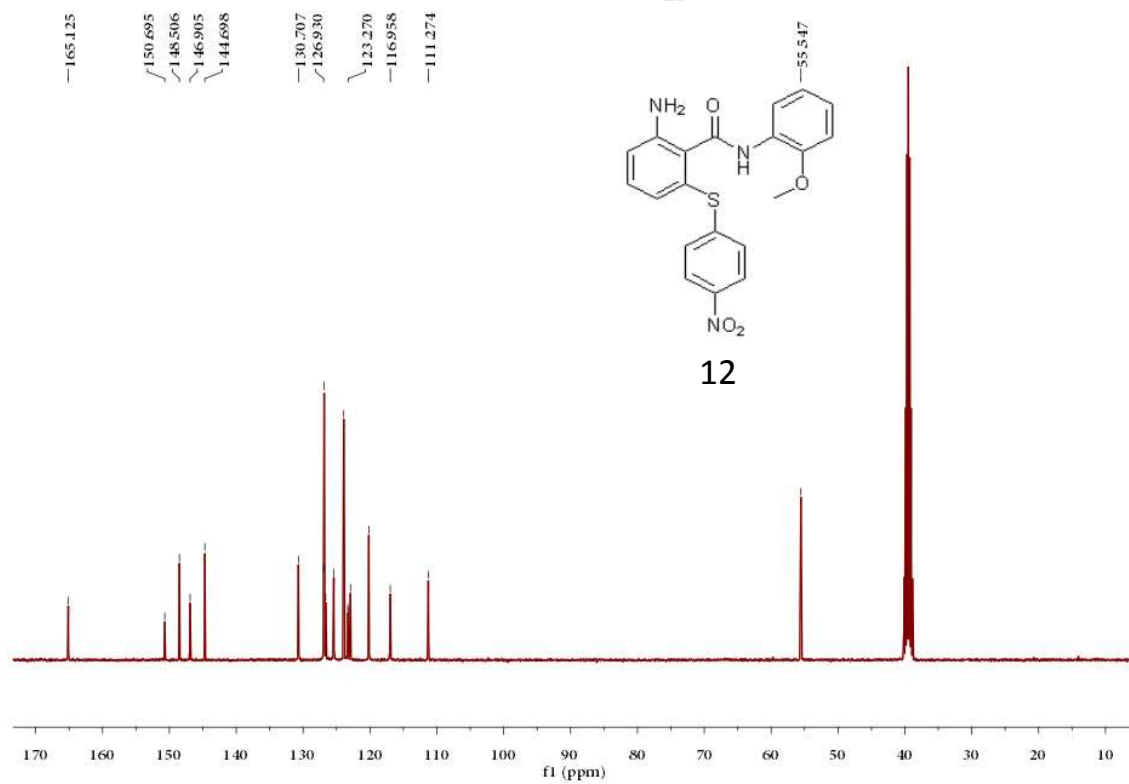
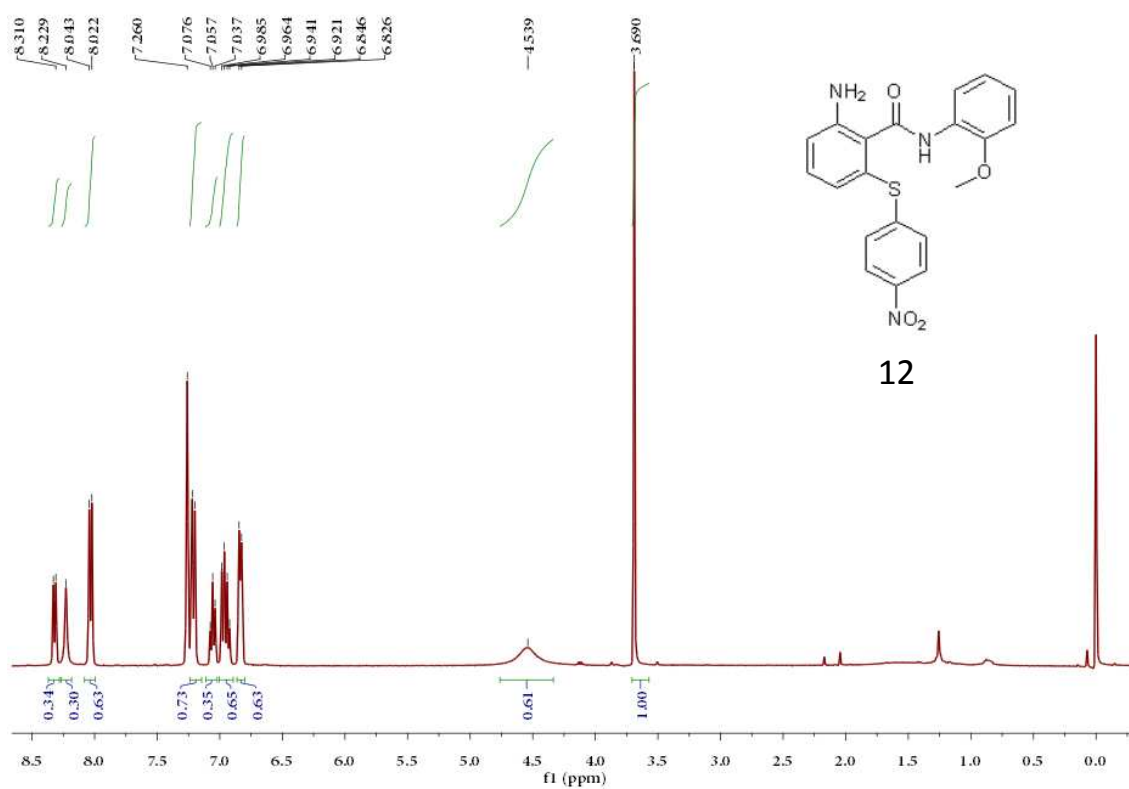
<sup>1</sup>H NMR spectra of **8**<sup>1</sup>H NMR spectra of **9**

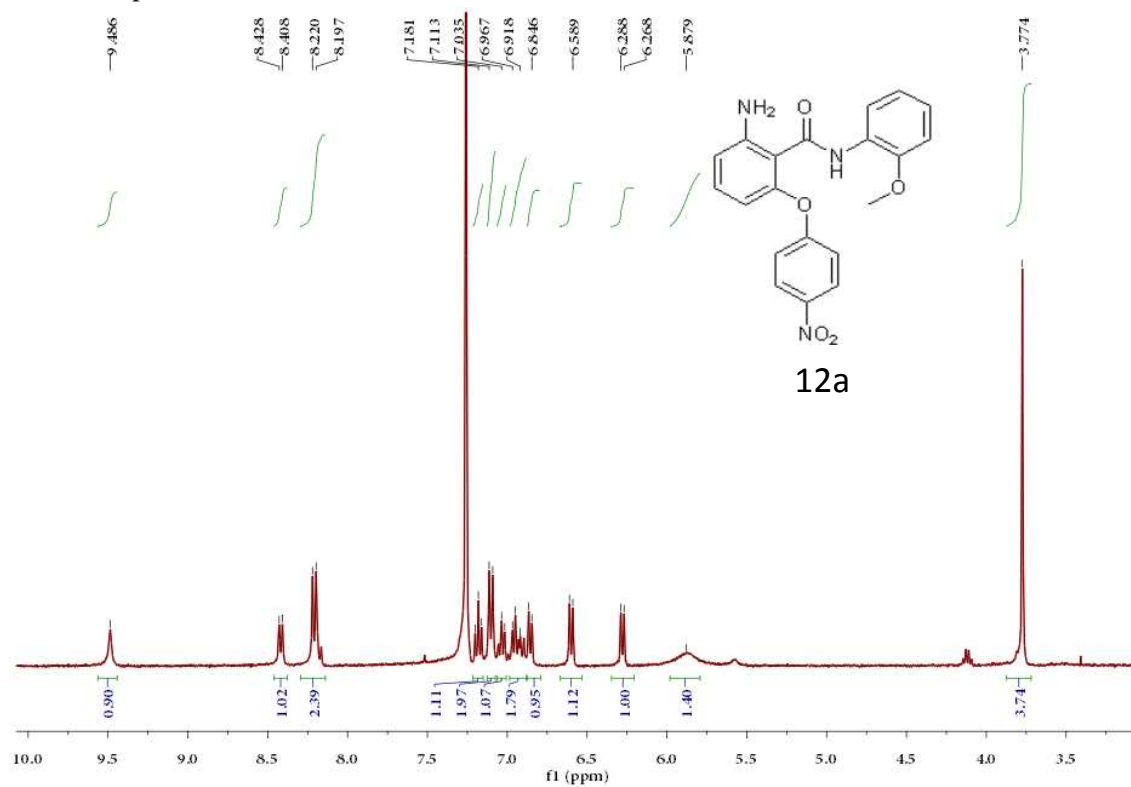
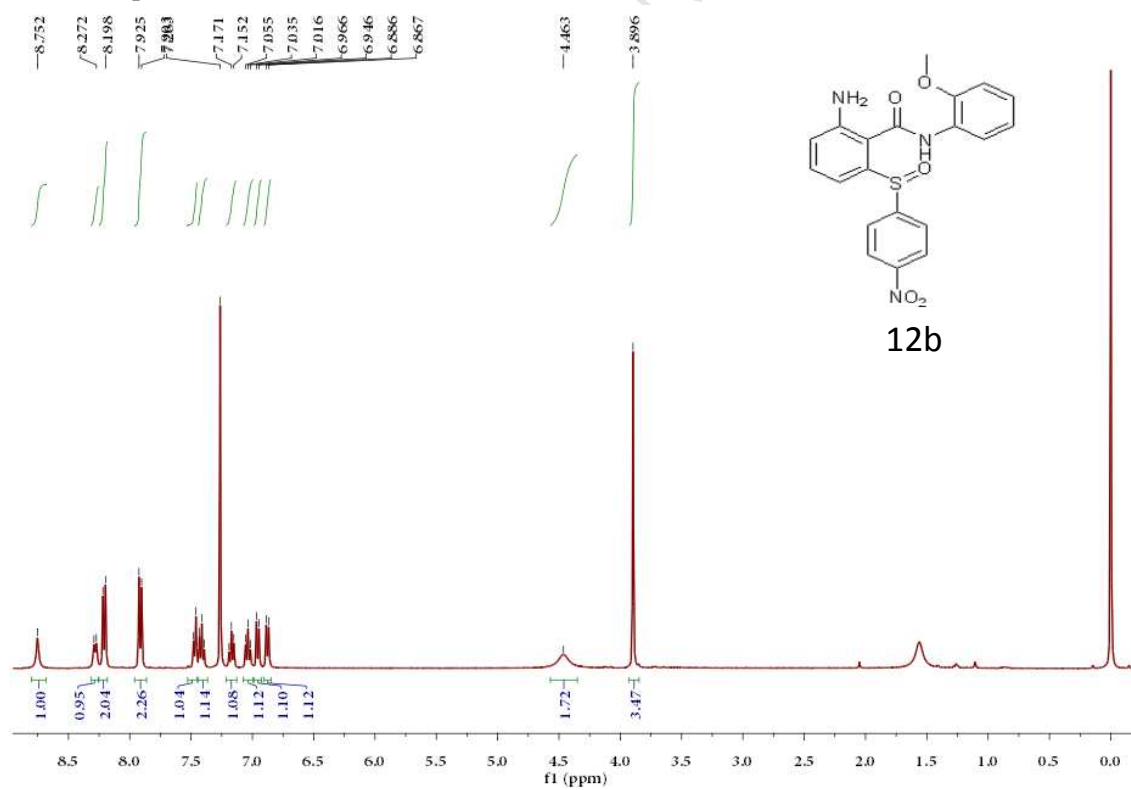
<sup>1</sup>H NMR spectra of **10**<sup>1</sup>H NMR spectra of **11**

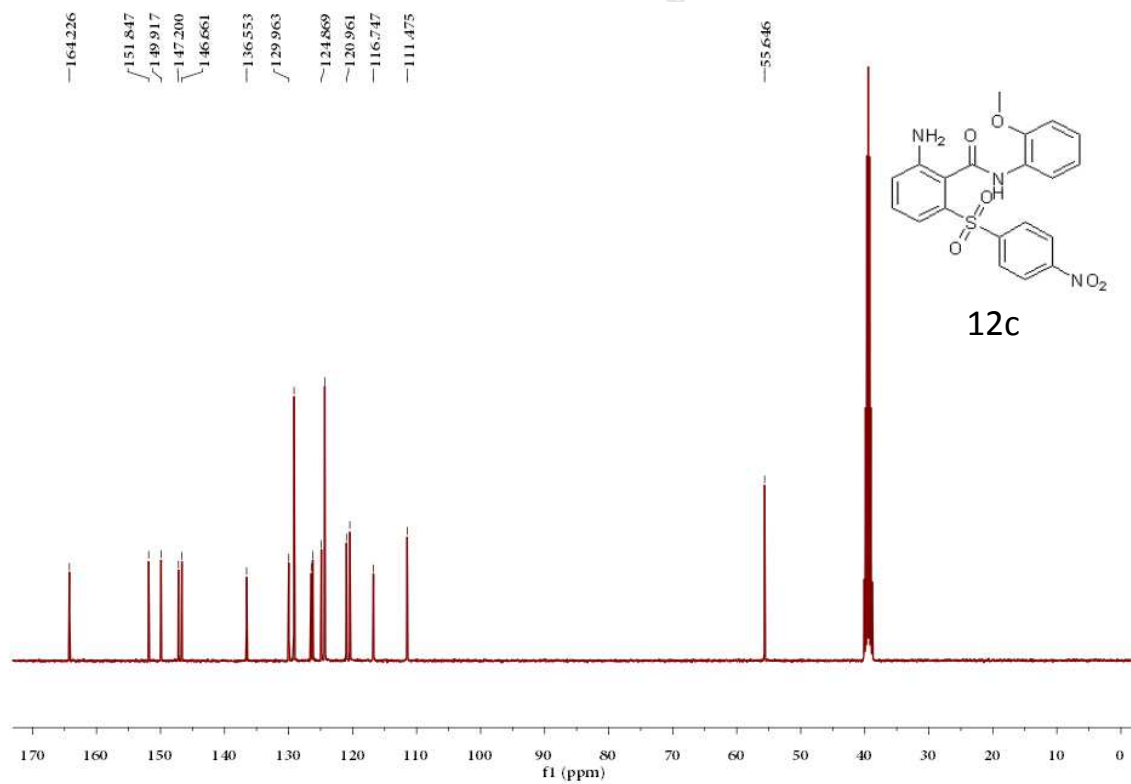
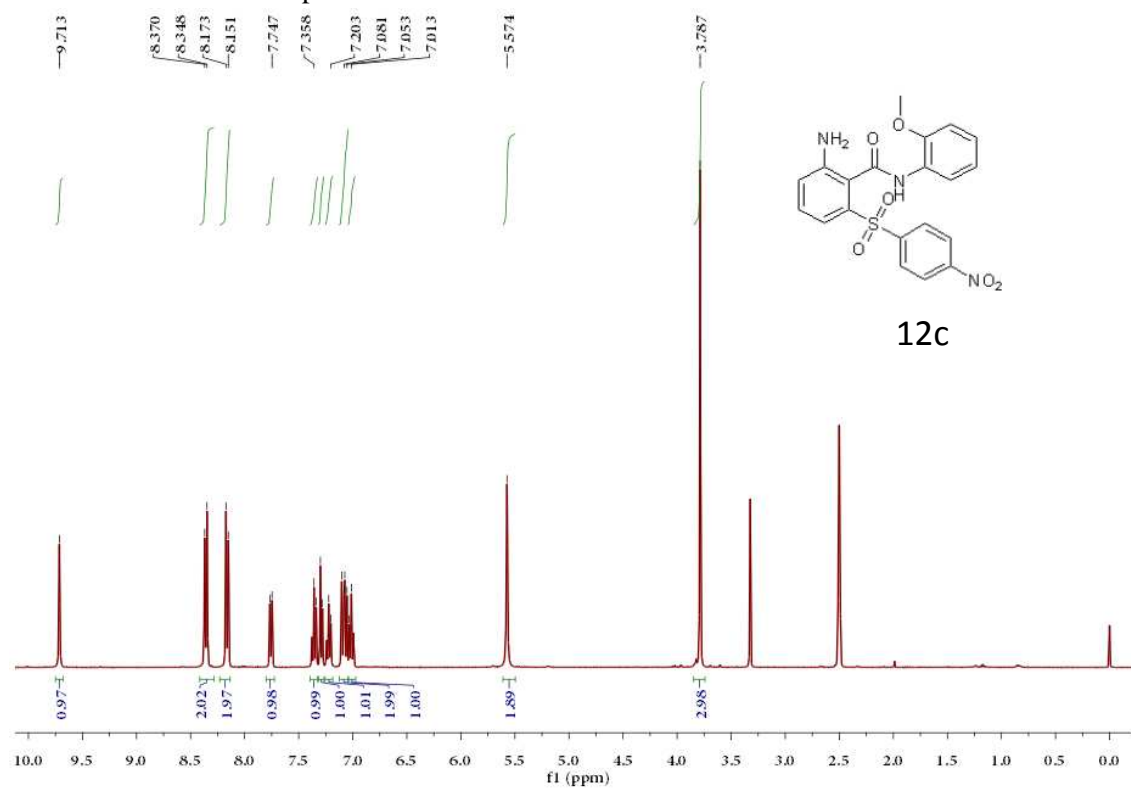
<sup>1</sup>H NMR spectra of **11a**<sup>1</sup>H NMR spectra of **11b**

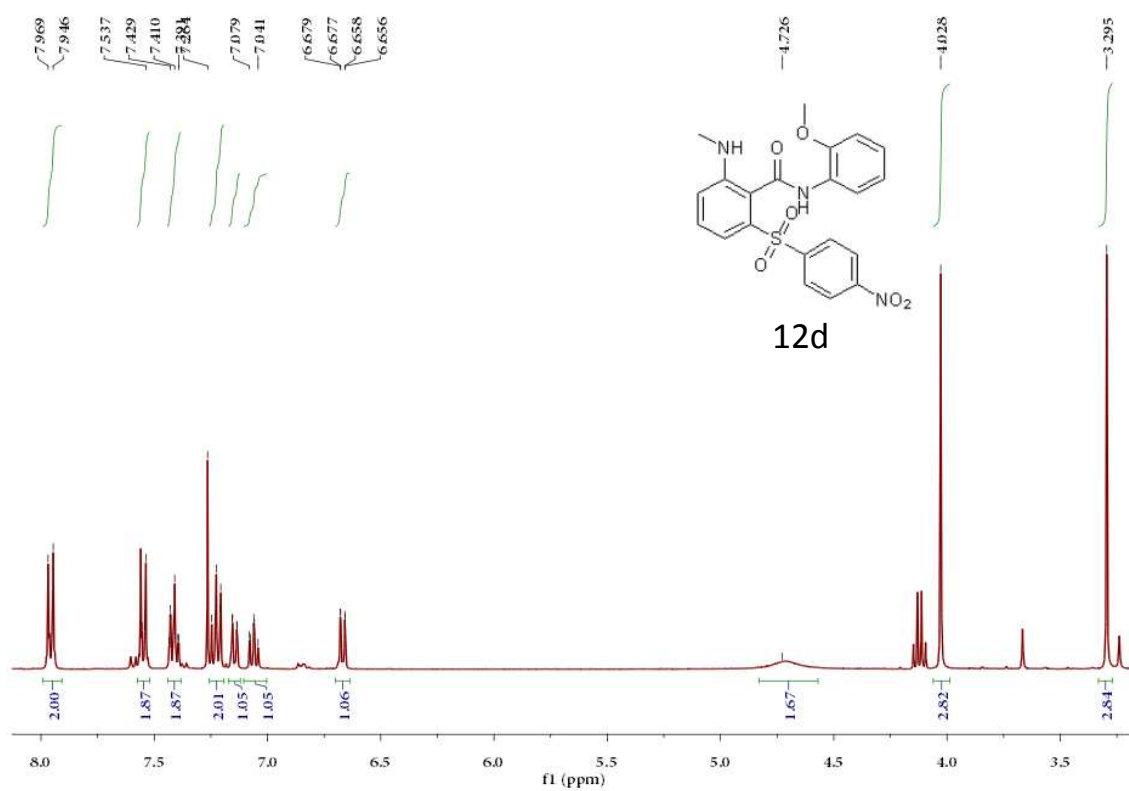
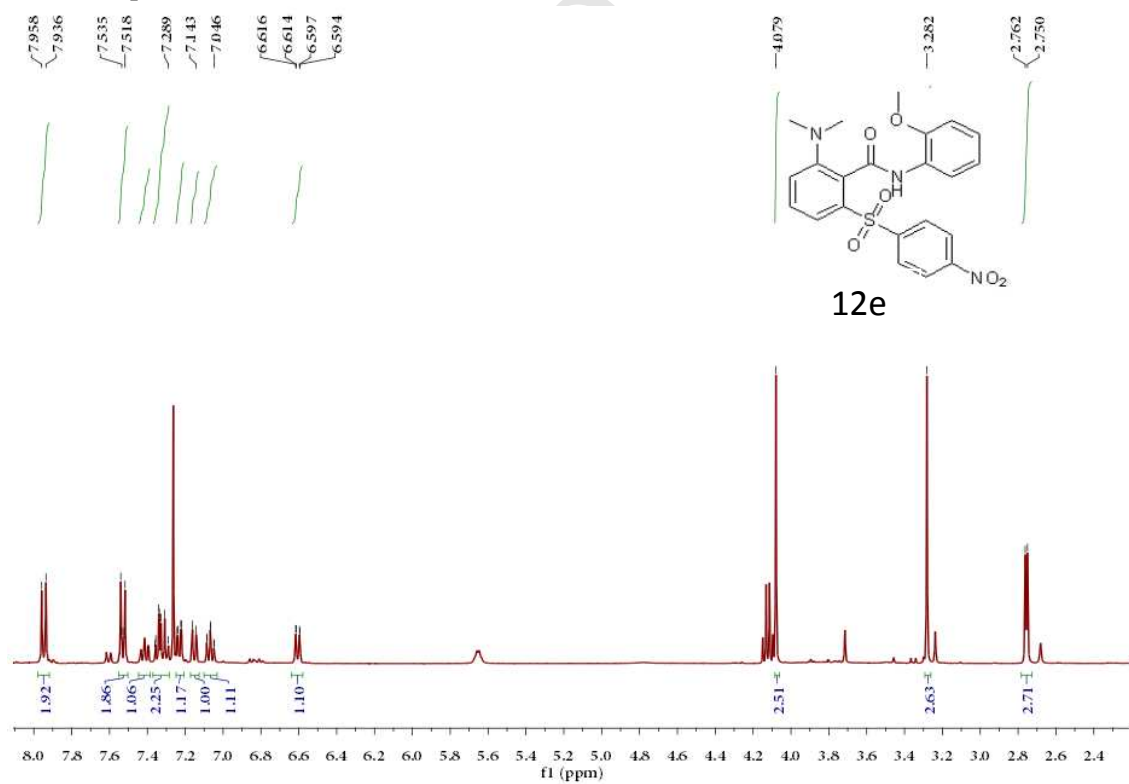
<sup>1</sup>H NMR spectra of **11c**

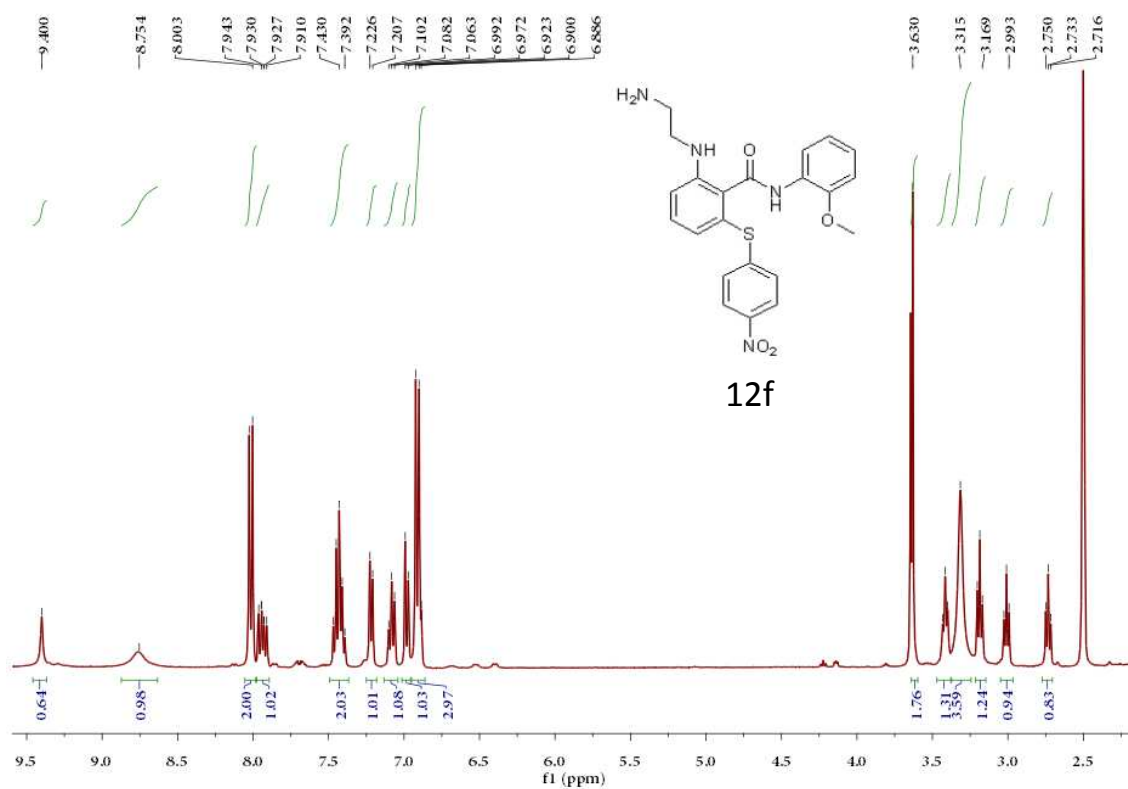
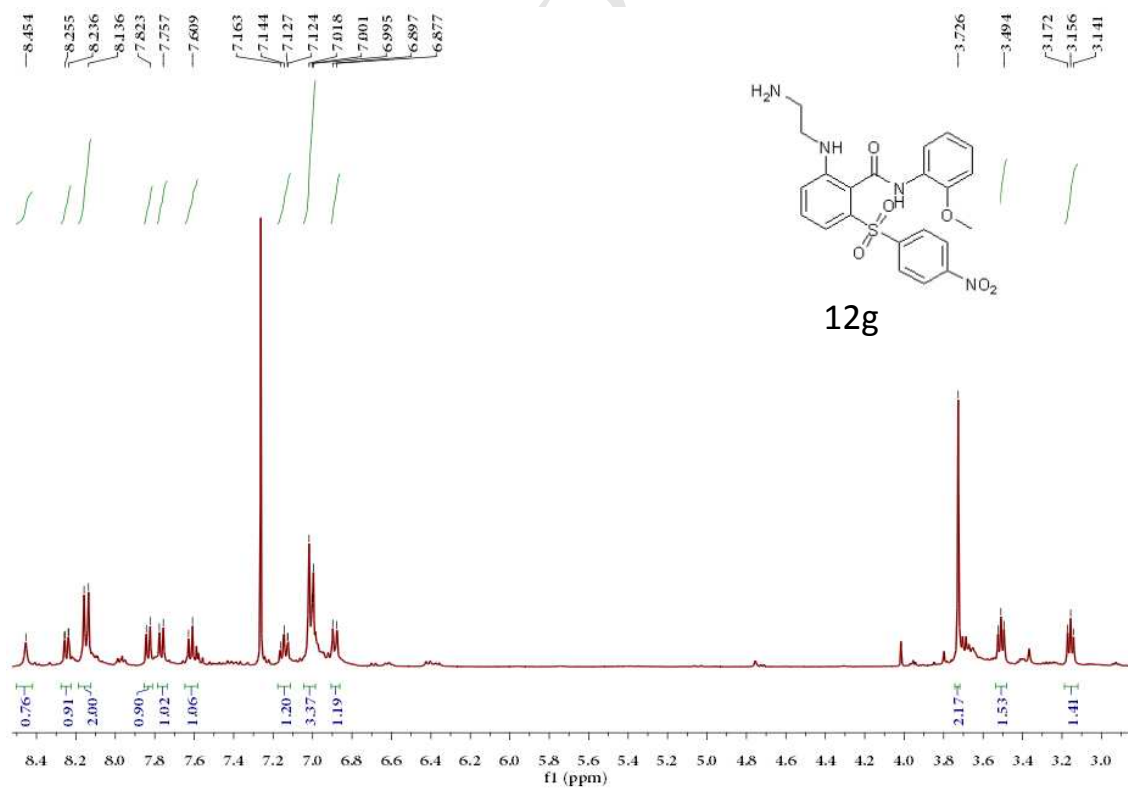
$^1\text{H}$  NMR and  $^{13}\text{C}$  NMR spectra of **12I**

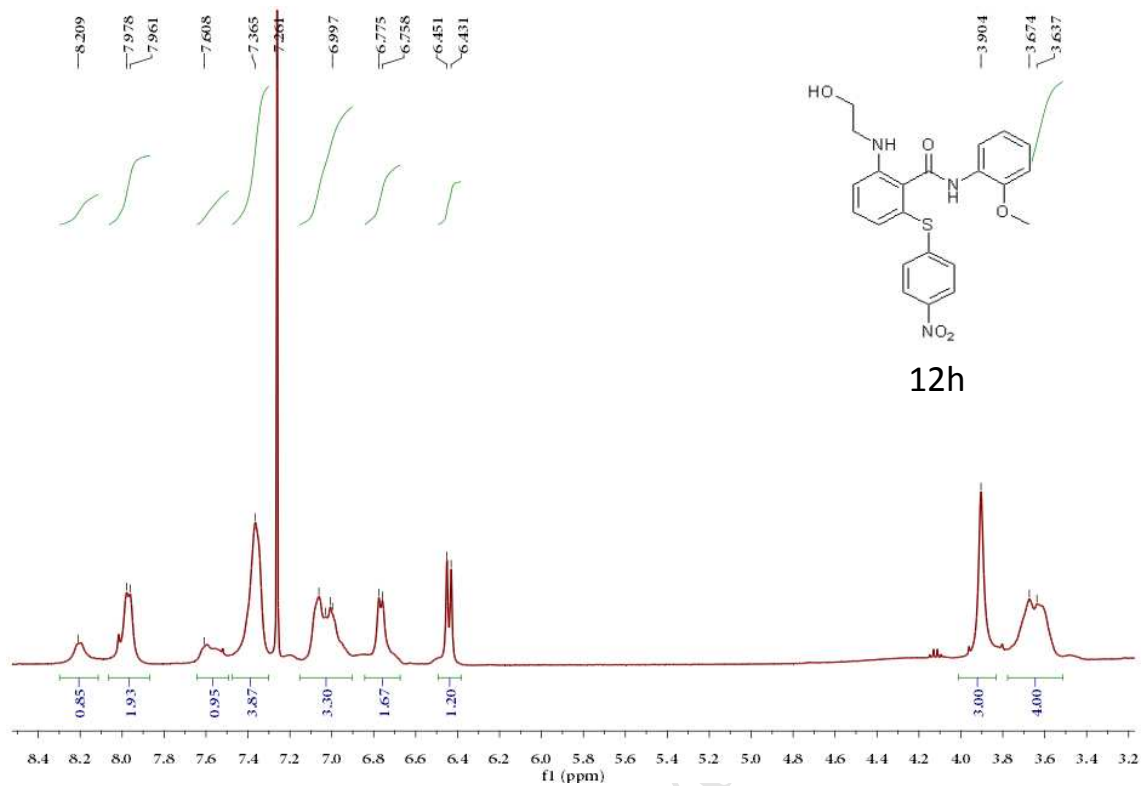
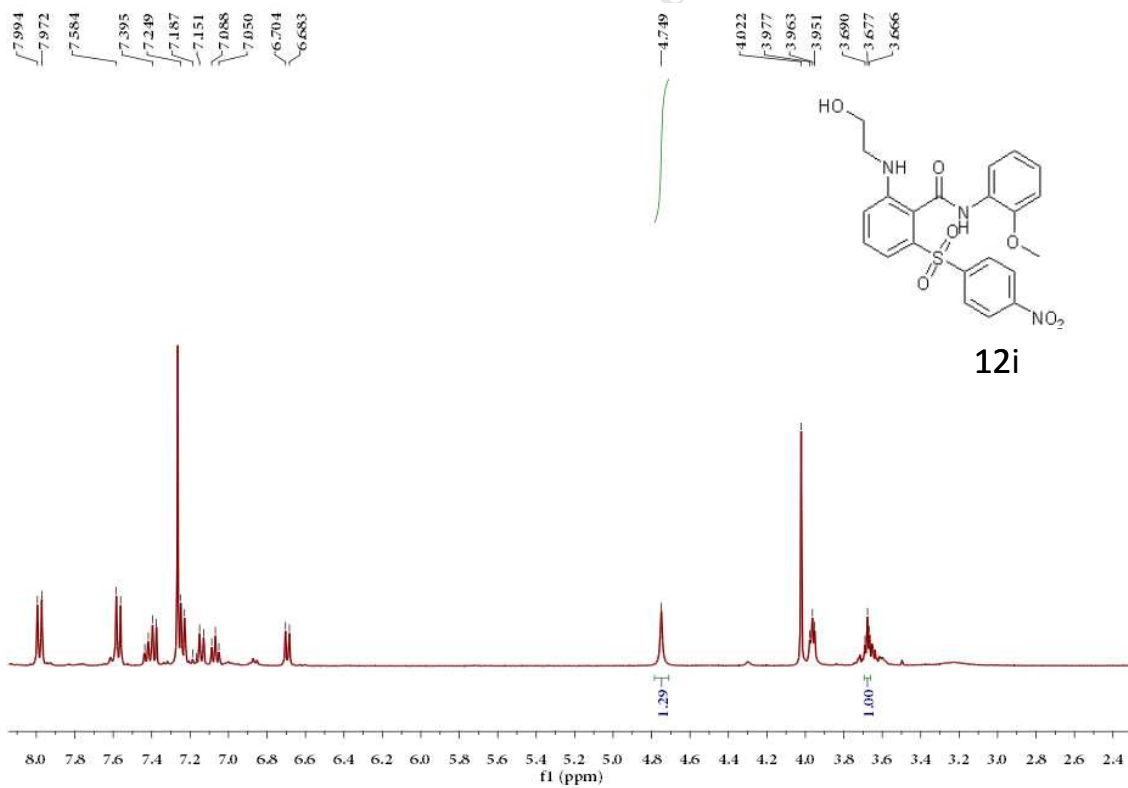
$^1\text{H}$  NMR and  $^{13}\text{C}$  NMR spectra of **12**

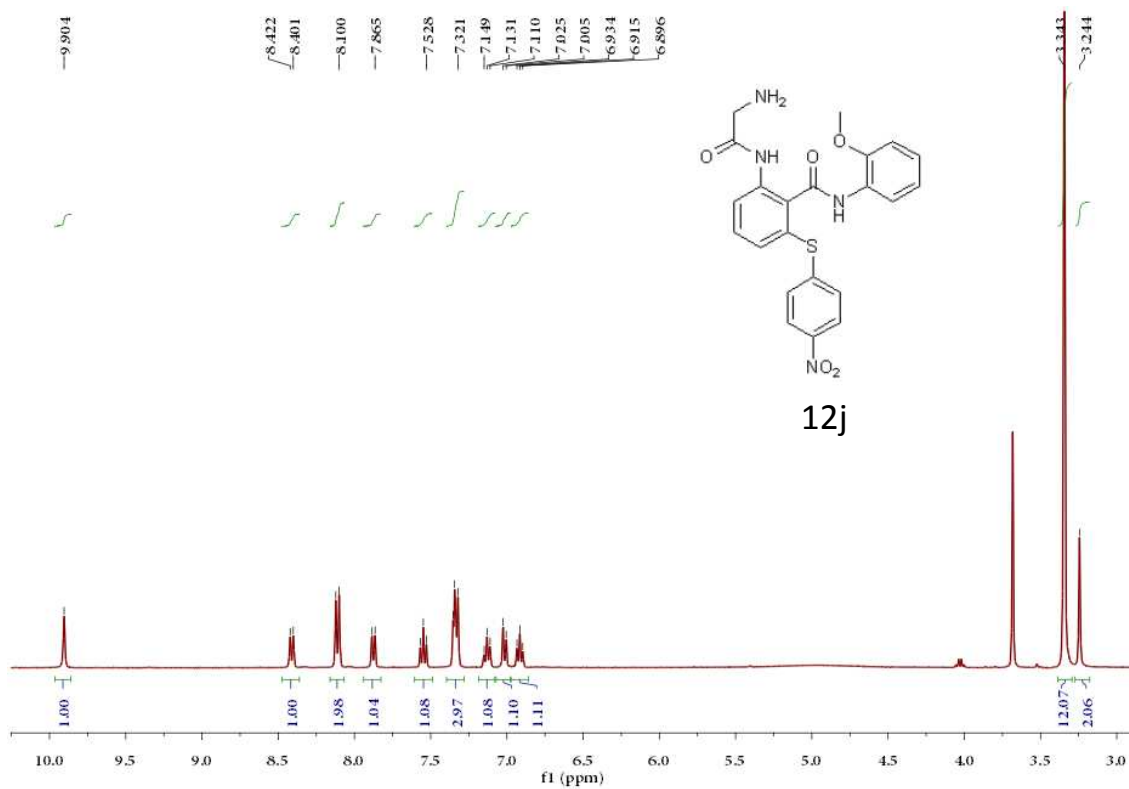
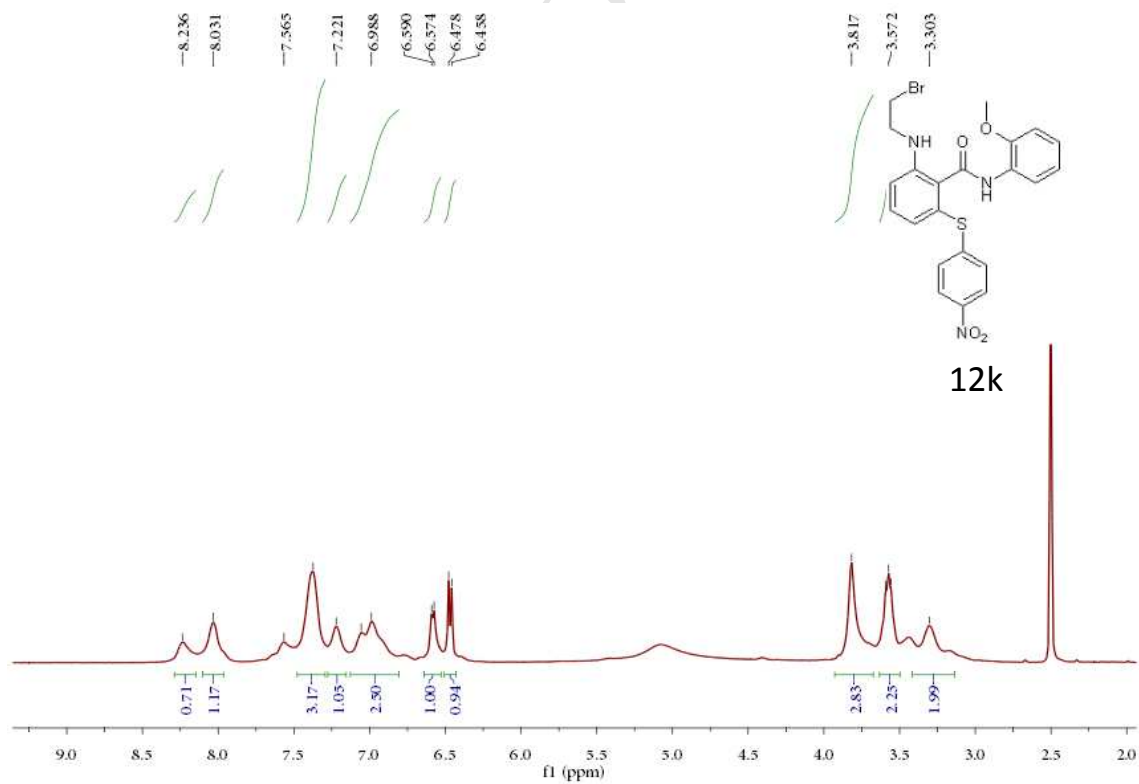
<sup>1</sup>H NMR spectra of **12a**<sup>1</sup>H NMR spectra of **12b**

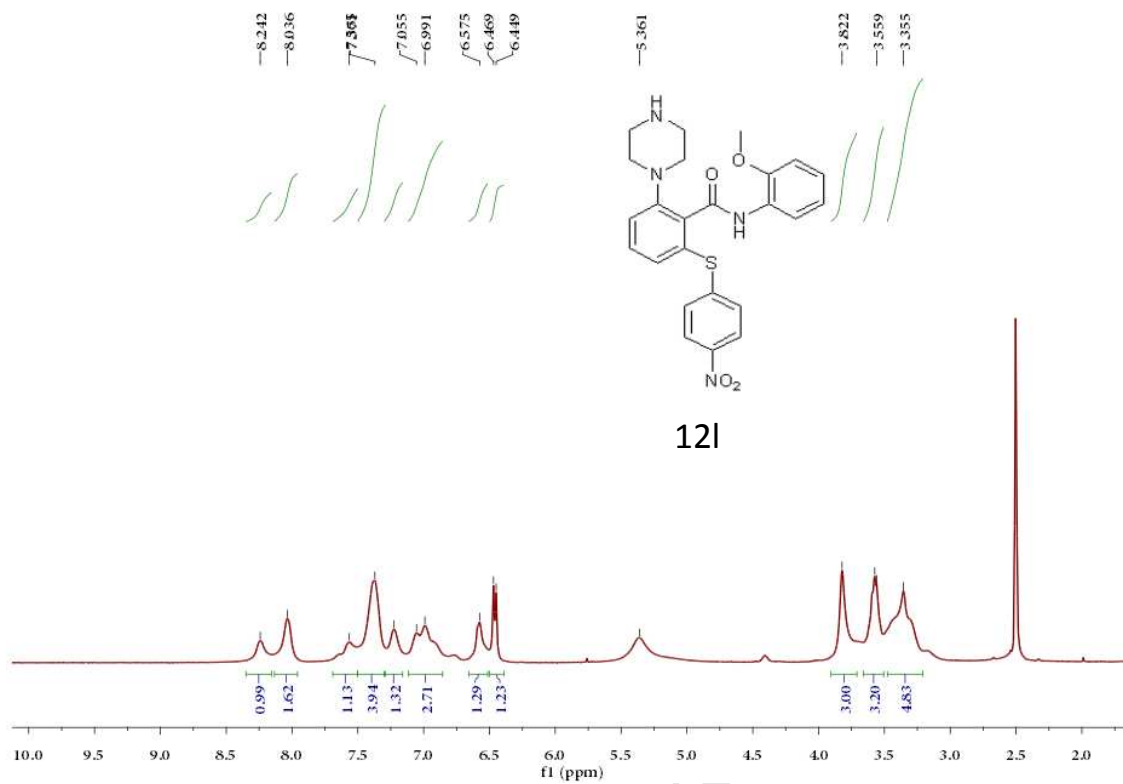
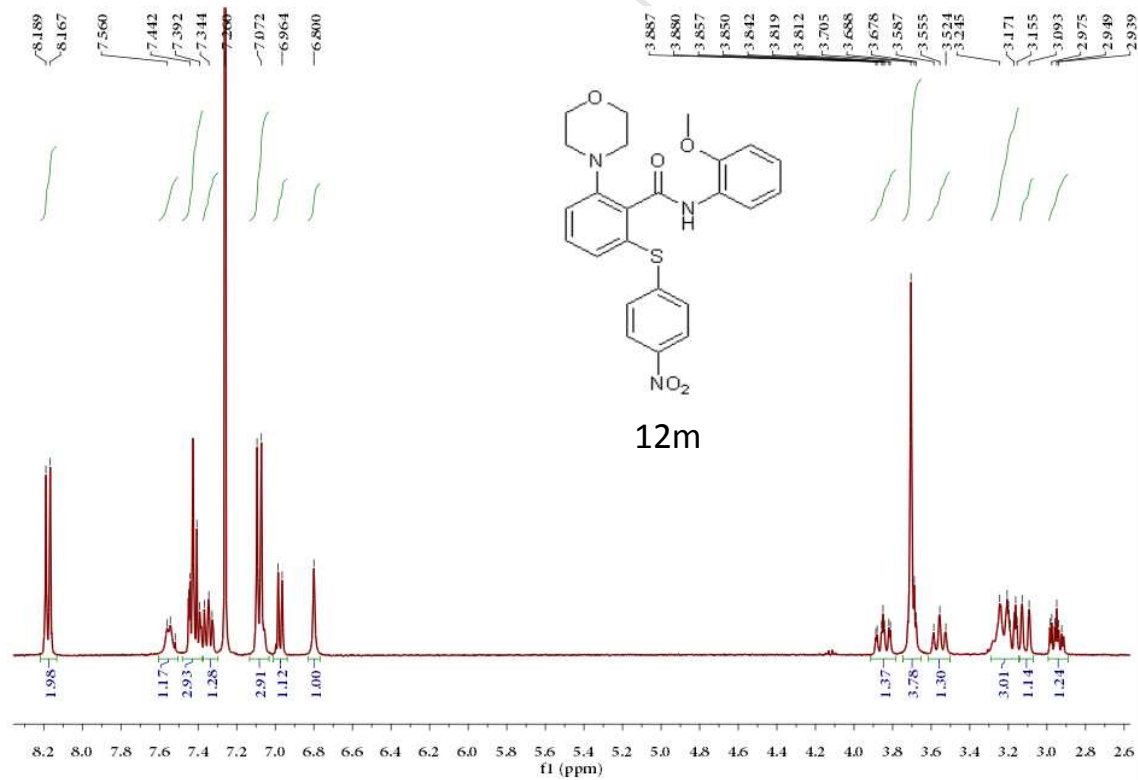
$^1\text{H}$  NMR and  $^{13}\text{C}$  NMR spectra of **12c**

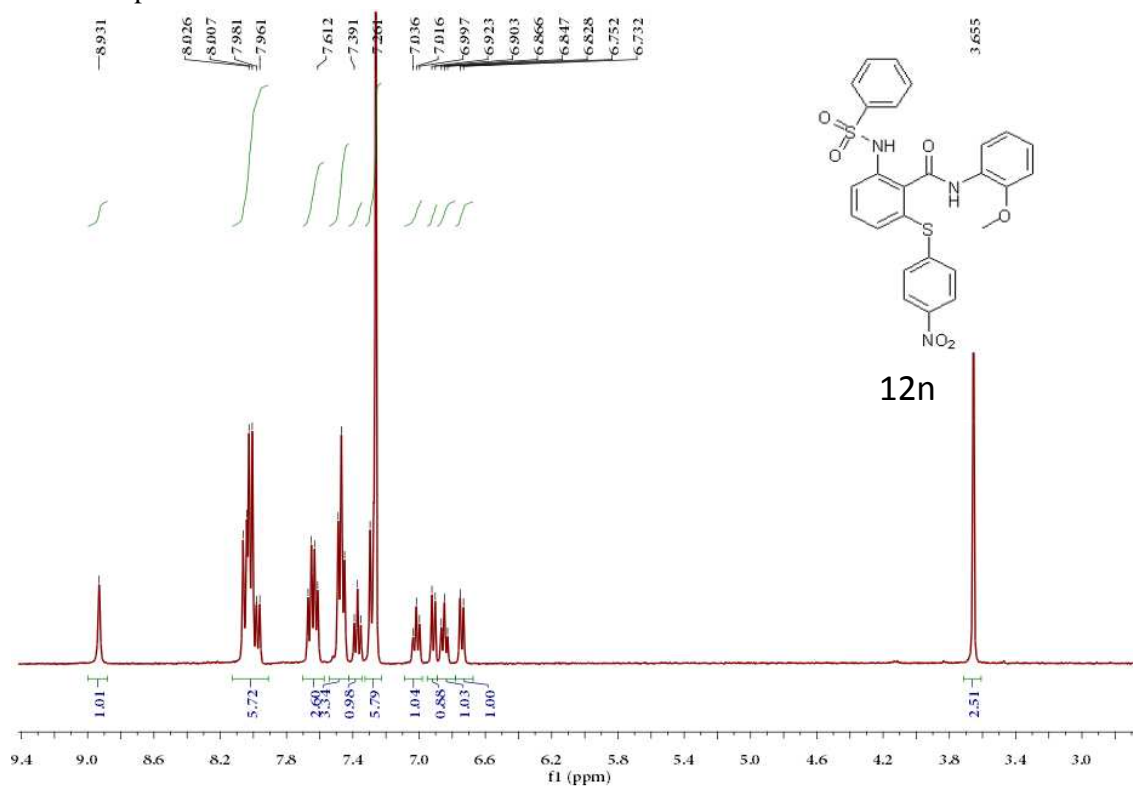
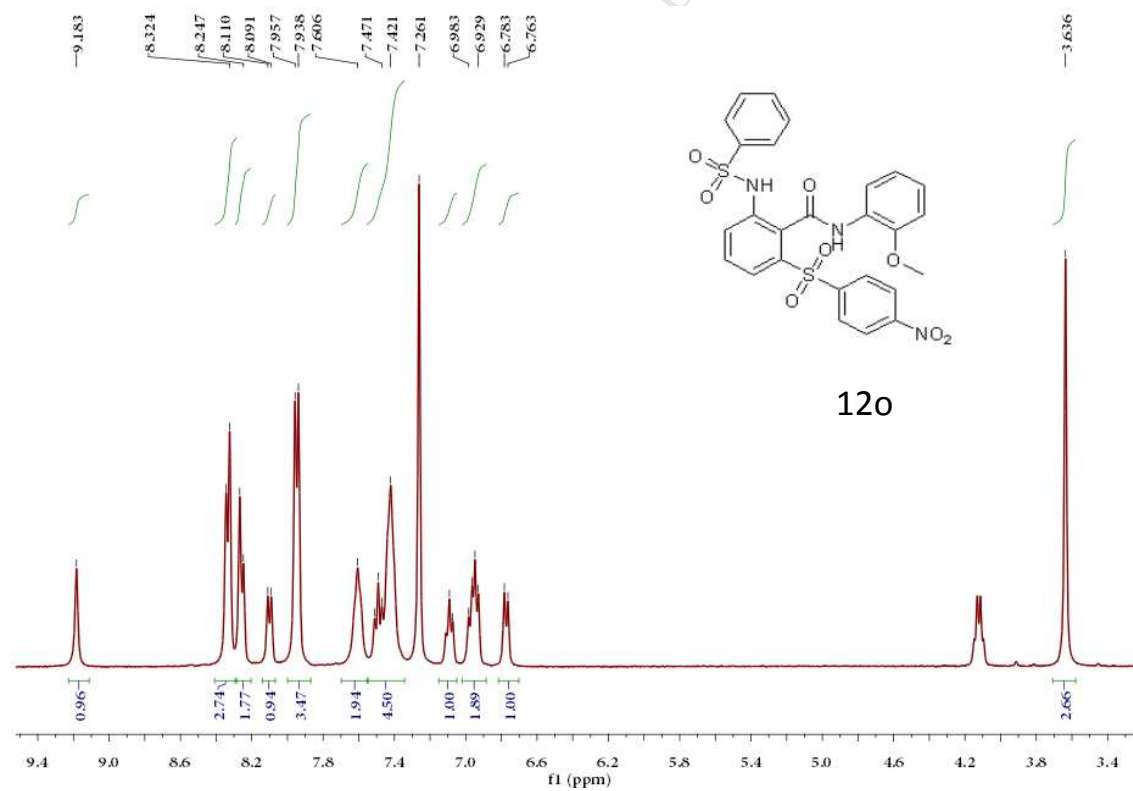
<sup>1</sup>H NMR spectra of **12d**<sup>1</sup>H NMR spectra of **12e**

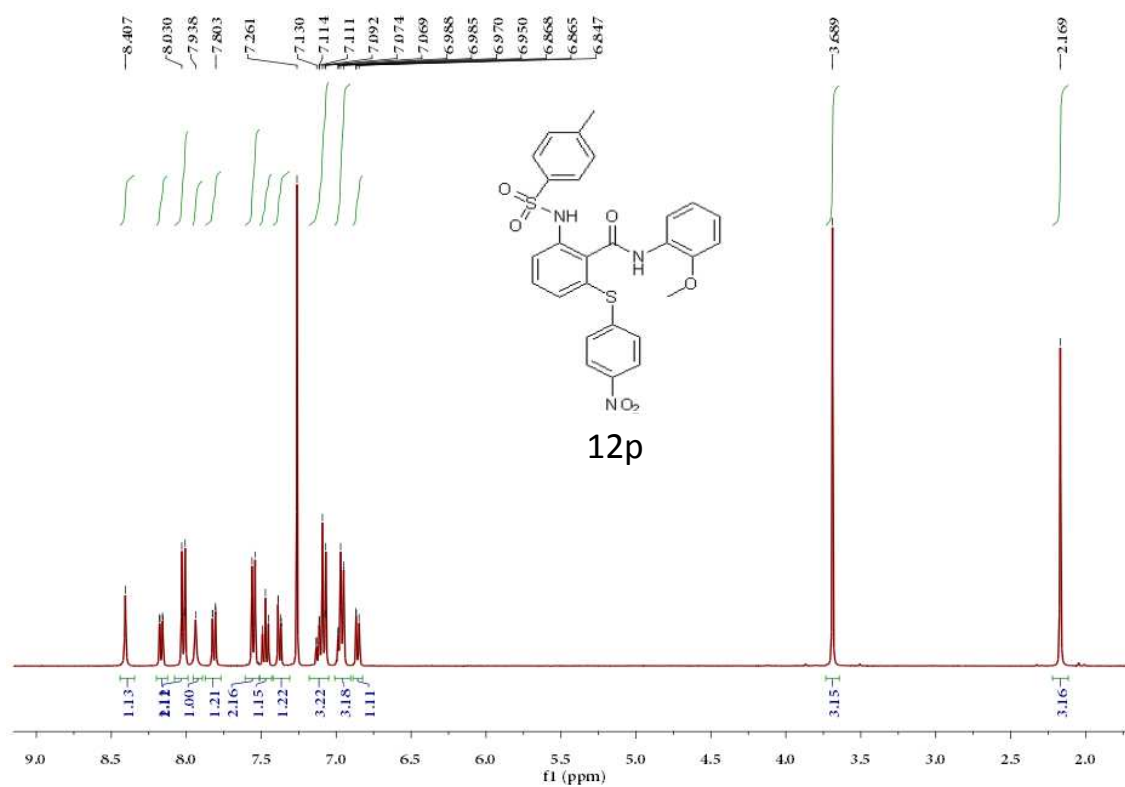
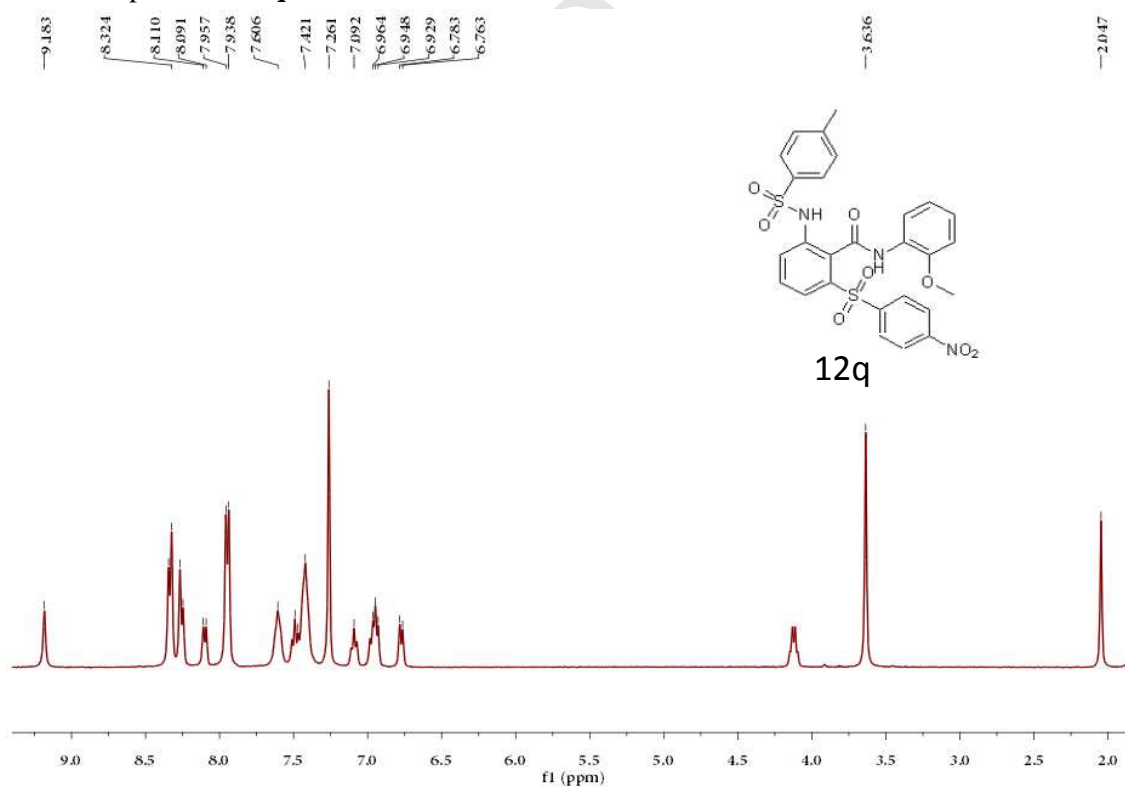
<sup>1</sup>H NMR spectra of **12f**<sup>1</sup>H NMR spectra of **12g**

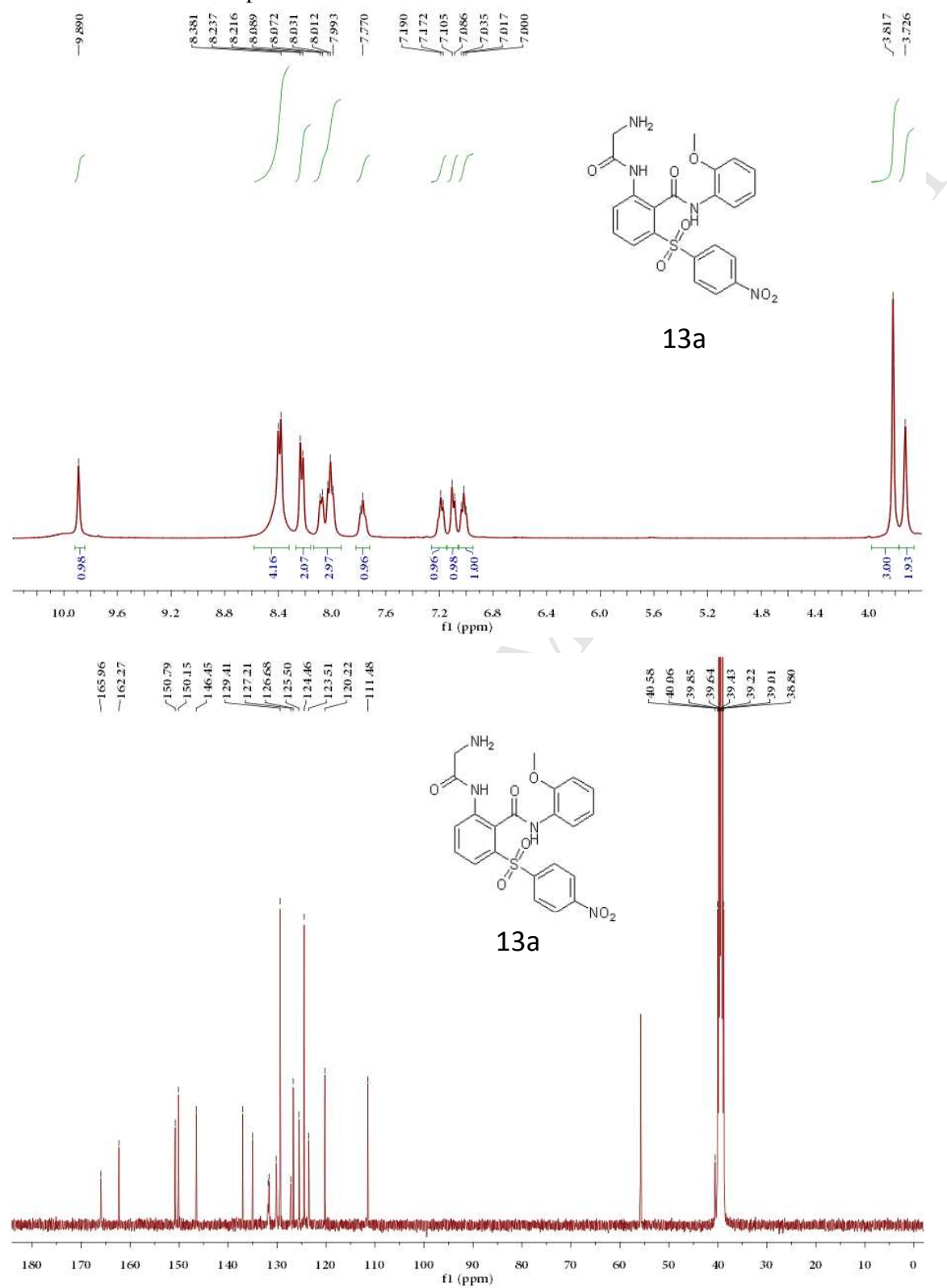
<sup>1</sup>H NMR spectra of **12h**<sup>1</sup>H NMR spectra of **12i**

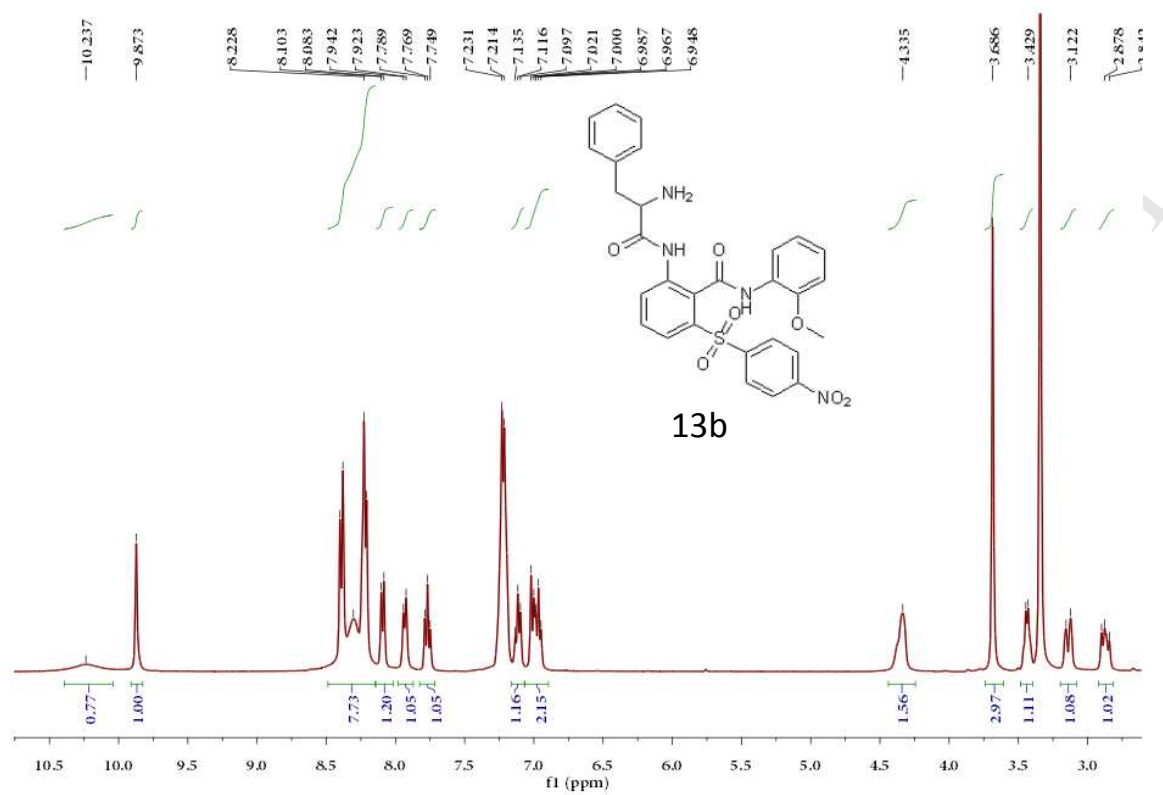
<sup>1</sup>H NMR spectra of **12j**<sup>1</sup>H NMR spectra of **12k**

<sup>1</sup>H NMR spectra of 12l<sup>1</sup>H NMR spectra of 12m

<sup>1</sup>H NMR spectra of **12n**<sup>1</sup>H NMR spectra of **12o**

<sup>1</sup>H NMR spectra of **12p**<sup>1</sup>H NMR spectra of **12q**

$^1\text{H}$  NMR and  $^{13}\text{C}$  NMR spectra of **13a**

<sup>1</sup>H NMR spectra of **13b**

ACCEPTED MANUSCRIPT

ACCEPTED MANUSCRIPT

ACCEPTED MANUSCRIPT